Time-Varying Volterra Analysis of Nonlinear Circuits

by

Hassan Sarbishaei

A thesis
presented to the University of Waterloo
in fulfillment of the
thesis requirement for the degree of
Master of Applied Science
in
Electrical and Computer Engineering

Waterloo, Ontario, Canada, 2009

AUTHOR'S DECLARATION

I hereby declare that I am the sole author of this thesis. This is a true copy of the thesis, including any required final revisions, as accepted by my examiners.

I understand that my thesis may be made electronically available to the public.

Hassan Sarbishaei

Abstract

Today's advances in communication systems and VLSI circuits increases the performance requirements and complexity of circuits. The performance of RF and mixed-signal circuits is normally limited by the nonlinear behavior of the transistors used in the design. This makes simulation of nonlinear circuits more important. Volterra series is a method used for simulation of mildly nonlinear circuits. Using Volterra series the response of the nonlinear circuit is converted into a sum of multiple linear circuit responses. Thus, using Volterra series, simulation of nonlinear circuits in frequency-domain analysis becomes possible. However, Volterra series is not able to simulate strongly nonlinear circuits such as saturated Power Amplifiers.

In this thesis, a new time-varying Volterra analysis is presented. The time-varying Volterra analysis is the generalization of conventional Volterra analysis where instead of using a DC expansion point a time-varying waveform has been used. Employing a time-varying expansion waveform for Volterra analysis, time-varying Volterra achieves better accuracy than conventional Volterra. The time-varying expansion waveforms are derived using a fast pre-analysis of the circuit. Using numerical examples, it has been shown that the time-varying Volterra is capable of simulating nonlinear circuits with better accuracy than conventional Volterra analysis. The time-varying Volterra analysis in both time and frequency domains are discussed in this thesis. The time-varying Volterra analysis has been used to simulate a saturated Class-F Power Amplifier in frequency-domain. The simulation results show good agreement with ELDO® steady-state and Harmonic Balance simulation results.

The proposed method manages to simulate nonlinear circuits, such as saturated Power Amplifier, mixers and nonlinear microwave circuits, with good accuracy. Also, this method can be used to simulate circuit with large number of nonlinear elements without the convergence issues of Harmonic Balance.

Acknowledgements

I would like to take this opportunity to express my sincere gratitude to my supervisor, Professor Ajoy Opal, for his valuable guidance, encouragement and support throughout my graduate studies. Also, I am grateful to Professor Nairn and Professor Barby for reading my thesis and providing me with valuable comments.

I would like to thank all my friends who have provided me with joy and warmth through these years. Last but not least, I would like to thank my parents and my family for their continued love, support and understanding.

Table of Contents

List of Figures

List of Tables

Chapter 1
Introduction

Circuit designers, before fabricating or manufacturing a design, need to ensure the functionality of their design before settling on a final design. Thus, Computer-Aided Design (CAD) tools, as well as circuit simulators, are important in design verification. Computation efficiency, memory resources and accuracy are important parameters of any circuit simulator. Simulation of linear circuits has been widely investigated and efficient methods are available in literature to simulate linear circuits in either the time or frequency domains [1]. Recent advances in telecommunication systems and VLSI circuits, continuously increases the complexity of circuits that need to be simulated. Also, due to stringent specifications for RF and mixed-mode circuits, the nonlinearity of such circuits becomes increasingly important. Thus, there is an increasing need for nonlinear circuit simulators with better efficiency and accuracy. Numerous nonlinear circuit simulators are available which simulate nonlinear circuits in either the time or frequency domains, e.g. [37], [38]. This thesis presents new methods for the simulation of nonlinear circuits in the time and frequency domains.

1.1 Nonlinear Circuit Simulation

Simulation of nonlinear circuits is generally more difficult than linear circuits. Different methods are available in literature for nonlinear circuit simulation. Time-domain numerical integration [1, 33], Harmonic Balance [3, 34] and Shooting method [35, 36] are traditional methods for nonlinear circuit simulation. Time-domain numerical integration and Shooting methods solve the differential algebraic equations of the circuit directly in time-domain using the appropriate numerical integration method. Shooting method simulates the steady-st ate response of the circuit directly, and time-domain numerical integration is used to calculate the transient response of the circuit. Both these methods require Newton-Raphson iterations at each step of transient simulation, which makes the simulation time-consuming. Harmonic Balance calculates the frequency components of the linear portion of the circuit in frequency-domain and nonlinear portion of the circuit in time-domain. Using an initial guess, the frequency components are calculated using Newton-Raphson iterations. Harmonic Balance faces convergence issues when dealing with large number of nonlinearities in the circuit [34]. When there is more than one tone at the input of the circuit, multi-tone Harmonic Balance (or generalized Harmonic Balance) [3] is employed. The simulation methods mentioned calculate only the response of the circuit and do not indicate which part of the circuit is responsible for the nonlinear behavior of the circuit. This information is valuable to the designer for low distortion designs [28].

Volterra series analysis is another commonly used nonlinear circuit simulation method. Volterra analysis uses a Taylor series expansion of all nonlinearities, and simplifies the nonlinear circuit analysis into sum of linear circuit responses [4, 5, 6]. In practical cases, Volterra analysis employs low degree polynomial approximations, typically 3rd order, due to complexity for high order polynomials [4]. This limits the application of the Volterra analysis to mildly nonlinear circuits, such as Low Noise Amplifier (LNA), Opamp and filter. When dealing with strongly nonlinear circuits, such as nonlinear Power Amplifiers (PA) and mixers, the Volterra analysis fails to give accurate results [8]. Volterra analysis is performed completely in frequency-domain because the circuit is linearized at each step of the analysis and handles multiple input frequencies easily. This makes Volterra analysis useful for multi-tone distortion analysis. Also, Volterra analysis can be used to separate different distortion contribution from different nonlinear elements. An efficient numerical method has been proposed in [28] to simulate per-element distortion analysis for nonlinear circuits using Volterra analysis. In the literature different methods have been proposed that combine different nonlinear circuit simulation methods. For example, by combining Harmonic Balance and Volterra analysis a simulation method for mixers has been proposed in [20].

1.2 Proposed Method

In this thesis a new simulation method which is an extension of the conventional Volterra analysis is presented. The proposed method uses time-varying expansion point for Taylor series, instead of a fixed DC expansion point. Due to time-varying nature of the method, the proposed Volterra analysis manages to simulate strongly nonlinear circuits with better accuracy than conventional Volterra. The details of the time-varying Volterra simulation in both time and frequency domains is presented in the thesis. The time-varying Volterra analysis can be used to simulate nonlinear circuits, such as RF/microwave mixers and Power Amplifiers. Simulation of a nonlinear Class-F Power Amplifier using the time-varying Volterra is presented in the thesis. It is shown that the time-varying Volterra series simulates the circuit with comparable accuracy as ELDO® steady-state simulations, but with a reduced computational cost.

1.3 Thesis Organization

Chapter 2 reviews different simulation methods for nonlinear circuits. Common time-domain and frequency-domain simulation methods are presented in this section. Different properties of these methods are discussed in this chapter. Chapter 3 introduces the time-varying Volterra analysis in time-domain. The concept of time-varying Volterra circuits and pre-analysis is discussed in this chapter. Using a numerical example, it is shown that the proposed method handles stronger nonlinearities and its simulation results are more accurate than conventional time-invariant Volterra. Also, this chapter presents a discussion on

the accuracy requirements for pre-analysis for different nonlinearities. A modification of the time-varying Volterra is also presented in this chapter which achieves better computation efficiency. Chapter 4 presents the time-varying Volterra analysis in frequency-domain. Using the same method described in Chapter 3, the time-varying Volterra circuits are solved in frequency-domain. The numerical results are compared with Harmonic Balance and Shooting method. Chapter 5 presents the simulation of a Class-F RF Power Amplifier in frequency-domain using time-varying Volterra. The simulation results show good agreement with the Shooting method. Chapter 6 concludes the thesis with discussion on the application of the time-varying Volterra. Also, possible future work related to per-element distortion analysis, as well as, applications in modeling is presented.

Chapter 2
Background: Nonlinear Circuit Simulation

In this chapter different simulation methods for nonlinear circuits are reviewed. These methods are categorized into two main groups, time-domain numerical integration methods and frequency-domain (or series expansion) methods. Time-domain methods can (but not necessarily do) simulate both transient and steady-state response of linear to strongly nonlinear circuits for almost all kinds of input signals. On the other hand frequency-domain methods can only simulate the steady-state response of the circuits for specific class of inputs. Furthermore, not all frequency-domain methods can handle strong nonlinearities or large number of nonlinear elements in the circuits. The details of these methods and their specifications will be discussed in more detail in the rest of this chapter.

The rest of this chapter is organized as follows. Section 2.1 deals mainly with Linear Multi-Step Predictor-Corrector (LMS-PC) algorithms and its pros and cons as a general time-domain simulation method. Volterra Series and Harmonic Balance are discussed in section 2.2 as two common frequency-domain methods for simulation of nonlinear circuits. Their advantages and shortcomings are addressed in section 2.2 as well.

2.1 Time-Domain Simulation Methods

The behavior of linear and nonlinear circuits can be modeled in time-domain using differential equations which usually have the form of Differential Algebraic Equations (DAE). For linear circuits the systems of Differential Algebraic Equations of the circuit are formulated using Modified Nodal Analysis (MNA) or Tableau formulation [1],

$$GX(t) + C\frac{d}{dt}\big(X(t)\big) = W(t), \qquad X(0) = X_0 \tag{2.1}$$

where G and C are constant matrices, $X(t)$ is the unknown vector with initial value X_0 and $W(t)$ is the input vector. For nonlinear circuits the circuit equations are nonlinear and more complex,

$$f\big(X(t)\big) + \frac{d}{dt}\Big(Q\big(X(t)\big)\Big) = W(t), \qquad X(0) = X_0 \tag{2.2}$$

where $f(.)$ and $Q(.)$ are, in general, nonlinear functions. By adding the charge of the nonlinear capacitors and flux of nonlinear inductors to the unknown vector one can rewrite the system of equations as [1],

$$GX(t) + E\frac{dX(t)}{dt} + P(X(t)) = W(t), \tag{2.3}$$

where both G and E are constant matrices and all the nonlinearities are collected in the nonlinear function $P(.)$. The next step in transient simulation is the discretization of time. The derivative of the unknown vector is replaced with a discrete-time approximation (usually a particular discrete-time approximation is called an integration method), which results in a finite-difference equation, instead of Differential Algebraic Equations. The resulting system of finite-difference equations can be solved using appropriate numerical method.

A common integration method widely used in circuit simulators is the Linear Multi-Step Predictor-Corrector (LMS-PC) algorithm. Predictor algorithm explicitly defines (predicts) the current time point as a function of past values and derivatives. A k^{th} order predictor algorithm uses the past k values and derivatives to evaluate the current time point, i.e. [1],

$$X(t_{n+k}) \cong \sum_{j=1}^{k} a_j^P X(t_{n+k-j}) - h\sum_{j=1}^{k} b_j^P \dot{X}(t_{n+k-j}), \tag{2.4}$$

where a_j^P and b_j^P are predictor constants and $h = t_{k+1} - t_k$ is the step size. Since predictor algorithm does not include the circuit differential equation, i.e. (2.3), the error will propagate in the algorithm and can grow unboundedly and result in the instability of the simulation (or from another point of view, there is no feedback in the method from the circuit). Thus, this algorithm must be used with the corrector algorithm to correct the predicted values and control the error in the system. The corrector algorithm is an implicit method that expresses the derivative of the current time point as a function of past values, derivatives and current time point [1],

$$\dot{X}(t_{n+k}) \cong \frac{-1}{h}\left\{\sum_{j=0}^{k} a_j^C X(t_{n+k-j}) - h\sum_{j=1}^{k} b_j^C \dot{X}(t_{n+k-j})\right\}, \tag{2.5}$$

where a_j^C and b_j^C are corrector constants. Using the corrector formula and (2.3) one can solve for the unknown vector, X, at each time point assuming the past k values and derivatives are available. In general, this system of equation is nonlinear, thus a numerical method needs to be used. The Newton-Raphson algorithm is commonly used to solve the system of nonlinear equations due to quadratic

convergence rate when the initial guess is close to the final solution [1]. Usually the predicted value using the predictor algorithm is taken as the initial estimate for Newton-Raphson algorithm. Gear2 or second-order Backward Difference Formula (BDF) is an integration method commonly used by different simulators [1], [2]. Predictor and corrector of Gear2 are defined as [1],

$$X(t_{n+2}) = 3X(t_{n+1}) - 3X(t_n) + X(t_{n-1})$$

$$\frac{d}{dt}X(t_{n+2}) = \frac{3}{2h}X(t_{n+2}) - \frac{2}{h}X(t_{n+1}) + \frac{1}{2h}X(t_n). \tag{2.6}$$

Replacing the corrector formula in (2.3) results in,

$$f(t_{n+2}) = \frac{3}{2h}EX(t_{n+2}) - \frac{2}{h}EX(t_{n+1}) + \frac{1}{2h}EX(t_n) + GX(t_{n+2}) + P\big(X(t_{n+2})\big) - W(t_{n+2}) = 0. \tag{2.7}$$

Using the Newton-Raphson, the value of $X(t_{n+2})$, the current time point, is found iteratively with the initial guess found using predictor algorithm, i.e. $X(t_{n+2}) = 3X(t_{n+1}) - 3X(t_n) + X(t_{n-1})$. Newton-Raphson algorithm requires the Jacobian matrix of the nonlinear function, $f(t_{n+2})$, which is defined as [1],

$$M_{n+2} = \frac{\partial f(t_{n+2})}{\partial X(t_{n+2})} = \frac{3}{2h}E + G + \frac{\partial P\big(X(t_{n+2})\big)}{\partial X(t_{n+2})}. \tag{2.8}$$

Using the Jacobian matrix one can find the next iteration value of unknown vector using,

$$X^{k+1}(t_{n+2}) = X^k(t_{n+2}) + t^k \Delta X^k(t_{n+2}), \tag{2.9}$$

where,

$$M_{n+2}\Delta X^k(t_{n+2}) = -f\left(X^k(t_{n+2})\right), \tag{2.10}$$

and parameter t^k is selected such that $0 < t^k \leq 1$. Solving for each time point using LMS-PC algorithm requires,

- Evaluation of Jacobian matrix (2.8), (which requires the first derivative of all the nonlinearities in the circuit)
- Solving (2.10) by LU factorization and forward/backward substitution of the Jacobian matrix,

for each iteration of the Newton-Raphson algorithm. As long as the initial guess is close to the final solution, few Newton-Raphson iterations are sufficient to reach good accuracy. However, when dealing with strong nonlinearities, the initial estimate will not be close to the final solution. This requires more iterations with reduced step sizes, i.e. small h, so that the Newton-Raphson algorithm will be able to converge. Most of the times a smaller transient simulation step is also required, i.e. small $h = t_{k+1} - t_k$, to avoid non-convergence in strongly nonlinear circuit simulation. In other words, the transient simulation step should be small when dealing with fast changes at the output nodes, whereas, a larger step size is sufficient for smoother part of the output. Thus, more sophisticated algorithms including variable step size control are necessary in order to be able to achieve a good accuracy. An example of a variable step size control algorithm for nonlinear circuits can be found in [1]. Variable step size control algorithms usually require multiple solutions of the circuit for each time point, thus increasing the computation cost of each time step significantly, especially for strongly nonlinear circuits.

It can be concluded that LMS-PC algorithms, while achieving good accuracy for nonlinear circuits, increase the simulation complexity and cost significantly (due to complex algorithms to avoid non-convergence when dealing with strong nonlinear circuits). Furthermore, when dealing with steady-state response of the circuits with widely separated frequencies, e.g. mixers where input and output frequencies can be more than a decade away from each other, LMS-PC algorithms are inefficient and require long simulation time. On one hand, the simulation step size should be small enough to account for the fast changes of the signals due to high frequency input component, on the other hand, the simulation time should be long enough to account at least one period of the output signal, determined by the period of the low frequency component. As an example, if the inputs of a mixer are two sinusoidal inputs with frequencies $f_1 = 1.05\,GHz$ and $f_2 = 1.0\,GHz$, with the output frequency $f_0 = 50\,MHz$, the simulation step size should be much smaller than $1/f_1 = 0.95\,ns$, e.g. 20 times smaller , also the simulation time should be at least $1/f_0 = 20\,ns$, which increases the simulation cost significantly. Another issue when trying to solve for steady-state response is the time that it takes for the circuit to reach steady-state, or the time it takes for transients to die down. Large time constants in the circuit dictate the time that it takes for transients to die (these large time constants can be due to biasing network), thus, forcing the transient simulation to run through many periods of the input signal, sometimes thousands of cycles, for transients to die [3].

Due to the issues discussed here, other simulation methods that eliminate these problems are beneficial (and sometimes necessary). “Shooting method” is a time-domain simulation method that calculates the steady-state response in time-domain using numerical integration, thus, eliminating the need for long transient simulation times [2]. However, it still requires complex numerical integration algorithms to overcome strong nonlinearities, as well as small step sizes to achieve good accuracy. Frequency-domain methods eliminate some of the problems associated with the time-domain simulators and achieve good accuracy with less computation cost. However, frequency-domain methods cannot handle all types of inputs and face problems when dealing with large strongly nonlinear circuits, which make it necessary to use time-domain numerical integration simulation methods. In the next section the basics and shortcomings of two popular frequency-domain methods, i.e. Volterra Series and Harmonic Balance, will be discussed in detail.

2.2 Frequency-Domain Simulation Methods

In this section two common frequency-domain approaches for nonlinear circuit simulation are discussed. Frequency-domain simulation methods calculate the steady-state response of circuits and cannot handle all types of continuous-time input sources. First, the Schetzen’s multi-linear method [4] for analyzing weakly nonlinear circuits, which is based on the Volterra Series analysis [5], is presented. Then, Harmonic Balance, which can handle stronger nonlinearities, will be discussed.

2.2.1 Schetzen’s Multi-Linear Method

Schetzen’s multi-linear method is based on Volterra analysis [5] and gives the same results for mildly nonlinear circuits [4]. However, Schetzen’s multi-linear method avoids the multiple integrals and kernels that usually appear in the original Volterra analysis, and thus gives the designer a better physical insight of the nonlinearity and their effect on the output. The first step in the Schetzen’s method is to expand the nonlinearity in the circuit using Taylor series. Taylor series of a nonlinear function $f(x)$ is expressed as,

$$f(x) = f(x_0) + (x - x_0)\frac{df}{dx}\Big|_{x=x_0} + \frac{1}{2!}(x - x_0)^2\frac{d^2f}{dx^2}\Big|_{x=x_0} + \cdots, \tag{2.11}$$

where x_0 is the expansion point, typically a DC value. For example, a nonlinear resistor is represented by [1],

$$v_R = f(i_R), \tag{2.12}$$

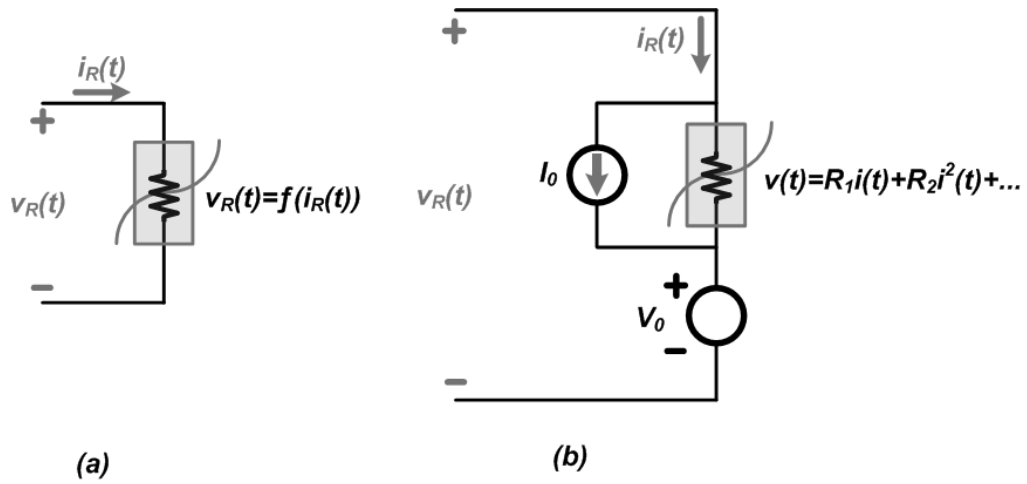

Fig. 2.1 - (a) Nonlinear resistor (b) Equivalent model for the nonlinear resistor

as shown in Fig. 2.1(a). Expanding the nonlinear function using the expansion point $V_0 = f(I_0)$, we have,

$$v_R = f(i_R) = V_0 + (i_R - I_0)\frac{df}{di_R}|_{i_R=I_0} + \frac{1}{2!}(i_R - I_0)^2\frac{d^2f}{di_R^2}|_{i_R=I_0} + \cdots. \tag{2.13}$$

Rewriting (2.13) results in,

$$v_R - V_0 = \hat{v} = R_1\hat{\imath} + R_2\hat{\imath}^2 + R_3\hat{\imath}^3 + \cdots, \tag{2.14}$$

where $\hat{\imath} = i_R - I_0$ represent the changes in the current of the resistor from the expansion point, I_0, which is usually the quiescent current of the resistor. The same thing can be said regarding $\hat{v} = v_R - V_0$, the changes in the voltage of the resistor from the expansion point, V_0. Also $R_1 = \frac{df}{di_R}\Big|_{i_R=I_0}$ is the linear (first order) resistance of the nonlinear element, which is the same as the resistor used for small signal analysis. Similarly $R_2 = \frac{1}{2!}\frac{d^2f}{di_R^2}\Big|_{i_R=I_0}$ is the second order coefficient of the resistance, $R_3 = \frac{1}{3!}\frac{d^3f}{di_R^3}\Big|_{i_R=I_0}$ is the third order coefficient and so on. The nonlinear resistor is modeled with a voltage source, V_0, current source I_0 and a nonlinear resistor with the characteristic function as shown in Fig. 2.1(b),

$$\hat{v} = \sum_{n=1}^{\infty} R_n \hat{\imath}^n. \tag{2.15}$$

Using this model we represent the nonlinear resistor by a power series. Because of linearity and superposition, we remove the constant voltage source,V_0, and current source, I_0, from the model and only discuss the nonlinear part of the model. If the independent variable of the nonlinear element, current in case of the resistor, is scaled by the factor α, then the n^{th} order term of the voltage of the resistor will be scaled by α^n. Using this method one can show the mechanism of the mixing and harmonic generation in a nonlinear circuit. If the current of the resistor only contains a single tone, $A\sin(\omega_0 t)$, then due to the nonlinearity, or non-zero higher order terms in the resistor characteristics, the voltage of the resistor will contain second order term, $R_2 \sin^2(\omega_0 t) = R_2(0.5 - 0.5\cos(2\omega_0 t))$ (which contains $2\omega_0$ and DC), third order term, $R_3 \sin^3(\omega_0 t) = R_3(0.75\sin(\omega_0 t) - 0.25\sin(3\omega_0 t))$ (which contains $3\omega_0$ and ω_0), and so on. Thus the output will contain not only the input frequency, ω_0, but also the harmonics of that frequency (theoretically infinite number of harmonics). When there is more than one tone at the input, the output spectrum will contain the harmonics of the input frequencies as well as the mixing of these frequencies which will result in a complex output frequency spectrum.

The next step in the Schetzen's multi-linear method is breaking up the complete response of the circuit into response of the circuits of different orders, i.e.,

$$\hat{v} = \sum_{n=1}^{\infty} \hat{v}_n \quad and \quad \hat{\imath} = \sum_{n=1}^{\infty} \hat{\imath}_n, \tag{2.16}$$

where $(\hat{v}_1, \hat{\imath}_1)$ represent the response of the first order circuit, i.e. linearized circuit, $(\hat{v}_2, \hat{\imath}_2)$ represent the response of the second order circuit and so on. Replacing (2.16) in (2.15) and scaling the current of the resistor by α, we have,

$$\hat{v} = \sum_{n=1}^{\infty} \alpha^n \hat{v}_n = \sum_{n=1}^{\infty} R_n \hat{\imath}^n = \sum_{n=1}^{\infty} R_n \left(\sum_{n=1}^{\infty} \alpha^n \hat{\imath}_n \right)^n. \tag{2.17}$$

Expanding the summations and rewriting (2.17), it can be shown that,

$$\begin{aligned}\alpha\hat{v}_1 + \alpha^2\hat{v}_2 + \alpha^3\hat{v}_3 + \cdots = {} & R_1(\alpha\hat{\imath}_1 + \alpha^2\hat{\imath}_2 + \alpha^3\hat{\imath}_3 + \cdots) \\ & + R_2(\alpha\hat{\imath}_1 + \alpha^2\hat{\imath}_2 + \alpha^3\hat{\imath}_3 + \cdots)^2 \\ & + R_3(\alpha\hat{\imath}_1 + \alpha^2\hat{\imath}_2 + \alpha^3\hat{\imath}_3 + \cdots)^3 + \cdots.\end{aligned} \tag{2.18}$$

Collecting the terms with the same power of α on both sides, one will get,

$$\begin{aligned}\alpha\hat{v}_1 + \alpha^2\hat{v}_2 + \alpha^3\hat{v}_3 + \cdots = {} & \alpha(R_1\hat{\imath}_1) \\ & +\alpha^2(R_2\hat{\imath}_2 + R_1\hat{\imath}_1^2) \\ & +\alpha^3(R_3\hat{\imath}_3 + 2R_1R_2\hat{\imath}_1\hat{\imath}_2 + R_1\hat{\imath}_1^3) + \cdots.\end{aligned} \tag{2.19}$$

Taking into account that this is true for all values of α, it can be concluded that the coefficient of different powers of α on both sides should be equal, i.e.,

$$\begin{aligned}\hat{v}_1 &= R_1\hat{\imath}_1 \\ \hat{v}_2 &= R_1\hat{\imath}_2 + R_1\hat{\imath}_1^2 \\ \hat{v}_3 &= R_1\hat{\imath}_3 + 2R_1R_2\hat{\imath}_1\hat{\imath}_2 + R_1\hat{\imath}_1^3\end{aligned} \tag{2.20}$$

As it can be seen, the response of the circuit of each order is expressed as the response of a linear circuit ($\hat{v}_n(linear) = R_1\hat{\imath}_n$) and a nonlinear part which depends only on the response of the circuit of lower orders ($\hat{v}_n(nonlinear) = f(\hat{\imath}_1, \hat{\imath}_2, \cdots, \hat{\imath}_{n-1})$. For example, for the third order circuit we have, $\hat{v}_3 = R_1\hat{\imath}_3 + 2R_1R_2\hat{\imath}_1\hat{\imath}_2 + R_1\hat{\imath}_1^3$, which can be thought of as the sum of the linear part, $R_1\hat{\imath}_3$, plus the nonlinear part, $2R_1R_2\hat{\imath}_1\hat{\imath}_2 + R_1\hat{\imath}_1^3$, that depends on $\hat{\imath}_1$ and $\hat{\imath}_2$ (solution of the circuit of lower orders). In other words, the nonlinear resistor for the n^{th} order circuit, can be modeled as a linear resistor, R_1, in series with a dependent voltage source, $e_n = f(\hat{\imath}_1, \hat{\imath}_2, \cdots, \hat{\imath}_{n-1})$, as shown in Fig. 2.2. Assuming the response of the lower orders circuits are already available, one can solve for the response of the circuit of n^{th} order by solving the n^{th} order circuit which is a linear circuit with nonlinear dependent sources whose value depends on the lower order circuit responses.

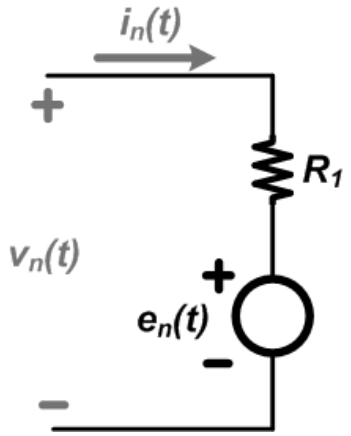

Fig. 2.2 - Equivalent model for the nonlinear resistor for nth order circuit

The derivations above can be easily generated for a nonlinear capacitor (charge of the capacitor expressed as a nonlinear function of the voltage, $q_C = f(v_C)$), nonlinear inductor (flux of the inductor expressed as a nonlinear function of the current, $\Psi_L = f(i_L)$) and nonlinear dependent sources. Fig. 2.3 summarizes the nonlinear elements and their Volterra circuit model [30]. It should be mentioned that, in case of nonlinear capacitors and inductors, it is better to add the charge of the capacitors and flux of the inductors to the unknown vector of the circuit, instead of their current (for a capacitor) and voltage (for an inductor). This way we can avoid numerical problems that can occur during simulation due to taking the derivatives of charge and flux [2]. To summarize, the steps required in Schetzen's multi-linear method are:

- First the nonlinear elements are replaced by their quiescent sources (voltage and current) along with a nonlinear element that is represented by, $\hat{v} = \sum_{n=1}^{\infty} R_n \hat{\imath}^n$. Of course the DC simulation must be carried out before this step to calculate the quiescent currents and voltages [1].
- Next, the first order circuit is solved, since response of the first order is required for all the higher order circuits. To construct the first order circuit, we replace all the nonlinear elements with their first order Volterra model, i.e. a linear element with the quiescent voltage and current source. All the inputs of the circuit should be taken into account for the first order circuit.
- After solving the first order circuit, higher order circuits are solved sequentially. This can done by replacing all the nonlinear elements with their n^{th} order Volterra model, i.e. a linear element and a dependent source as shown in Fig. 2.3, while all the inputs to the circuit are now turned-off (they only affect the first order circuit).

- Finally, the response of different orders should be added to get the complete answer of the circuit.

There are some interesting points regarding Schetzen's method that are worth noting here. It can be seen that, the Volterra circuits of different orders are all linear, and have the same G and C matrices. Thus, superposition can be applied to each Volterra circuit, but not across different orders. Furthermore, the linearity makes it easy to use frequency-domain approaches to solve the circuit [7]. In other words, the circuit of order n can be described in frequency-domain as [1],

$$(G + (j\omega)C)X_n(j\omega) = T(j\omega)X_n(j\omega) = W_n(j\omega), \tag{2.21}$$

where, G and C are constant matrices for all the orders, and thus $T(j\omega)$ do not change for different orders. Knowing $W_n(j\omega)$, the input vector, the circuit is solved for different frequencies using LU factorization of $T(j\omega)$ and forward/backward substitution [1]. Calculating $W_n(j\omega)$ requires taking the Fourier transform of all the sources. $W_n(j\omega)$ includes dependent sources of the Volterra models, which have the form of $e_n = f(\hat{\imath}_1, \hat{\imath}_2, \cdots, \hat{\imath}_{n-1})$, for a nonlinear resistor. Since $f(\hat{\imath}_1, \hat{\imath}_2, \cdots, \hat{\imath}_{n-1})$ contains multiplication of the currents of lower orders (which are known), one can find its Fourier transform by convolving the Fourier transform of lower orders. For the third order model of a resistor we have,

$$\begin{aligned} & e_3(t) = 2R_1R_2\hat{\imath}_1(t)\hat{\imath}_2(t) + R_1\hat{\imath}_1^3(t) \\ & \xrightarrow{\mathcal{F}} E_3(j\omega) = 2R_1R_2\{\widehat{I_1}(j\omega) \otimes \widehat{I_2}(j\omega)\} + R_1\{\widehat{I_1}(j\omega) \otimes \widehat{I_1}(j\omega) \otimes \widehat{I_1}(j\omega)\}, \end{aligned} \tag{2.22}$$

where $\otimes$ denotes convolution.

As it can be seen when the input contains multiple tones, the size of the frequency vector will increase rapidly, due to inter-modulation and harmonic generation. It makes the calculation of $W_n(j\omega)$, which requires convolution, more expensive. But in case of few tones at the input, Schetzen's method can be performed efficiently. For mildly nonlinear circuits, it is expected that the Taylor series of the nonlinear elements converges rapidly, thus only a few terms are needed in the Taylor series. In other words, a few orders of Volterra circuits are sufficient to achieve good accuracy, usually 3 or 5. From another point of view, it can be said that the rest of nonlinear terms in the Taylor series are small enough, i.e.,

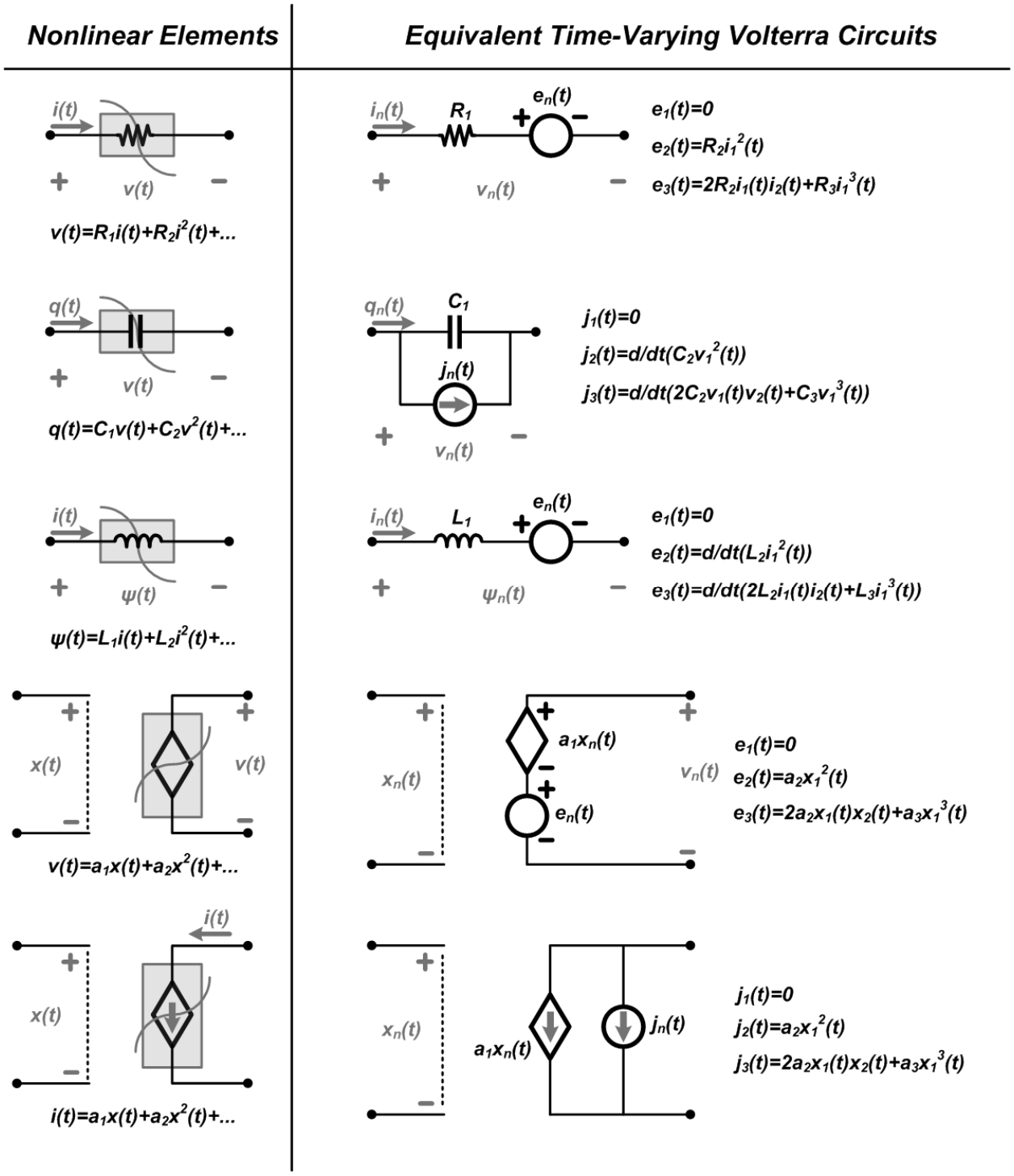

Fig. 2.3 - Volterra model for the nonlinear elements

$$R_{N+1}\hat{\imath}^{N+1} + R_{N+2}\hat{\imath}^{N+2} + \cdots \approx 0, \tag{2.23}$$

where N is the order of the Volterra analysis. This is achieved by either employing small $\hat{\imath}$, i.e. small input, or small R_{N+1}, i.e. weak nonlinearity. One might suggest using more terms in the Taylor series when dealing with strongly nonlinear circuits. However, this approach has two main issues when dealing with practical cases. First, as the order of Volterra series increases, the complexity of the dependent sources for each order increases exponentially. Thus, the frequency-domain method requires lots of convolutions to find the Fourier transform of the dependent sources, which increases the computation cost significantly. The second issue, which is more serious, is the convergence radius of the Taylor series [8]. This issue becomes significant when dealing with exponential nonlinearities. For example, the drain current of a MOSFET as a function of gate voltage has the form of [9],

$$i_D(V_{GS}) = ln\left(1 + exp\left(\frac{V_{GS} - V_T}{2\eta\Phi_t}\right)\right)^2. \tag{2.24}$$

Complex singularity of the nonlinearity at $V_{GS} = V_T + j2\pi\eta\Phi_t$, limits the convergence radius of the Taylor series. Thus, when the input signal is large, the Taylor series diverges, which results in large simulation errors (especially when MOSFET's region of operation changes). This error cannot be reduced by using higher order Volterra circuits.

The problems discussed here, limit the application of ordinary Volterra analysis to mildly nonlinear circuits [8]. Hence, other frequency-domain simulation methods should be considered when dealing with strong nonlinearities. Harmonic Balance is a common method for simulation of strongly nonlinear circuits in frequency-domain. The basics and drawbacks of Harmonic Balance are discussed in the next section.

2.2.2 Harmonic Balance

Time-domain numerical integration is not the best choice for simulating all kinds of circuits. For example, in cases where only the steady-state response of the circuit is of interest, frequency-domain approaches are more efficient simulation methods comparing to time-domain integration methods. Furthermore, microwave circuits, that contain dispersive transmission-lines and transmission-lines discontinuity, cannot be easily handled in time-domain integration methods [10]. Time-domain integration methods are not the best choice for simulation of microwave circuits. Mildly nonlinear circuits are efficiently handled using Volterra analysis as described before. Since Volterra analysis can be done in

frequency-domain, transmission-lines can be easily handled in such simulators using their S- or Y-parameters. However, Volterra analysis faces problems when dealing with strongly nonlinear circuits. Harmonic Balance is a common frequency-domain method which handles strongly nonlinear circuits.

The first step in Harmonic Balance is grouping the circuit into two parts. Linear part, that contains the input sources and all the linear elements, and the nonlinear part, which contains only the nonlinear elements. The linear part of the circuit is solved efficiently in frequency-domain. The nonlinear part, on the other hand, is solved in the time-domain, so that it will be able to achieve good accuracy when dealing with strongly nonlinear circuits. When dealing with nonlinear microwave circuits, usually there are only a few nonlinear elements in the circuits, e.g. transistors, whereas in Radio-Frequency Integrated Circuits (RFIC) the number of nonlinear elements is more as compared to microwave circuits. Assuming there are N nonlinear elements in the circuit (e.g. in case of microwave Power Amplifier (PA) N is as low as one or two) the nonlinear circuit is redrawn as shown in Fig. 2.4.

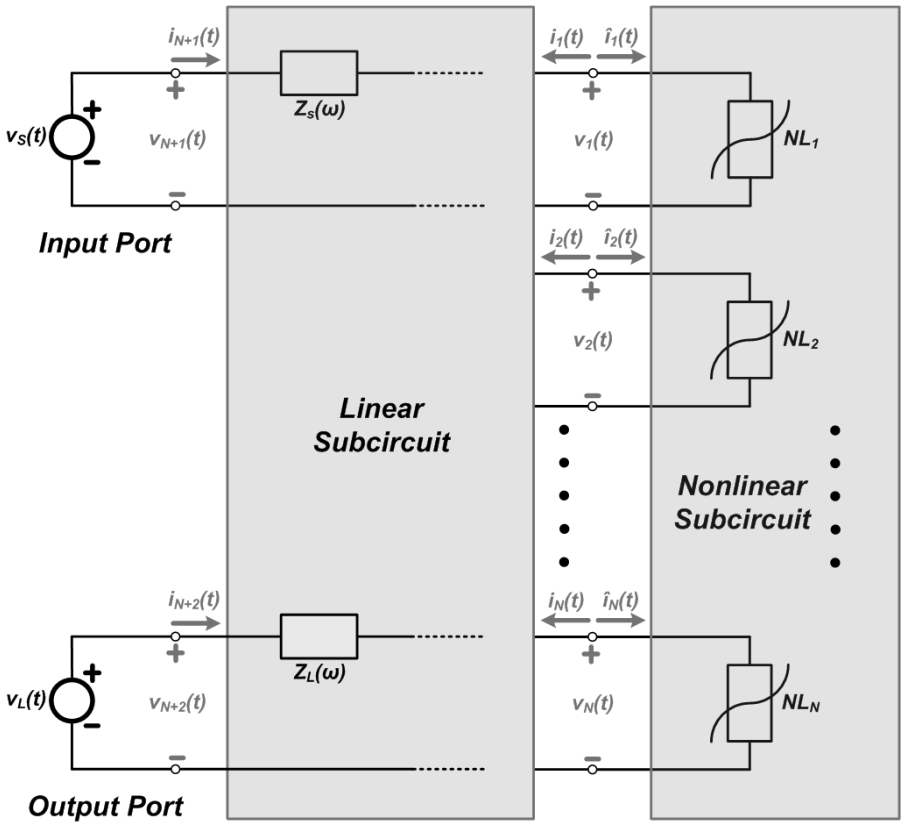

Fig. 2.4 - Nonlinear circuit divided into linear and nonlinear subcircuits for Harmonic Balance analysis

The linear part is described using admittance parameters (Y-parameters). Before proceeding further with solution of the circuit, let's assume the input of the circuit is a single-tone sinusoidal signal. Since the circuit is nonlinear, the steady-state response of the circuit will contain the excitation frequency and its harmonics. In theory, an infinite number of harmonics exist at the output. However, in practice, the first K harmonics can describe the output, and all the node voltages and branch current, with good accuracy [10]. K depends on the nonlinearity of the circuit as well as the input power. For mild to strong nonlinearities, a small number of harmonics, e.g. 5 harmonics, is usually sufficient, whereas when strongly nonlinear circuits require larger number of harmonics to achieve good accuracy. For single frequency at the input, knowing the magnitude and phase of the K harmonics of all voltages and currents, the time-domain solution of the circuit is found using the inverse Fourier transform,

$$v(t) = \sum_{n=-K}^{K} V_n e^{jn\omega_0 t} . \tag{2.25}$$

Thus, the solution of the circuit is now reduced to finding the magnitude and phase of the K harmonics for all voltages and currents. Using Kirchhoff's current law in the time-domain we have,

$$\begin{cases} i_1(t) + \hat{\imath}_1(t) = 0 \\ i_2(t) + \hat{\imath}_2(t) = 0 \\ \vdots \\ i_N(t) + \hat{\imath}_N(t) = 0 \end{cases} . \tag{2.26}$$

Taking the Fourier transform of (2.26), results in,

$$\begin{cases} I_{1,0} + \hat{I}_{1,0} = 0 \\ I_{1,1} + \hat{I}_{1,1} = 0 \\ \vdots \\ I_{1,K} + \hat{I}_{1,K} = 0 \\ I_{2,0} + \hat{I}_{2,0} = 0 \\ I_{2,1} + \hat{I}_{2,1} = 0 \\ \vdots \\ I_{2,K} + \hat{I}_{2,K} = 0 \\ \vdots \\ I_{N,K} + \hat{I}_{N,K} = 0 \end{cases} , \tag{2.27}$$

where $I_{n.k}$ represents the kth harmonic of the current $i_n(t)$ and similarly, $\hat{I}_{n.k}$ represent the kth harmonic of the current $\hat{\imath}_n(t)$. One can solve the linear part of the circuit using Y-parameters in frequency-domain. The linear analysis must be carried out at the excitation frequency, ω_0, and also, at the harmonics of the excitation frequency. The admittance equations for the linear part of the circuit at the excitation frequency is written as,

$$\begin{aligned}
I_{1,1} &= Y_{11}(\omega_0)V_{1,1} + Y_{12}(\omega_0)V_{2,1} + \cdots + Y_{1(N+2)}(\omega_0)V_{N+2,1} \\
I_{2,1} &= Y_{21}(\omega_0)V_{1,1} + Y_{22}(\omega_0)V_{2,1} + \cdots + Y_{2(N+2)}(\omega_0)V_{N+2,1} \\
&\vdots \\
I_{N,1} &= Y_{N1}(\omega_0)V_{1,1} + Y_{N2}(\omega_0)V_{2,1} + \cdots + Y_{N(N+2)}(\omega_0)V_{N+2,1} \\
I_{(N+1),1} &= Y_{(N+1)1}(\omega_0)V_{1,1} + Y_{(N+1)2}(\omega_0)V_{2,1} + \cdots + Y_{(N+1)(N+2)}(\omega_0)V_{N+2,1} \\
I_{(N+2),1} &= Y_{(N+2)1}(\omega_0)V_{1,1} + Y_{(N+2)2}(\omega_0)V_{2,1} + \cdots + Y_{(N+2)(N+2)}(\omega_0)V_{N+2,1},
\end{aligned} \tag{2.28}$$

where $V_{n.k}$ represent the kth harmonic of the voltage $v_n(t)$. Since we have an $(N+2)$ port network, the size of the admittance equations will be $(N+2) \times (N+2)$. Similarly, the admittance equations for the harmonics are written for the linear part of the circuit knowing the Y-parameters of the linear circuit at $2\omega_0$, $3\omega_0$, … and $K\omega_0$. Combining all the admittance equations in the matrix form we'll get,

$$\begin{bmatrix} I_1 \\ I_2 \\ \vdots \\ I_N \\ I_{N+1} \\ I_{N+2} \end{bmatrix} = \begin{bmatrix} Y_{1,1} & Y_{1,2} & \cdots & Y_{1,N} & Y_{1,(N+1)} & Y_{1,(N+2)} \\ Y_{2,1} & Y_{2,2} & & Y_{2,N} & Y_{2,(N+1)} & Y_{2,(N+2)} \\ \vdots & & \ddots & & \vdots & \\ Y_{N,1} & & & Y_{N,N} & Y_{N,(N+1)} & Y_{N,(N+2)} \\ Y_{(N+1),1} & \cdots & & Y_{(N+1),N} & Y_{(N+1),(N+1)} & Y_{(N+1),(N+2)} \\ Y_{(N+2),1} & & & Y_{(N+2),N} & Y_{(N+2),(N+1)} & Y_{(N+2),(N+2)} \end{bmatrix} \begin{bmatrix} V_1 \\ V_2 \\ \vdots \\ V_N \\ V_{N+1} \\ V_{N+2} \end{bmatrix}, \tag{2.29}$$

where,

$$I_n = \begin{bmatrix} I_{n,0} \\ I_{n,1} \\ I_{n,2} \\ \vdots \\ I_{n,K} \end{bmatrix} \quad \text{and} \quad V_n = \begin{bmatrix} V_{n,0} \\ V_{n,1} \\ V_{n,2} \\ \vdots \\ V_{n,K} \end{bmatrix}, \tag{2.30}$$

and,

$$Y_{m,n} = \begin{bmatrix} Y_{mn}(0) & 0 & \cdots & 0 \\ 0 & Y_{mn}(\omega_0) & & 0 \\ \vdots & & \ddots & \vdots \\ 0 & 0 & \cdots & Y_{mn}(K\omega_0) \end{bmatrix}. \tag{2.31}$$

It can be seen that the size of the complete admittance equations is $(K+1)(N+2) \times (K+1)(N+2)$. When solving the circuit, all the voltages and currents, except V_{N+1} and V_{N+2}, are unknown. Also, I_{N+1} and I_{N+2}, are not of interest. Thus, taking out I_{N+1}, I_{N+2}, V_{N+1} and V_{N+2} from the unknown vector, we'll get,

$$I = \begin{bmatrix} I_1 \\ I_2 \\ \vdots \\ I_N \end{bmatrix} = \begin{bmatrix} Y_{1,(N+1)} & Y_{1,(N+2)} \\ Y_{2,(N+2)} & Y_{2,(N+2)} \\ \vdots & \vdots \\ Y_{N,(N+1)} & Y_{N,(N+2)} \end{bmatrix} \begin{bmatrix} V_{N+1} \\ V_{N+2} \end{bmatrix} + \begin{bmatrix} Y_{1,1} & Y_{1,2} & \cdots & Y_{1,N} \\ Y_{2,1} & Y_{2,2} & & Y_{2,N} \\ \vdots & & \ddots & \vdots \\ Y_{N,1} & Y_{N,2} & \cdots & Y_{N,N} \end{bmatrix} \begin{bmatrix} V_1 \\ V_2 \\ \vdots \\ V_N \end{bmatrix}, \tag{2.32}$$

$$\rightarrow I = I_S + Y_{N\times N} V,$$

where I_S is the known vector due to the input sources at port $N+1$ and $N+2$. Replacing (2.32) in (2.27), results in,

$$I + \hat{I}(Nonlinear) = I_S + Y_{N\times N} V + \hat{I}(Nonlinear) = 0, \tag{2.33}$$

where $\hat{I}(Nonlinear)$ is the current of the nonlinear elements. The next step is to calculate $\hat{I}(Nonlinear)$ as a function of the unknown vector, V. In order to be able to handle strong nonlinearities, the nonlinear section of the circuit is solved in time-domain. Nonlinear resistors, conductances and controlled sources are characterized by their current-voltage relation, i.e.,

$$i_{g,n}(t) = f_n\big(v_1(t), v_2(t), \cdots, v_N(t)\big). \tag{2.34}$$

Taking the Fourier Transform of $i_{g,n}(t)$, part of the $\hat{I}(Nonlinear)$ vector that is due to nonlinear conductance and controlled sources is calculated as,

$$I_G = \begin{bmatrix} I_{G1} \\ I_{G2} \\ \vdots \\ I_{GN} \end{bmatrix} = \mathcal{F} \begin{bmatrix} i_{g,1}(t) \\ i_{g,2}(t) \\ \vdots \\ i_{g,N}(t) \end{bmatrix} = \mathcal{F} \begin{bmatrix} f_1(v_1(t), v_2(t), \cdots, v_N(t)) \\ f_2(v_1(t), v_2(t), \cdots, v_N(t)) \\ \vdots \\ f_N(v_1(t), v_2(t), \cdots, v_N(t)) \end{bmatrix}. \tag{2.35}$$

Nonlinear capacitors are characterized by their charge-voltage relation, i.e.,

$$\begin{gathered} q_{c,n}(t) = f_{qn}\big(v_1(t), v_2(t), \cdots, v_N(t)\big), \\ \rightarrow i_{c,n}(t) = dq_{c,n}(t)/dt. \end{gathered} \tag{2.36}$$

Similarly, taking the Fourier transform of the charge in (2.36) and then taking the first derivative of charge to get the current, we'll get,

$$\begin{gathered} Q = \begin{bmatrix} Q_1 \\ Q_2 \\ \vdots \\ Q_N \end{bmatrix} = \mathcal{F} \begin{bmatrix} q_{c,1}(t) \\ q_{c,2}(t) \\ \vdots \\ q_{c,N}(t) \end{bmatrix} = \mathcal{F} \begin{bmatrix} f_{q1}(v_1(t), v_2(t), \cdots, v_N(t)) \\ f_{q2}(v_1(t), v_2(t), \cdots, v_N(t)) \\ \vdots \\ f_{qN}(v_1(t), v_2(t), \cdots, v_N(t)) \end{bmatrix}, \\ \rightarrow I_C = j\Omega Q, \end{gathered} \tag{2.37}$$

where I_C is the part of nonlinear current due to nonlinear capacitors and,

$$\Omega = \begin{bmatrix} \Omega_0 & 0 & \cdots & 0 & 0 \\ 0 & \Omega_0 & & 0 & 0 \\ \vdots & & \ddots & \vdots & \\ 0 & 0 & & \Omega_0 & 0 \\ 0 & 0 & \cdots & 0 & \Omega_0 \end{bmatrix}, \tag{2.38}$$

$$\Omega_0 = \begin{bmatrix} 0 & 0 & \cdots & 0 \\ 0 & \omega_0 & & 0 \\ \vdots & & \ddots & \vdots \\ 0 & 0 & \cdots & K\omega_0 \end{bmatrix}.$$

Replacing I_G and I_C in (2.33), results in,

$$F(V) = I_S + Y_{N\times N}V + I_G + I_C = 0. \tag{2.39}$$

Finally, the last step in Harmonic Balance is to solve (2.39) for the unknown vector V, called Harmonic Balance equation [10]. However, I_G and I_C are both nonlinear functions of the unknown vector V, which results in a nonlinear function $F(V)$. Solving (2.39) requires iterative methods, for example Newton-Raphson algorithm. Newton-Raphson algorithm starts with an initial guess of the solution, and then corrects the initial guess in the next iterations based on the first derivative of the nonlinear function with respect to all parameters (the Jacobian matrix) [1]. The Jacobian matrix for the Harmonic Balance equation is found as,

$$M(V) = \frac{\partial F(V)}{\partial V} = Y_{N\times N} + \frac{\partial I_G}{\partial V} + \frac{\partial I_C}{\partial V} = Y_{N\times N} + \frac{\partial I_G}{\partial V} + j\Omega\frac{\partial Q}{\partial V}. \tag{2.40}$$

Also, the next iteration value, V^{i+1}, is found using,

$$\left.\frac{\partial F(V)}{\partial V}\right|_{V=V^i}\left(V^{i+1} - V^i\right) = -F\left(V^i\right). \tag{2.41}$$

Calculating the Jacobian matrix requires the first derivative of all the nonlinear elements which is complex and time-consuming (especially when a close-form expression for nonlinearities is not available). Furthermore, solving (2.41) requires considerable memory and computation when dealing with large and/or strongly nonlinear circuits. The reader is referred to [10] for the details of the method. The steps required to solve the Harmonic Balance equation are,

- Start with an initial guess for the time-domain unknown vector $v(t)$ and then take its Fourier Transform to obtain V^0. If the initial guess is not close enough to the final solution, the algorithm faces convergence issues [10].
- Find the time-domain current of nonlinear resistors and controlled sources, and the charge of the nonlinear capacitors based on the initial guess, $v^0(t)$. Then, take the Fourier transform of the currents and charges to find with I_G and I_C matrices.

- Calculate the Harmonic Balance equation, $F(V^0) = I_S + Y_{N\times N}V^0 + I_G + I_C$.
- Calculate the Jacobian matrix using (2.40).
- Calculate the next iteration value, V^{i+1}, using (2.41).
- Using the new value of V^{i+1}, calculate the Harmonic Balance equation, $F\left(V^{i+1}\right)$.
- If the error of "all" the unknowns in $F\left(V^{i+1}\right)$ are small enough, the solution has been found. Otherwise, use the inverse Fourier transform to find $v^{i+1}(t)$ and go back to the second step.

Note that, Harmonic Balance requires one Fourier Transform and Inverse Fourier Transform, calculating Jacobian matrix and solving (2.41) per iteration. As the size of matrices increases, (due to larger circuits and/or stronger nonlinearities), computation cost increases significantly [10]. The method described here deals with the case where inputs contain a single tone. However, in practical situations, it is necessary to simulate circuits with multiple tones at input. When dealing with multiple tones, not only the harmonics of the input frequencies exist at the output, also, the inter-modulation products of the input frequencies should be taken into account. This increases the size of matrices significantly, especially for strongly nonlinear circuits. For example, in case of two-tone excitation (ω_1 and ω_2) the frequencies need to be taken into account at the output are,

$$\omega_k = m\omega_1 + n\omega_2\,, \qquad m,n = \cdots,-2,-1,0,+1,+2,\cdots \tag{2.42}$$

The only difference in the Harmonic Balance analysis for multi-tone inputs is larger matrices. Also, since the input tones to the circuit are usually non-commensurate, the voltages and currents are not periodic, which requires generation of "almost-periodic" Fourier transform. The associated problems and algorithms regarding this issue are beyond the scope of this chapter and the reader is referred to [10] for a detailed discussion of this problem.

Chapter 3
Time-Varying Volterra Analysis: Time-Domain Approach

In this chapter, a new time-domain method to simulate nonlinear circuits is proposed. The method is a modification of the conventional Volterra analysis, which enables it to simulate nonlinear circuits more accurately. Conventional Volterra analysis is not accurate enough when analyzing strongly nonlinear circuits, as discussed in chapter 2. The Taylor series truncation error and its limited convergence radius are the two main sources of these issues. The proposed method changes the Taylor expansion point as the signal varies, i.e. a time-varying expansion waveform. Hence, the truncation error of the Taylor series will be reduced, and the convergence issue of Taylor expansion will be solved. The details of the proposed method are discussed in this chapter. The method is particularly useful when sinusoidal waveforms are used and frequency-domain analysis is possible. Details of the method in frequency-domain will be discussed in the next chapter. The concept of time-varying Volterra analysis has been proposed in the literature before [20], [21]. However, all the methods are either applicable for one specific circuit, e.g. mixers, or should be used with another simulation method, e.g. Harmonic Balance. For example, in [20] the application of time-varying Volterra for analysis of a FET mixer is discussed. The mixer is first analyzed using Harmonic Balance with the presence of the larger input, i.e. local oscillator input. Then using the result of Harmonic Balance as the expansion point for the nonlinear elements, Volterra analysis is applied to solve the circuit. This method is only applicable for mixers where one of the inputs is much larger than other inputs. Also, the method requires Harmonic Balance analysis to be done first, thus, increasing the computation cost of the method.

The rest of this chapter is organized as follows. Section 3.1 describes the proposed method, gives its properties and compares it with the other time-domain simulation methods. Section 3.2 presents the application of the proposed method to simulate nonlinear RC circuits. Three different cases of nonlinear RC circuits are simulated using the proposed method and conventional time-domain approaches. Section 3.3 discusses the effect of pre-analysis on the proposed method in more detail. Generalization of the proposed method for multi-dimensional nonlinearities is presented in section 3.4. In section 3.5 a modification of the time-varying Volterra will be presented that achieves better computation efficiency comparing to time-varying Volterra. The advantages and shortcomings of the proposed method are summarized in section 3.6.

3.1 Method Description

The conventional Volterra analysis uses a truncated Taylor series to express the behavior of the nonlinear elements of the circuit. Usually the quiescent voltages/currents (DC) of the nonlinear devices are used as

the expansion point of the Taylor series [4]. The 3rd order truncated Taylor series of a nonlinear resistor is written as,

$$v_R(t) \cong V_0 + R_1(i_R(t) - I_0) + R_2(i_R(t) - I_0)^2 + R_3(i_R(t) - I_0)^3, \tag{3.1}$$

where $V_0 = f(I_0)$, which is a DC value, is the expansion point of the Taylor series. In order to clarify that usually both current and voltage of the resistor are time-dependent, $i_R(t)$ and $v_R(t)$ are used in (3.1). The truncation error of the series is approximated by, $\varepsilon_{truncation} \cong R_4(i_R(t) - I_0)^4$ [11]. As the input signal gets larger, the current and voltage of the resistor, $i_R(t)$ and $v_R(t)$, will deviate more from the expansion point, I_0 and V_0. In other words, $|i_R(t) - I_0|$ becomes larger as the input gets stronger, which results in larger truncation error. The truncation error can be reduced by either reducing R_4 or $|i_R(t) - I_0|$. The first method is presented in [8]. Knowing that a truncated Chebyshev series is the best n^{th} order polynomial approximation of a function, Chebyshev series is applied to model nonlinearities in [8]. Employing Chebyshev series will not only reduce the truncation error of the expansion, thus increasing the accuracy of the Volterra analysis, but also solves the convergence issue of Taylor series as discussed in [8]. The second method, is reducing $|i_R(t) - I_0|$. In order to lower truncation error, one must reduce $|i_R(t) - I_0|$ at all times. Using a time-varying expansion point for Taylor series, $v_0(t) = f\big(i_0(t)\big)$, we are able to reduce the truncation error compared to Taylor series with a fixed expansion point. As long as the time-varying expansion point is chosen in a way so that $\|i_R(t) - i_0(t)\| < \|i_R(t) - I_0\|$, the accuracy of the expansion will improve. Using this method, the 3rd order truncated Taylor series is written as,

$$v_R \cong v_0(t) + R_1(t)\big(i_R - i_0(t)\big) + R_2(t)\big(i_R - i_0(t)\big)^2 + R_3(t)\big(i_R - i_0(t)\big)^3. \tag{3.2}$$

Since a time-varying expansion point is used, the resistor coefficients, i.e. R_1, R_2, R_3,…, are also time dependent, and defined as,

$$\begin{aligned} R_1(t) &= \frac{df}{di_R}\bigg|_{i_R = i_0(t)} \\ R_2(t) &= \frac{1}{2!}\frac{d^2f}{di_R^2}\bigg|_{i_R = i_0(t)} \\ R_3(t) &= \frac{1}{3!}\frac{d^3f}{di_R^3}\bigg|_{i_R = i_0(t)} \\ &\vdots \end{aligned} \tag{3.3}$$

Schetzen's multi-linear method can now be applied for the nonlinear element described using (3.2). Rewriting (3.2), we get,

$$v_R(t) - V_0(t) = \hat{v}(t) = R_1(t)\hat{\imath}(t) + R_2(t)\hat{\imath}(t)^2 + R_3(t)\hat{\imath}(t)^3 + \cdots. \tag{3.4}$$

where $\hat{\imath}(t) = i_R(t) - i_0(t)$ and $\hat{v}(t) = v_R(t) - v_0(t)$. The Nonlinear resistor can be modeled with two independent sources, $v_0(t)$ and $i_0(t)$ (which are time-dependent), and a nonlinear element with the characteristic function,

$$\hat{v}(t) = \sum_{n=1}^{\infty} R_n(t)\hat{\imath}(t)^n, \tag{3.5}$$

as shown in Fig. 3.1.

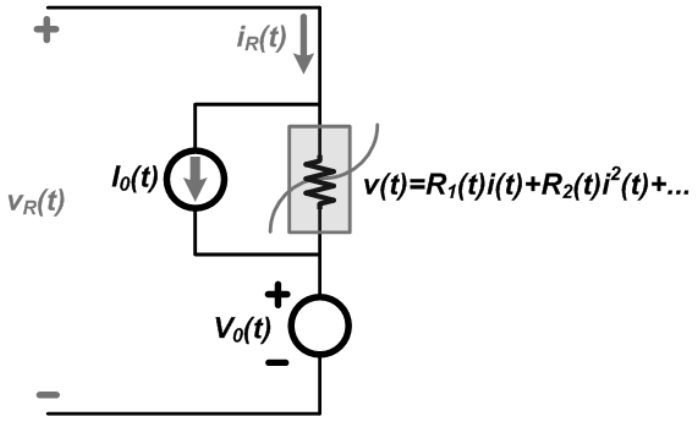

Fig. 3.1 - Equivalent model for the nonlinear resistor with time-varying expansion point

The time-varying sources $v_0(t)$ and $i_0(t)$ appear in the right-hand side of the formulation equations, so we can remove them from the model and concentrate on the nonlinear part. Breaking up the complete response into response of different orders, as done in conventional Schetzen's method, results in,

$$\hat{v}(t) = \sum_{n=1}^{\infty} \hat{v}_n(t) \quad and \quad \hat{\imath}(t) = \sum_{n=1}^{\infty} \hat{\imath}_n(t). \tag{3.6}$$

Replacing (3.6) in (3.5) and equating terms of different orders on both sides, the response of different orders is found as,

$$\hat{v}_1(t) = R_1(t)\hat{\imath}_1(t)$$

$$\hat{v}_2(t) = R_1(t)\hat{\imath}_2(t) + R_1(t)\hat{\imath}_1(t)^2$$

$$\hat{v}_3(t) = R_1(t)\hat{\imath}_3(t) + 2R_1(t)R_2(t)\hat{\imath}_1(t)\hat{\imath}_2(t) + R_1(t)\hat{\imath}_1(t)^3 \quad (3.7)$$

$$\vdots$$

The response of each order contains a linear, but time-varying, part ($\hat{v}_n(linear) = R_1(t)\hat{\imath}_n(t)$) and a nonlinear time-varying part which depends only on the response of the circuit of lower orders ($\hat{v}_n(nonlinear) = f\big(\hat{\imath}_1(t), \hat{\imath}_2(t), \cdots, \hat{\imath}_{n-1}(t)\big)$). The response of each order is modeled using a linear time-varying resistor, $R_1(t)$, and a dependent source, $e_n(t) = f\big(\hat{\imath}_1(t), \hat{\imath}_2(t), \cdots, \hat{\imath}_{n-1}(t)\big)$, as shown in Fig. 3.2. Since the dependent source, $e_n(t)$, depends upon the response of lower order circuits, it will appear on the right-hand side of the formulation for each order.

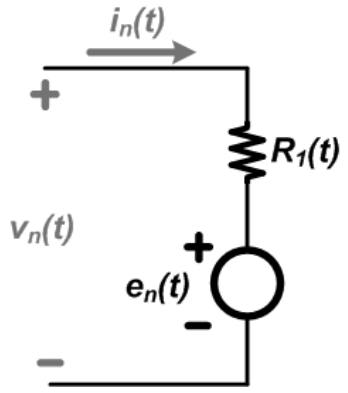

Fig. 3.2 - Nth order time-varying Volterra equivalent model for the nonlinear resistor

Generalizing the derivations above similar models is created for nonlinear capacitors, inductors and dependent sources. Fig. 3.3 summarizes the Volterra models of different orders for nonlinear elements.

There are two issues regarding the time-varying expansion point. First, how can one find $I_0(t)$ for any given circuit? Secondly, how close the time-varying expansion point, $I_0(t)$, should be to the exact

response of the circuit, $i_R(t)$? $I_0(t)$ is chosen to get an acceptable truncation error at all times, i.e. for a 3rd order truncated Taylor series we have,

$$\max\left\{\left|\frac{\varepsilon_{truncation}}{v_R(t)}\right|\right\} \cong max\left\{\left|\frac{R_4(t)\left(i_R(t)-i_0(t)\right)^4}{v_R(t)}\right|\right\} < \varepsilon_{max}, \tag{3.8}$$

where ε_{max} is the maximum acceptable error. It should be noted, $\varepsilon_{truncation}$ is the error only due to truncation. The total simulation error is the truncation error plus the error of transient simulation. Since the simulation accuracy is limited by the truncation error, the truncation error is a critical and important parameter. The time-varying expansion point for all the nonlinear devices is found with the aid of a preliminary simulation of the circuit, called *pre-analysis*. Unless very strongly nonlinear circuits are considered, the pre-analysis does not need to be very accurate. It will be shown with the aid of a simple numerical example that simulation of the linearized circuit, called linear pre-analysis, is sufficient to find the time-varying expansion points for all the nonlinear devices. It can be easily seen that more accurate pre-analysis results in better accuracy for the truncated Taylor series and Volterra analysis.

The derivations in equations (3.4) to (3.7) using time-varying expansion point is an extension of the Schetzen's original work in [4]. The model contains a time-varying resistor, which is the main difference between this method and conventional Volterra analysis. When using time-varying expansion point, a linear time-varying circuit must be analyzed in each order of Volterra analysis. Linear time-varying circuits are more expensive to analyze compared to linear time-invariant circuits. The simulation of the time-varying Volterra circuits will be discussed in more detail in section 3.2. In summary the steps required for time-varying Volterra analysis are,

- Pre-analysis: Simulate the linearized circuit, i.e. linear pre-analysis, to find time-varying expansion point for all nonlinear elements.
- Based on the expansion point, calculate time-varying nonlinear coefficients for all nonlinear elements.
- Solve the time-varying Volterra circuits of different orders sequentially using the proper numerical integration method.
- Finally, add the response of different orders to get the complete solution.

The advantages and limitations of the proposed method are discussed in the next section with the aid of a numerical example.

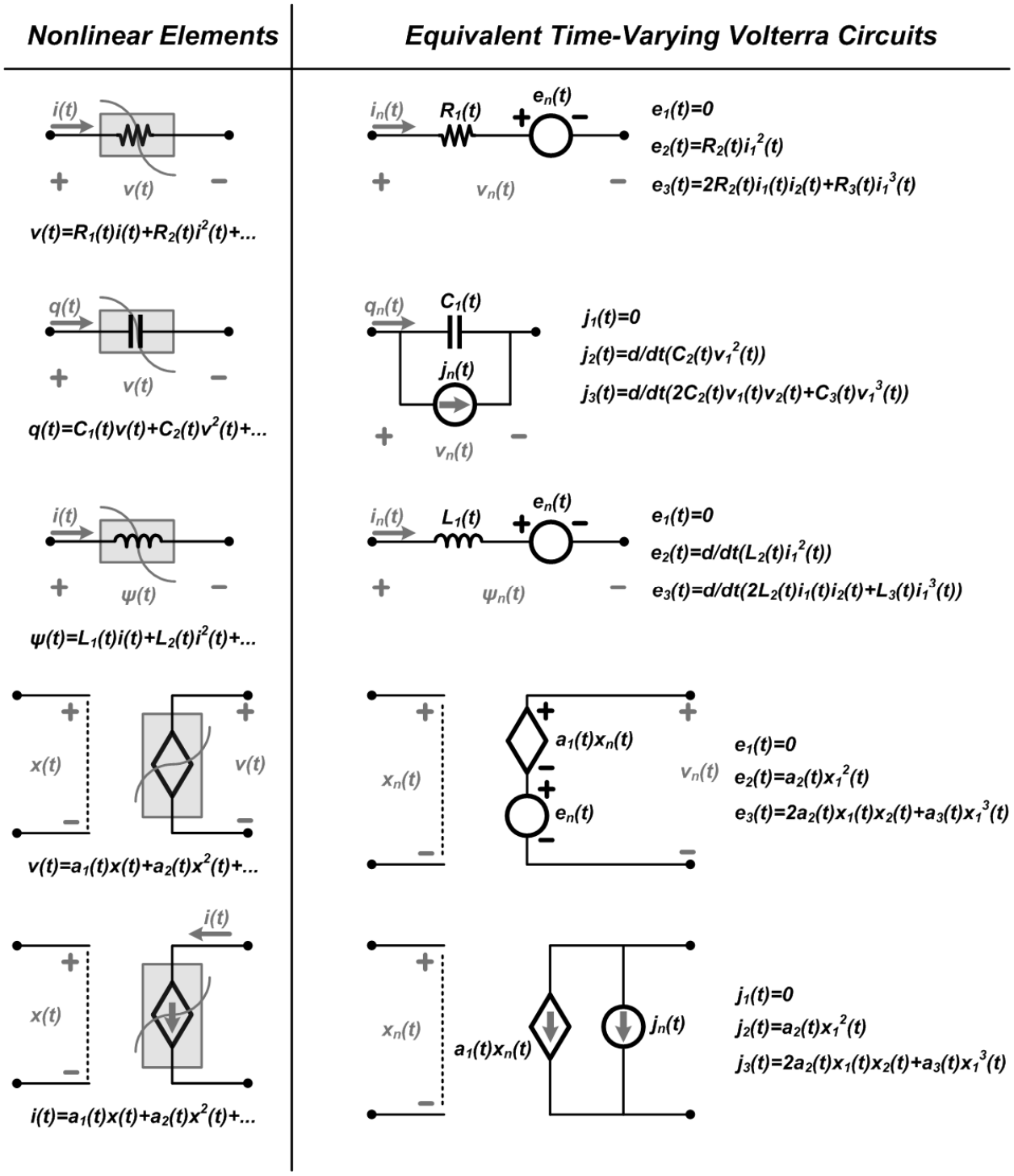

Fig. 3.3 - Nonlinear elements and their time-varying Volterra circuits

3.2 Numerical Example

In order to show the effectiveness of the method, a nonlinear RC circuit is simulated using the time-varying Volterra analysis. Furthermore, a comparison between the 3rd order time-varying Volterra, 3rd order and 5th order conventional Volterra and Newton-Raphson numerical integration is carried out in this section. The test circuit contains an input voltage source, nonlinear resistor and a linear capacitor as shown in Fig.3.4. It has been assumed that the nonlinearity of the resistor is modeled using a 3rd order polynomial. However, the results can be simply generalized for higher order nonlinearities and other nonlinear elements.

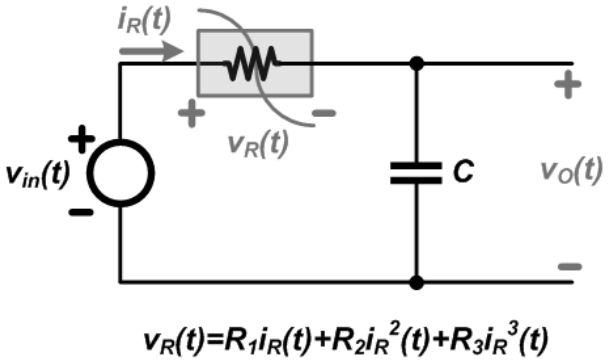

Fig. 3.4 - Nonlinear RC test circuit

First we analyze the circuit using conventional Volterra analysis. The circuit is broken into circuit of different orders, as shown in Fig. 3.5. It is assumed that DC of the input signal is zero, thus, DC operating point of the nonlinear resistor is zero. The circuits is formulated using MNA as,

$$GX_n(t) + C\frac{dX_n(t)}{dt} = W_n(t), \tag{3.9}$$

where,

$$G = \begin{bmatrix} 0 & 0 & 0 & 1 & 1 \\ 0 & 0 & 0 & -1 & 0 \\ 1 & 0 & 0 & 0 & 0 \\ 1 & -1 & 0 & 0 & 0 \\ 0 & 1 & -1 & 0 & -R_1 \end{bmatrix}, \tag{3.10}$$

$$C = \begin{bmatrix} 0 & 0 & 0 & 0 & 0 \\ 0 & 0 & C_0 & 0 & 0 \\ 0 & 0 & 0 & 0 & 0 \\ 0 & 0 & 0 & 0 & 0 \\ 0 & 0 & 0 & 0 & 0 \end{bmatrix},$$

and,

$$\begin{aligned} W_1(t) &= [0 \quad 0 \quad v_{in}(t) \quad 0 \quad 0]^T, \\ W_2(t) &= [0 \quad 0 \quad 0 \quad e_2(t) \quad 0]^T, \\ &\vdots \\ W_5(t) &= [0 \quad 0 \quad 0 \quad e_5(t) \quad 0]^T. \end{aligned} \tag{3.11}$$

Using the 2nd order BDF the circuits are solved as (with constant step-size) [1],

$$\left(G + \frac{3}{2h}C\right) X_n(t_{k+2}) = W_n(t_{k+2}) + \frac{2}{h}CX_n(t_{k+1}) - \frac{1}{2h}CX_n(t_k), \tag{3.12}$$

where $h = t_{k+2} - t_{k+1}$, is the simulation step-size. Solving (3.12) requires LU factorization of $T = G + (3/2h)C$ matrix once, and forward/backward substitution for each time-step. Finally, the total response is calculated as, $X(t) = X_1(t) + X_2(t) + X_3(t) + X_4(t) + X_5(t)$, for 5th order conventional Volterra. For 3rd order conventional Volterra, the 4th and 5th order simulation results are not considered.

The circuit is also simulated using 3rd order time-varying Volterra with linear pre-analysis. The first step is the linear pre-analysis. Linearizing the circuit around the DC operating point, i.e. $i_{R-DC} = 0$, the circuit is reduced to the 1st order conventional Volterra circuit. The linearized circuit is simulated using the same 2nd order BDF formulae described before. Using the result of pre-analysis for the current of the resistor, i.e. $i_{R-PE}(t)$, the 3rd order truncated time-varying expansion of the nonlinear resistor is found as,

$$\begin{aligned} v_R(t) \cong\ & f\big(i_{R-PE}(t)\big) + \hat{R}_1(t)\big(i_R(t) - i_{R-PE}(t)\big) \\ & + \hat{R}_2(t)\big(i_R(t) - i_{R-PE}(t)\big)^2 + \hat{R}_3(t)\big(i_R(t) - i_{R-PE}(t)\big)^3, \end{aligned} \tag{3.13}$$

where,

$$f\left(i_{R-PE}(t)\right) = R_1 i_{R-PE}(t) + R_2 i_{R-PE}^2(t) + R_3 i_{R-PE}^3(t),$$

$$\hat{R}_1(t) = \frac{df}{di_R}\bigg|_{i_R = i_{R-PE}(t)} = R_1 + 2R_2 i_{R-PE}(t) + 3R_3 i_{R-PE}^2(t),$$

(3.14)

$$\hat{R}_2(t) = \frac{1}{2!}\frac{d^2 f}{di_R^2}\bigg|_{i_R = i_{R-PE}(t)} = R_2 + 3R_3 i_{R-PE}(t),$$

$$\hat{R}_3(t) = \frac{1}{3!}\frac{d^3 f}{di_R^3}\bigg|_{i_R = i_{R-PE}(t)} = R_3.$$

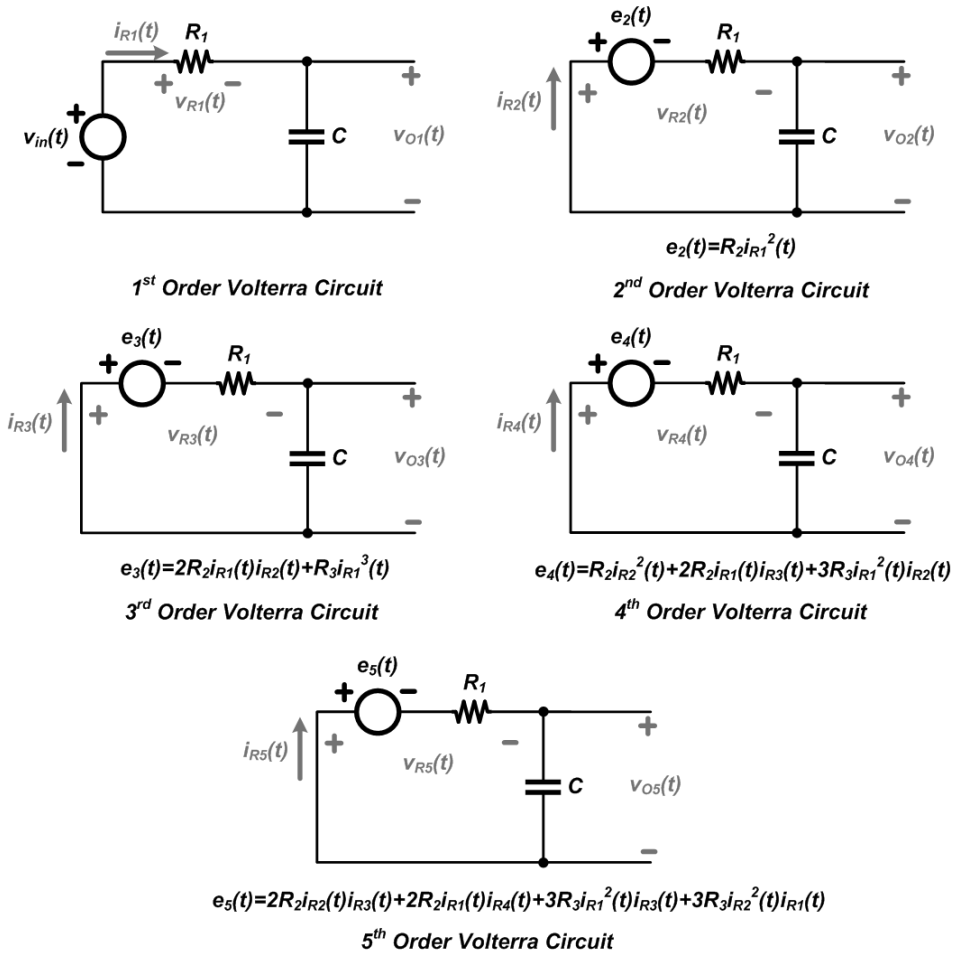

Fig. 3.5 - Volterra circuits for different orders

Using (3.13) the 1st, 2nd and 3rd order time-varying Volterra circuits are constructed as shown in Fig. 3.6. All the circuits contain linear time-varying resistors, while the rest of the circuit is similar to the conventional Volterra circuits.

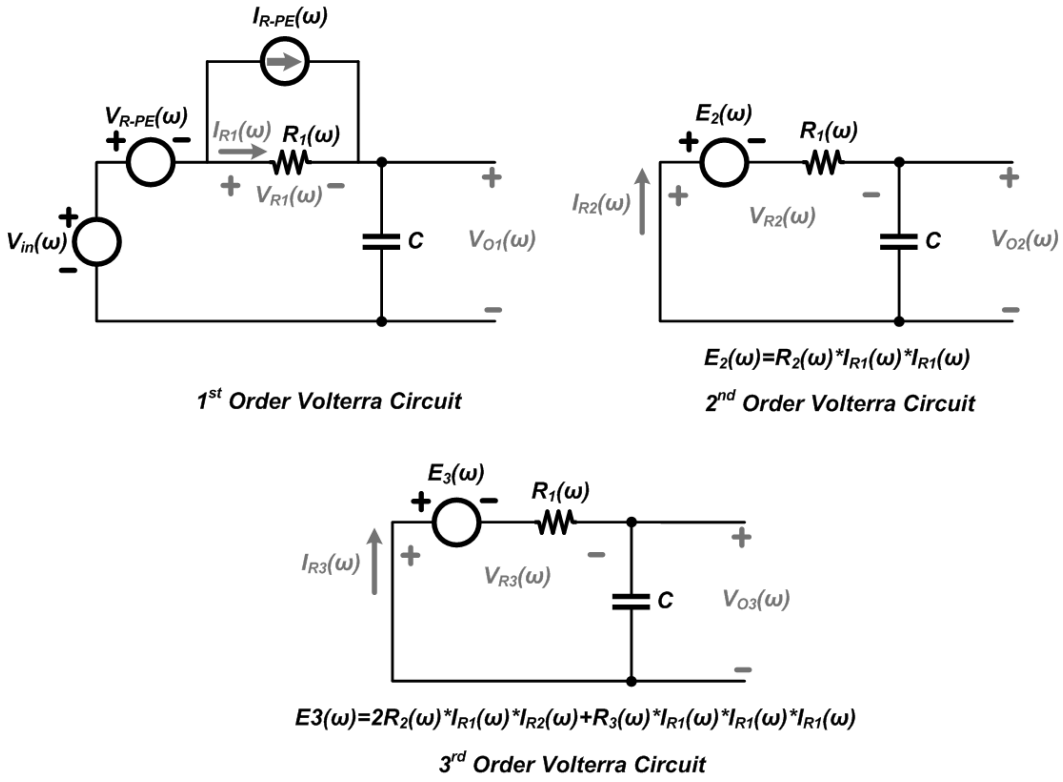

Fig. 3.6 – Time-Varying Volterra circuits for different orders

Similarly, the time-varying Volterra circuits are formulated as,

$$\hat{G}(t)X_n(t) + \hat{C}\frac{dX_n(t)}{dt} = \widehat{W}_n(t), \tag{3.15}$$

where,

$$\hat{G}(t)=\begin{bmatrix} 0 & 0 & 0 & 1 & 1 \\ 0 & 0 & 0 & -1 & 0 \\ 1 & 0 & 0 & 0 & 0 \\ 1 & -1 & 0 & 0 & 0 \\ 0 & 1 & -1 & 0 & -\hat{R}_1(t) \end{bmatrix},$$

$$\hat{C}=\begin{bmatrix} 0 & 0 & 0 & 0 & 0 \\ 0 & 0 & C_0 & 0 & 0 \\ 0 & 0 & 0 & 0 & 0 \\ 0 & 0 & 0 & 0 & 0 \\ 0 & 0 & 0 & 0 & 0 \end{bmatrix},$$

(3.16)

and,

$$\begin{aligned} \widehat{W}_1(t) &= \begin{bmatrix} i_{R-PE}(t) & -i_{R-PE}(t) & v_{in}(t) & f\big(i_{R-PE}(t)\big) & 0 \end{bmatrix}^T, \\ \widehat{W}_2(t) &= [0 \quad 0 \quad 0 \quad e_2(t) \quad 0]^T, \\ \widehat{W}_3(t) &= [0 \quad 0 \quad 0 \quad e_3(t) \quad 0]^T. \end{aligned}$$

(3.17)

Solving the circuits using 2nd order BDF, we have (with constant step-size),

$$\left(\hat{G}(t_{k+2})+\frac{3}{2h}\hat{C}\right)X_n(t_{k+2})=\widehat{W}_n(t_{k+2})+\frac{2}{h}\hat{C}X_n(t_{k+1})-\frac{1}{2h}\hat{C}X_n(t_k),$$

(3.18)

where $h=t_{k+2}-t_{k+1}$, is the simulation step-size. Solving (3.18) requires LU factorization of $T(t)=\hat{G}(t)+(3/2h)\hat{C}$ and forward/backward substitution for each time-step. The total response is calculated as, $X(t)=X_1(t)+X_2(t)+X_3(t)$.

For the purpose of comparison, 3 different cases of nonlinearities for the resistor will be examined in this section. First, a mildly nonlinear resistor is taken into account, i.e. $R_2, R_3 \ll R_1$. As it will be shown, both time-varying Volterra and conventional Volterra analysis are capable of simulating such circuits. However, time-varying Volterra (with linear pre-analysis) gives better accuracy comparing to conventional Volterra. For the second and third cases stronger nonlinear resistor is considered. In these cases the coefficients R_2 and R_3 are comparable to, or larger than R_1. Conventional Volterra series cannot simulate the circuit, whereas, time-varying Volterra manages to simulate the circuit with good accuracy.

3.2.1 Case I

First case deals with a mildly nonlinear resistor. The input of the circuit is a sinusoidal voltage with a unity frequency and amplitude, i.e. $v_{in}(t) = \sin(2\pi t)$. The circuit parameters along with transient simulation parameters are summarized in Table 3.1.

Table 3.1 – Specifications of the test circuit and simulation parameters for Case I

Parameter	Value
Input Frequency, f_{in} (Hz)	1
Input Amplitude, A_{in} (Volts)	1
Resistor Parameters, R_1, R_2, R_3	$1, 0.05, 0.05$
Capacitor Values (F)	1
Simulation Step-Size, h (sec)	5×10^{-4}
Simulation Stop-Time (sec)	10

The circuit is simulated using 3rd and 5th order conventional Volterra and 3rd order time-varying Volterra (with linear pre-analysis). In order to be able to compare the accuracy of the results, the circuit is also simulated using ELDO® [12], an all purpose circuit simulator. ELDO® uses Gear2 numerical integration method with Newton-Raphson iterations. Variable step-size control algorithm is incorporated in the ELDO® software to ensure a good simulation accuracy at all times [12]. Fig. 3.7 shows the output voltage of the 3rd order time-varying Volterra analysis, 3rd and 5th order conventional Volterra as well as ELDO® simulation results. The results of all the methods are in good agreement with ELDO® simulation results. The absolute error of the 3rd order time-varying Volterra and 3rd and 5th order conventional Volterra simulation results are also shown in Fig. 3.8 to Fig. 3.10. The absolute error of the 3rd order time-varying Volterra is 3 orders of magnitude lower than the 3rd order conventional Volterra. Even when conventional Volterra with higher order is used, i.e. 5th order, the absolute error is 2 orders of magnitude higher than 3rd order time-varying Volterra (with linear pre-analysis). Better accuracy for time-varying Volterra is due to time-varying expansion point for nonlinear resistor. 3rd and 5th order conventional Volterra analysis use $i_{R-DC} = 0$ as the expansion point, whereas time-varying Volterra uses the result of the simulation of linearized circuit as the expansion point.

One can increase the order of conventional Volterra further to achieve the same accuracy as 3rd time-varying Volterra analysis. However, as the order of Volterra increases the complexity of the Volterra circuit increases exponentially making the analysis too complicated and impractical. Furthermore, in

order to ensure that the absolute error is not due to transient numerical integration and only Volterra analysis, the simulations were repeated for smaller transient step-sizes. The absolute error remained constant which shows that the error is dominated by the Volterra analysis error.

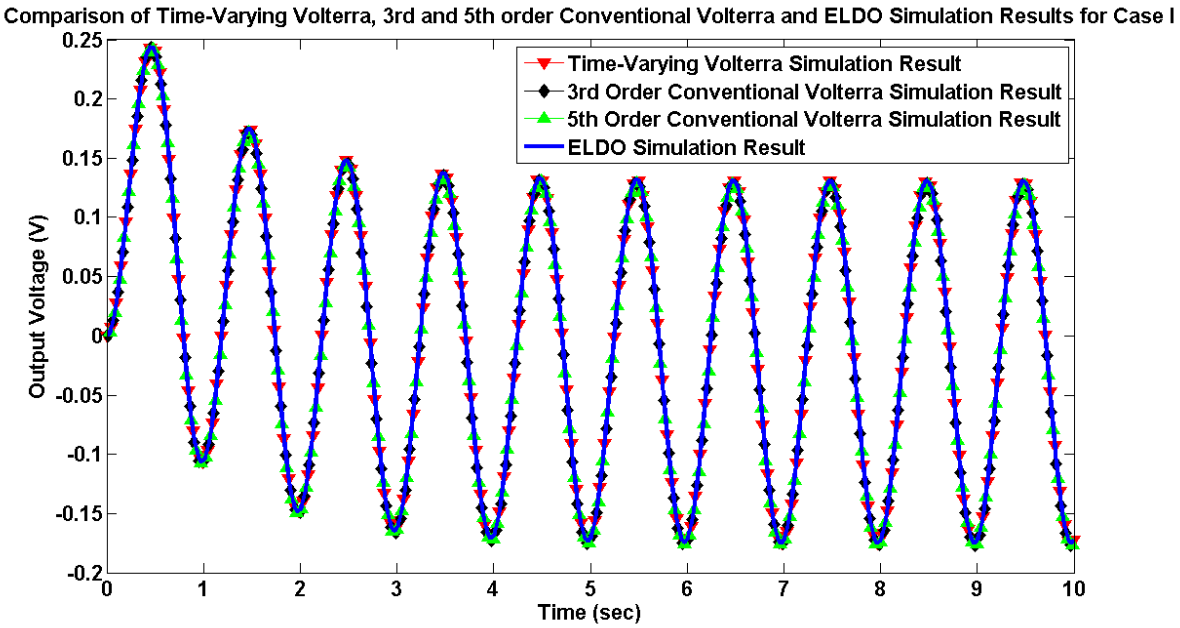

Fig. 3.7 – Output Voltage using 3rd order Time-Varying Volterra, 3rd and 5th order conventional Volterra and ELDO® for Case I

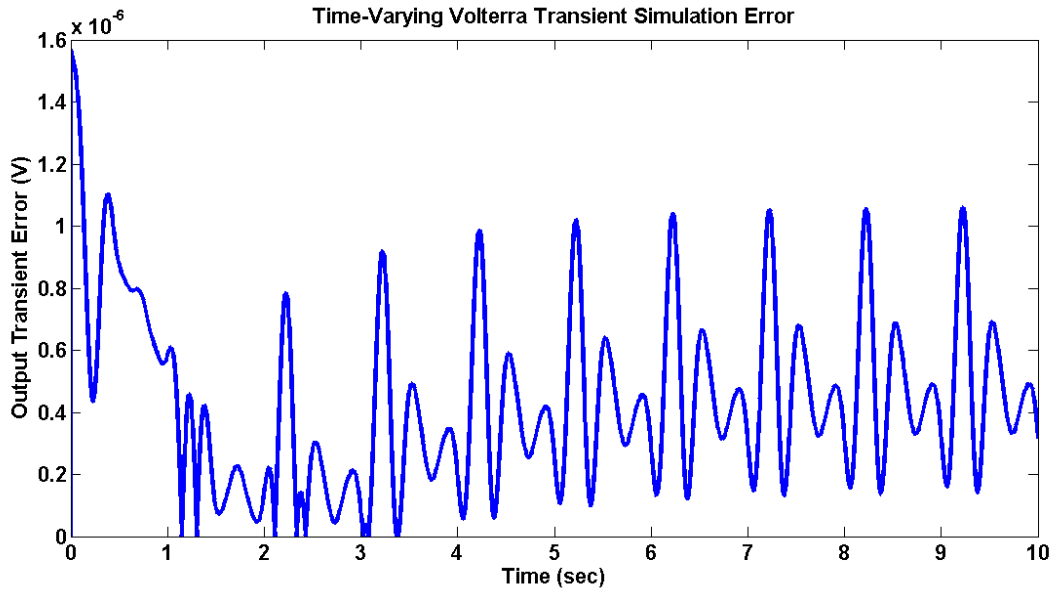

Fig. 3.8 – Absolute error of the simulation using 3rd order Time-Varying Volterra for Case I

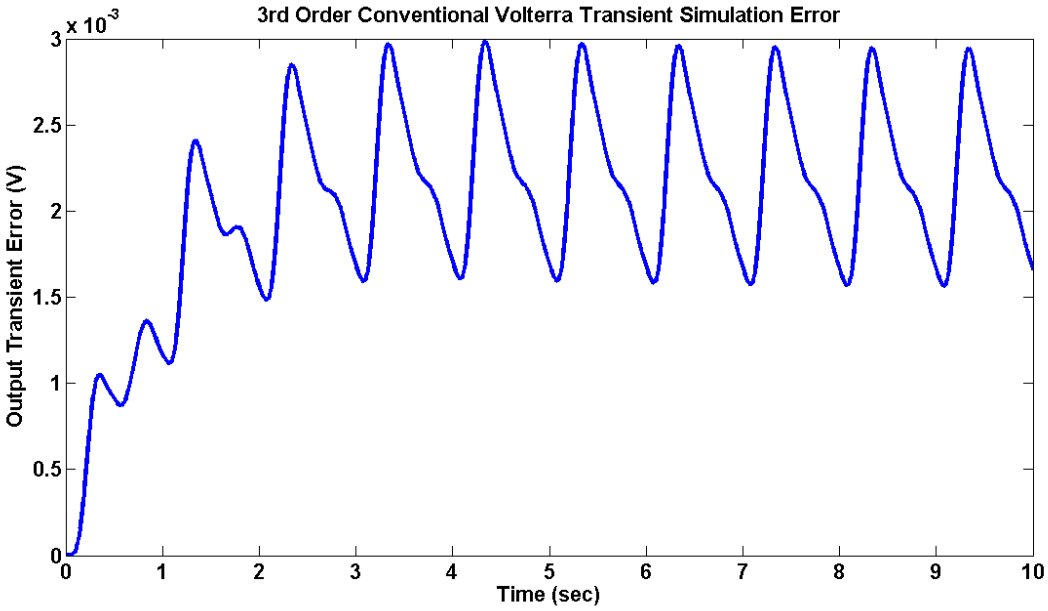

Fig. 3.9 - Absolute error of the simulation using 3rd order conventional Volterra for Case I

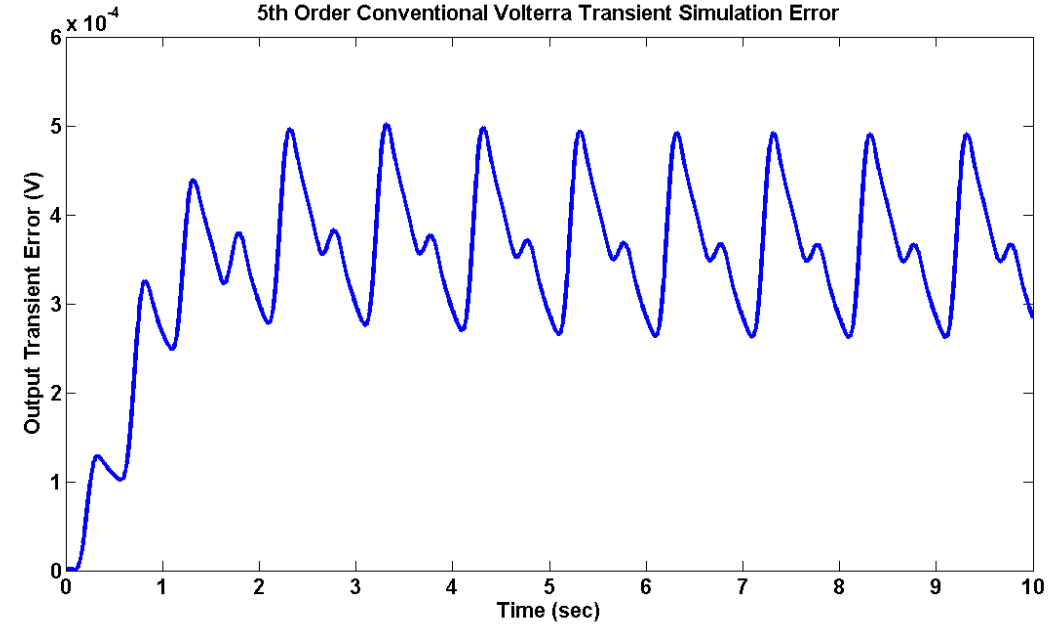

Fig. 3.10 - Absolute error of the simulation using 5th order conventional Volterra for Case I

3.2.2 Case II

Second case uses a stronger nonlinear resistor, compared to Case I. This can be achieved by increasing R_2 and R_3, while keeping the rest of the parameters in the circuit constant. Table 3.2 shows the circuit and simulation parameters for Case II.

Table 3.2 - Specifications of the test circuit and simulation parameters for Case II

Parameter	Value
Input Frequency, f_{in} (Hz)	1
Input Amplitude, A_{in} (Volts)	1
Resistor Parameters, R_1, R_2, R_3	$1, 0.5, 0.5$
Capacitor Values (F)	1
Simulation Step-Size, h (sec)	5×10^{-4}
Simulation Stop-Time (sec)	10

The simulation results of the 3rd order time-varying Volterra, 3rd and 5th order conventional Volterra and ELDO® are shown in Fig. 3.11. Both 3rd and 5th order conventional Volterra fail to give accurate results for Case II, with relative error as high as 50%. On the other hand, 3rd order time-varying Volterra manages to simulate the circuit with good accuracy, maximum relative error of 0.2%. The absolute error of time-varying Volterra simulation is shown in Fig. 3.12.

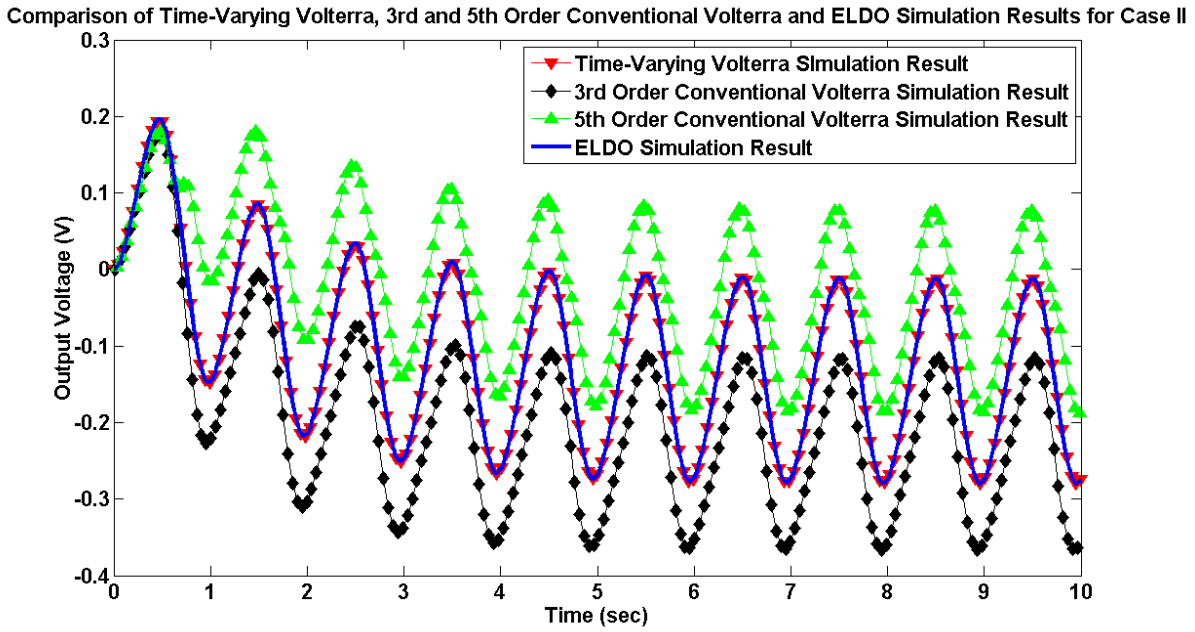

Fig. 3.11 - Output Voltage using 3rd order Time-Varying Volterra, 3rd and 5th order conventional Volterra and ELDO® for Case II

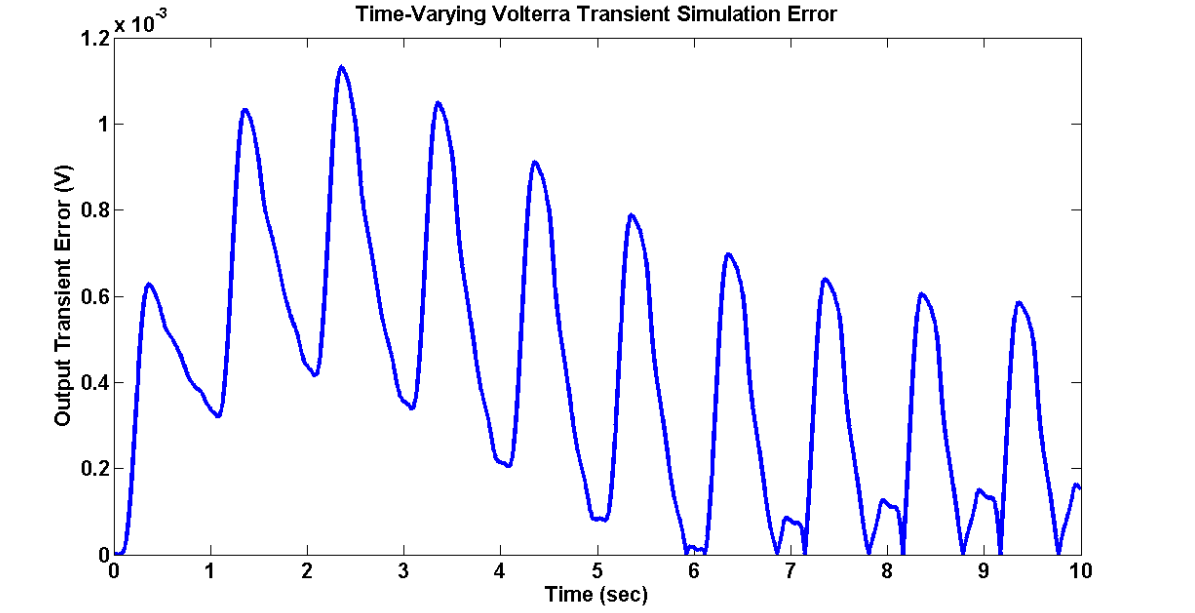

Fig. 3.12 - Absolute error of the simulation using 3rd order Time-Varying Volterra for Case II

3.2.3 Case III

Finally, the third case increases the nonlinearity of the resistor further. Table 3.3 shows the circuit and simulation parameters for Case III.

Table 3.3 - Specifications of the test circuit and simulation parameters for Case III

Parameter	Value
Input Frequency, f_{in} (Hz)	1
Input Amplitude, A_{in} (Volts)	1
Resistor Parameters, R_1, R_2, R_3	$1, 1, 1.5$
Capacitor Values (F)	1
Simulation Step-Size, h (sec)	5×10^{-4}
Simulation Stop-Time (sec)	10

Since nonlinearity of the resistor is stronger than Case II, it is evident that the conventional Volterra, which failed in Case II, cannot give accurate results for this nonlinear circuit. Simulation shows that the results of the 3rd and 5th order conventional Volterra suffers from relative error as high as 400%. The simulation results of the 3rd order time-varying Volterra, 3rd and 5th order conventional Volterra as well as ELDO® simulation results are shown in Fig. 3.13. The results of 3rd order time-varying Volterra shows larger error comparing to Case II, maximum absolute error of $14 \times 10^{-3}\ V$, as shown in Fig. 3.14. The accuracy of the time-varying Volterra drops as the nonlinearity becomes stronger. This is due to the fact that the error of the pre-analysis is larger as the nonlinearity becomes stronger. Thus, the expansion point of the resistor will be farther from the exact response of $i_R(t)$, i.e. larger $|i_R(t) - i_{R-PE}(t)|$. The simulation error can be reduced by applying a more accurate pre-analysis, e.g. 3rd order Volterra, and/or using higher order for time-varying Volterra analysis. However, this will make the simulation more expensive.

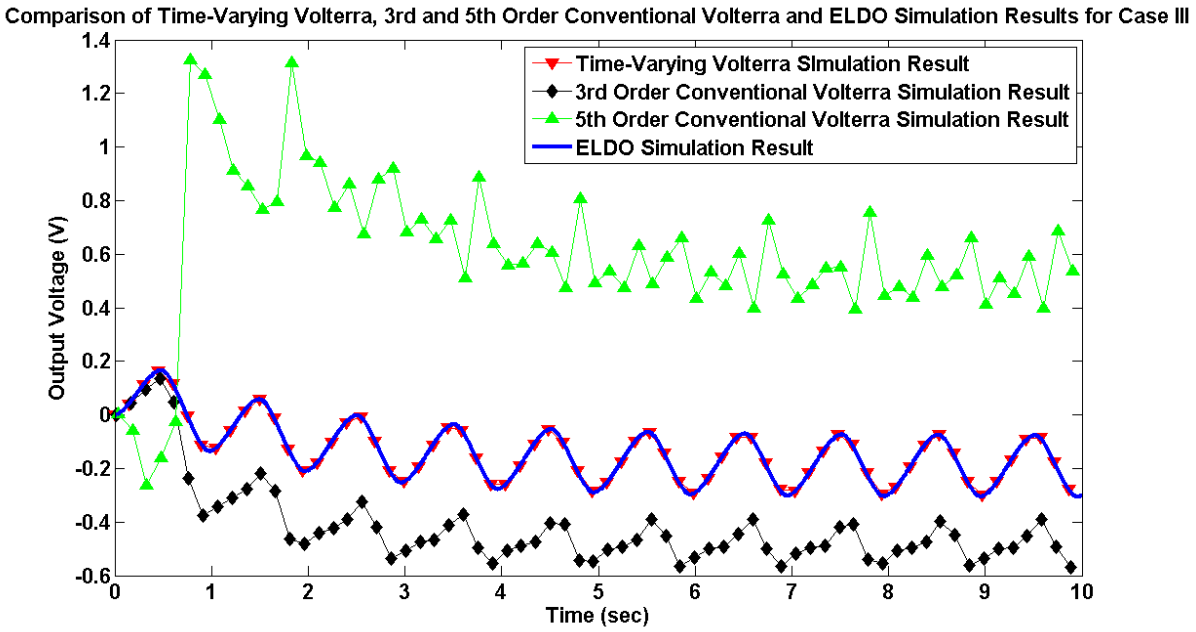

Fig. 3.13 - Output Voltage using 3rd order Time-Varying Volterra, 3rd and 5th order conventional Volterra and ELDO® for Case III

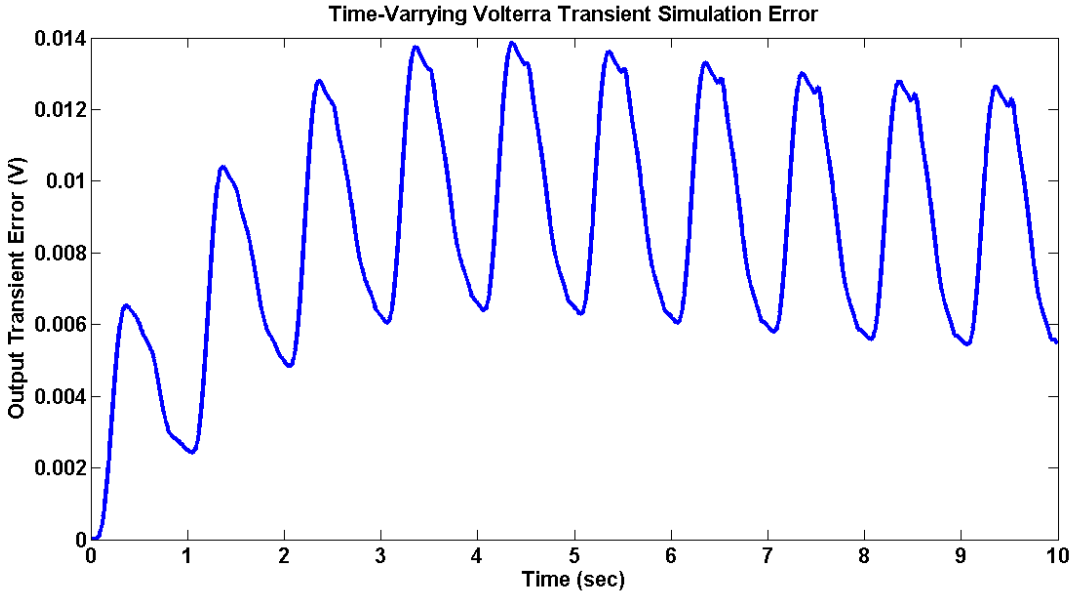

Fig. 3.14 - Absolute error of the simulation using 3rd order Time-Varying Volterra for Case III

3.2.4 Computation Cost Analysis of the method

Computation cost is an important parameter of any simulation method. Time-domain simulation of time-varying Volterra (with linear pre-analysis) requires the LU factorization of an $M \times M$ matrix and N forward/backward substitution for each time-step. M is the size of circuit matrix, e.g. we have $M = 5$ for the nonlinear RC example, and N is the order of time-varying Volterra, e.g. we have $N = 3$ for the nonlinear RC example. The cost of pre-analysis should be added to the total cost mentioned before. For this example, linear time-domain pre-analysis has been implemented which requires one LU factorization of a circuit with the same size, and one forward/backward substitution for each time-step. Assuming K number of simulation steps is required, e.g. we have $K = 10/5 \times 10^{-4} = 2 \times 10^4$ for the nonlinear RC example, and the overall cost of the time-varying Volterra is calculated as,

$$Total\ Cost = K \times C_{LU} + K \times N \times C_{F/B} + C_{Pre-Analysis}, \tag{3.19}$$

where C_{LU} is the cost of LU factorization, $C_{F/B}$ is the cost of forward/backward substitution and $C_{Pre-Analysis}$ is the pre-analysis computation. Replacing $C_{LU} = M^3/3 - M/3$ and $C_{F/B} = M^2$ [1] in (3.19), we have,

$$Total\ Cost \cong K\, M^3/3 + K \times N \times M^2. \tag{3.20}$$

Similarly, the computation cost of conventional Volterra is calculated as,

$$Total\ Cost \cong M^3/3 + K \times N \times M^2, \tag{3.21}$$

where M is the size of matrix of the circuit and N is the order of Volterra analysis. Conventional Volterra requires LU factorization, once, since the Volterra circuits are linear time-invariant. Thus, conventional Volterra analysis requires less computation comparing to time-varying Volterra. However, time-varying Volterra achieves better accuracy. Also, time-varying Volterra manages to simulate stronger nonlinearities compared to conventional Volterra, which makes the method useful to simulate larger set of nonlinear circuits, such as saturated Power Amplifiers. The detail of frequency-domain analysis of time-varying Volterra will be presented in the next chapter.

3.3 Discussion on the Accuracy of Pre-Analysis

In this section the effect of accuracy of pre-analysis on the overall performance of the method will be discussed in more detail. In section 3.1, it was mentioned that the time-varying expansion point should be chosen in a way to ensure small $|i_R(t) - i_0(t)|$ at all times, where $i_0(t) = i_{R-PE}(t)$ is the time-varying expansion point and $i_R(t)$ is the exact response of the circuit. A preliminary simulation, called "pre-analysis" is used to determine the time-varying expansion point. The more accurate the pre-analysis, smaller the $|i_R(t) - i_0(t)|$. With the aid of the numerical example, it was shown that linear pre-analysis is sufficient for time-varying Volterra analysis. In order to clarify the effect of the error of pre-analysis on the performance of the method, we present two examples. First, a diode (a strongly nonlinear device) is taken into account and the second example is an MOS transistor (less nonlinearity compared to the diode).

The current of a diode is defined as [13],

$$i_D = f(v_D) = I_s \exp\left(\frac{v_D}{V_T}\right), \tag{3.22}$$

where $V_T = kT/q$ is the thermal voltage, and I_s is the saturation current of the diode. 3rd order truncated Taylor series of the current of diode is written as,

$$i_D \cong i_0(t) + g_1(t)\big(v_D - v_0(t)\big) + g_2(t)\big(v_D - v_0(t)\big)^2 + g_3(t)\big(v_D - v_0(t)\big)^3, \tag{3.23}$$

where $i_0(t) = f\big(v_0(t)\big)$ is the time-varying expansion point. Also,

$$g_1(t) = \frac{df}{dv_D}\bigg|_{v_D = v_0(t)} = \frac{I_s}{V_T}\exp\left(\frac{v_0(t)}{V_T}\right),$$

$$g_2(t) = \frac{1}{2!}\frac{d^2f}{dv_D^2}\bigg|_{v_D = v_0(t)} = \frac{I_s}{2V_T^2}\exp\left(\frac{v_0(t)}{V_T}\right), \tag{3.24}$$

$$g_3(t) = \frac{1}{3!}\frac{d^3f}{dv_D^3}\bigg|_{v_D = v_0(t)} = \frac{I_s}{6V_T^3}\exp\left(\frac{v_0(t)}{V_T}\right).$$

The truncation error of this approximation is found using,

$$\varepsilon_{truncation}(t) \approx g_4(t)\big(v_D(t) - v_0(t)\big)^4 = \frac{I_s}{24V_T^4}\exp\left(\frac{v_0(t)}{V_T}\right)\big(v_D(t) - v_0(t)\big)^4. \tag{3.25}$$

Assume the voltage across the diode changes in the range of $-0.8\,V$ and $+0.8\,V$. Also, we have, $I_s = 10^{-16}\,A$ and $V_T = 0.025\,V$. The time-varying expansion point should be chosen so that, the maximum truncation error, which happens when $v_D(t)$ is maximum, is acceptable. Assuming 1% is the maximum acceptable error, we have,

$$\begin{gathered}\max\left\{\frac{\varepsilon_{truncation}(t)}{i_D(t)}\right\} = \frac{g_4(t_{max})\big(v_D(t_{max}) - v_0(t_{max})\big)^4}{i_D(t_{max})} < \varepsilon_{max} = 0.01 \\ \rightarrow \frac{\frac{I_s}{24V_T^4}\exp\left(\frac{V_0(t_{max})}{V_T}\right)\big(v_D(t_{max}) - v_0(t_{max})\big)^4}{i_D(t_{max})} < 0.01.\end{gathered} \tag{3.26}$$

Replacing, $v_D(t_{max}) = 0.8\,V$, and $i_D(t_{max}) = I_s\exp\left(\frac{v_D(t_{max})}{V_T}\right) = 7.9\,mA$, we will get,

$$\begin{gathered}\frac{10^{-16}}{24\times 0.025^4}\exp\left(\frac{v_0(t_{max})}{0.025}\right)\big(0.8 - v_0(t_{max})\big)^4/7.9\times 10^{-3} < 0.01 \\ \rightarrow 0.7787 < v_0(t_{max}) < 0.8123.\end{gathered} \tag{3.27}$$

As it can be seen, the acceptable error for time-varying expansion point is very small in case of strongly nonlinear circuits, i.e. 1.54%. In other words, the pre-analysis should have a maximum error of 1.54% at all times, which makes the pre-analysis expensive. For the second case, take an MOS transistor into account. Using simplified EKV model, the drain current of the transistor is characterized using [9],

$$i_D = 2\times\beta\times V_T^2\times\left(\ln\left(1 + exp\left(\frac{v_{GS} - V_{th}}{2V_T}\right)\right)\right)^2, \tag{3.28}$$

where $\beta = \mu_n C_{ox}\,W/L$ and V_{th} is the threshold voltage of the transistor. Using Taylor series with time-varying expansion point, the current of the transistor is approximated as,

$$i_D = i_0(t) + g_{m1}(t)\big(v_{GS} - v_0(t)\big) + g_{m2}(t)\big(v_{GS} - v_0(t)\big)^2 + g_{m3}(t)\big(v_{GS} - v_0(t)\big)^3, \tag{3.29}$$

where,

$$\begin{aligned} g_{m1}(t) &= \frac{di_D}{dv_{GS}}|_{v_{GS}=v_0(t)}, \\ g_{m2}(t) &= \frac{1}{2!}\frac{d^2 i_D}{dv_{GS}^2}|_{v_{GS}=v_0(t)}, \\ g_{m3}(t) &= \frac{1}{3!}\frac{d^3 i_D}{dv_{GS}^3}|_{v_{GS}=v_0(t)}. \end{aligned} \tag{3.30}$$

Due to complexity, the symbolic formulas for g_{m1}, g_{m2} and g_{m3} are not shown here. Truncation error of (3.29) is,

$$\varepsilon_{truncation}(t) \cong g_{m4}(t)\big(v_{GS}(t) - v_0(t)\big)^4, \tag{3.31}$$

where $g_{m4}(t) = \frac{1}{4!}d^4 i_D / dv_{GS}^4\,|_{v_{GS}=v_0(t)}$. Assuming v_{GS} swings from $-0.8\,V$ to $+0.8\,V$, maximum truncation error, which happens at $v_{GS}(t_{max}) = 0.8\,V$, is given by,

$$\max\{\varepsilon_{truncation}(t)\} = \varepsilon_{truncation}(t_{max}) \cong g_{m4}(t_{max})\big(v_{GS}(t_{max}) - v_0(t_{max})\big)^4. \tag{3.32}$$

Again, assuming 1% as the maximum acceptable relative truncation error, we have,

$$\frac{\varepsilon_{truncation}(t_{max})}{i_D(t_{max})} = \frac{g_4(t_{max})\big(v_{GS}(t_{max}) - v_0(t_{max})\big)^4}{2 \times \beta \times V_T^2 \times \left(\ln\left(1 + exp\left(\frac{v_{GS}(t_{max}) - V_{th}}{2V_T}\right)\right)\right)^2} < \varepsilon_{max} = 0.01. \tag{3.33}$$

Using the symbolic formulae for $g_{m4}(t)$, and substituting $\beta = 200 \times 10^{-6}\ V^2/A$, $V_{th} = 0.5\,V$ and $V_T = 0.025\,V$, one can solve (3.33) for $v_0(t_{max})$. We used MATLAB® to calculate $g_{m4}(t)$ and solve (3.33) for $v_0(t_{max})$. The result shows that, assuming $v_0(t_{max}) > 0.648\,V$ satisfies (3.33). For the case of the transistor, the time-varying expansion point is much more relaxed and can handle larger errors for the expansion point, i.e. 20%. This error can be easily satisfied using linear pre-analysis.

It can be concluded that, depending on the type of nonlinearity, the required accuracy for pre-analysis can changes significantly, from 1.54% for diode to 20% for the MOS transistor. As long as strong nonlinear devices, such as diodes, are not considered, the simulation method tolerates large errors for pre-analysis, up to 20%. Thus, simple and efficient pre-analysis, such as linear pre-analysis, is appropriate to find the time-varying expansion point of the nonlinear devices.

3.4 Multi-Dimensional Nonlinearity

In this section we generalize the method described in section 3.1 for multi-dimensional nonlinearities. Semiconductor devices are modeled using two- or three- dimensional nonlinear elements, thus, makes it necessary to consider multi-dimensional nonlinearities as well. For example, the drain current of an MOS transistor is modeled using a two-dimensional nonlinear voltage-controlled current source (assuming body is connected to source) where,

$$i_D = f(v_{GS}, v_{DS}). \tag{3.34}$$

Fig. 3.15 shows a two-dimensional nonlinear voltage-controlled current source. Expanding the output current using Taylor series with time-varying expansion point, we have,

$$\begin{aligned} i(t) = f\big(v_A(t), v_B(t)\big) \cong\ & i_0(t) + K_{1A}(t)\big(v_A(t) - v_{0A}(t)\big) + K_{1B}(t)\big(v_B(t) - v_{0B}(t)\big) \\ & + K_{2A}(t)\big(v_A(t) - v_{0A}(t)\big)^2 + K_{2B}(t)\big(v_B(t) - v_{0B}(t)\big)^2 \\ & + K_{1A1B}(t)\big(v_A(t) - v_{0A}(t)\big)\big(v_B(t) - v_{0B}(t)\big) \\ & + K_{3A}(t)\big(v_A(t) - v_{0A}(t)\big)^3 + K_{3B}(t)\big(v_B(t) - v_{0B}(t)\big)^3 \\ & + K_{2A1B}(t)\big(v_A(t) - v_{0A}(t)\big)^2\big(v_B(t) - v_{0B}(t)\big) \\ & + K_{1A2B}(t)\big(v_A(t) - v_{0A}(t)\big)\big(v_B(t) - v_{0B}(t)\big)^2 \\ & + K_{1A2B}(t)\big(v_A(t) - v_{0A}(t)\big)\big(v_B(t) - v_{0B}(t)\big)^2 + \cdots, \end{aligned} \tag{3.35}$$

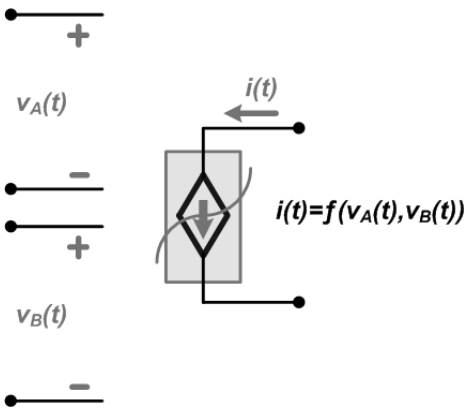

Fig. 3.15 – Nonlinear Voltage Controlled Current Source

where, $i_0(t) = f\big(v_{0A}(t), v_{0B}(t)\big)$ is the expansion point. The nonlinearity coefficients are defined as,

$$K_{mAnB}(t) = \frac{d^{m+n} f}{dv_A^m dv_B^n}\bigg|_{v_{0A}(t),\, v_{0B}(t)'} \tag{3.36}$$

Fig. 3.16 shows the equivalent model of the nonlinear controlled current source using the time-varying Taylor series. Similar to one-dimensional nonlinearities, Schetzen's multi-linear method is applied to find time-varying Volterra circuits for different orders. Fig. 3.17 shows the time-varying Volterra models for two-dimensional nonlinear controlled sources up to 3rd order. This method can be used to find the time-varying Volterra models for three-dimensional nonlinearities.

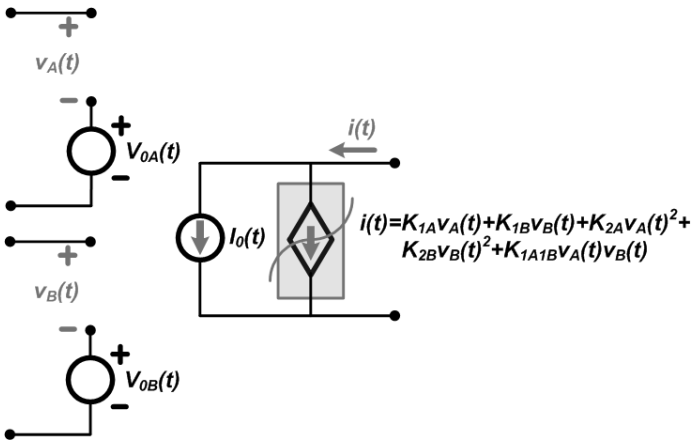

Fig. 3.16 - Equivalent model for the nonlinear controlled current source

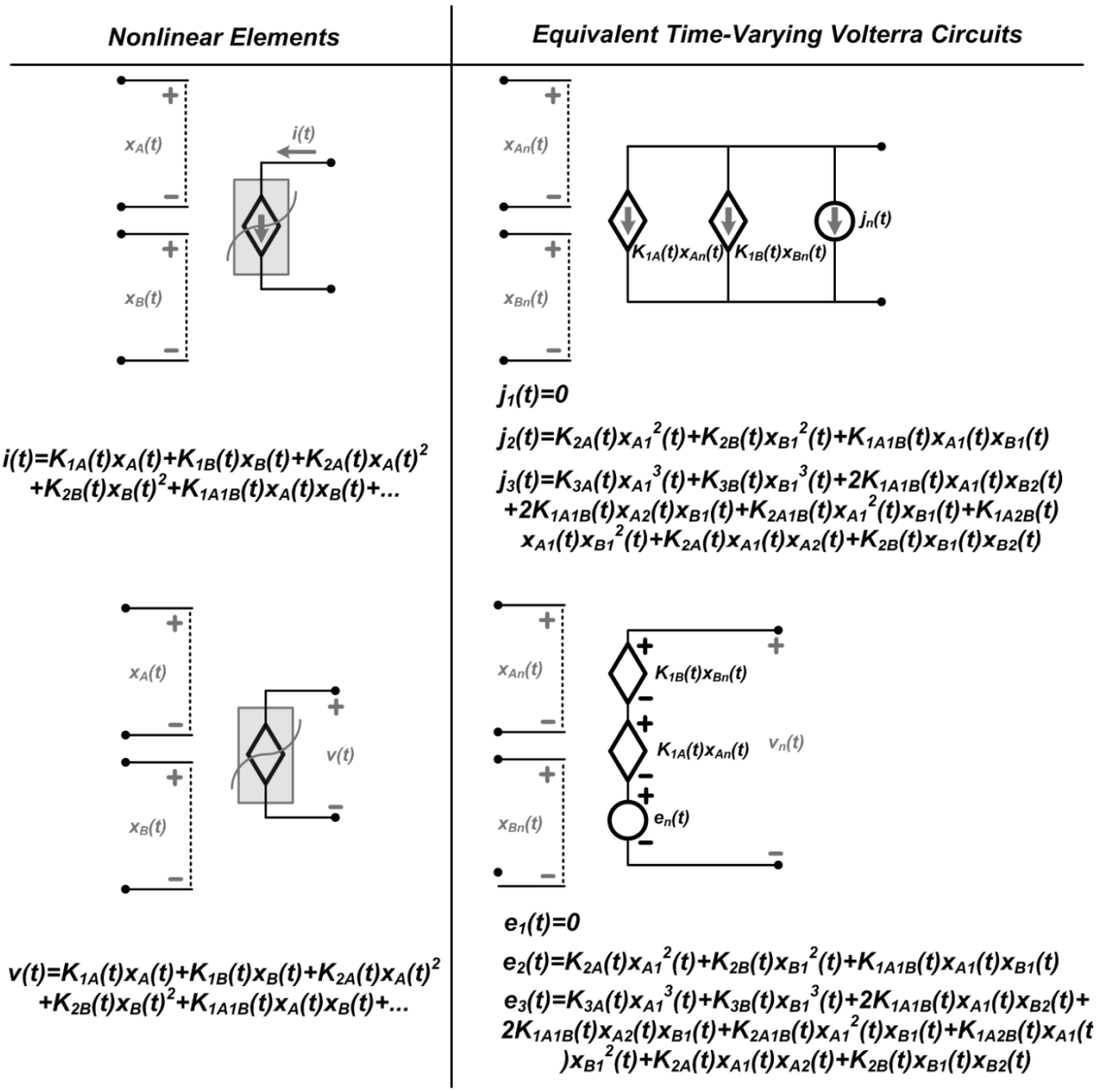

Fig. 3.17 – Two-dimensional nonlinear elements and their time-varying Volterra circuits

3.5 Modified time-varying Volterra

In this section a modification of the time-varying Volterra is presented. The modified time-varying Volterra employs multiple expansion points instead of continuously time-varying expansion point for Taylor series. Using this method the computation cost of the method is decreased, while similar accuracy is achieved. This method is beneficial specially when the input signal is periodic and we are only interested in the steady-state response of the circuit. Employing different expansion points for different

time periods, nonlinear elements are approximated using different Taylor series for different time periods. For example, for a nonlinear resistor we have,

$$v_R(t) = v_{0,i} + R_{1,i}\left(i_R(t) - i_{0,i}\right) + R_{2,i}\left(i_R(t) - i_{0,i}\right)^2 + R_{3,i}\left(i_R(t) - i_{0,i}\right)^3 + \cdots, \tag{3.37}$$

for the time period $T_i < t < T_{i+1}$, called the i^{th} phase. Similar expressions are derived for the nonlinear resistor for all other phases. Applying Schetzen multi-linear method for all the phases, Volterra circuits can be derived for all the phases as shown in Fig. 3.18. The Volterra circuits are modeled as switched linear circuits. The expansion points for different time periods, i.e. phases, are found using the pre-analysis similar to time-varying Volterra analysis. The Volterra switched linear circuits are simulated in time-domain using appropriate numerical integration method. Simple numerical integration methods, such as BDF, face difficulties when simulating switched circuits [25]. Due to inconsistent initial condition which happens in switching circuits, small simulation step sizes should be incorporated, especially at the switching instants, which increase the simulation cost [25]. Here, we employ sampled-data simulation algorithm [25, 31, 32] to simulate the Volterra circuits in time-domain. Sampled data simulation method is based on numerical Laplace inversion [1] that achieves high accuracy while solving the issue of inconsistent initial condition. For detailed discussion on the simulation of switched linear circuit using sampled-data simulation, the reader is referred to [25]. Simulating the switched linear circuit using sampled-data simulation requires calculating state transition matrix and zero-state vector of the circuit in each phase [25]. State transition matrix and zero-state vector are calculated using numerical Laplace inversion, which is an expensive task.

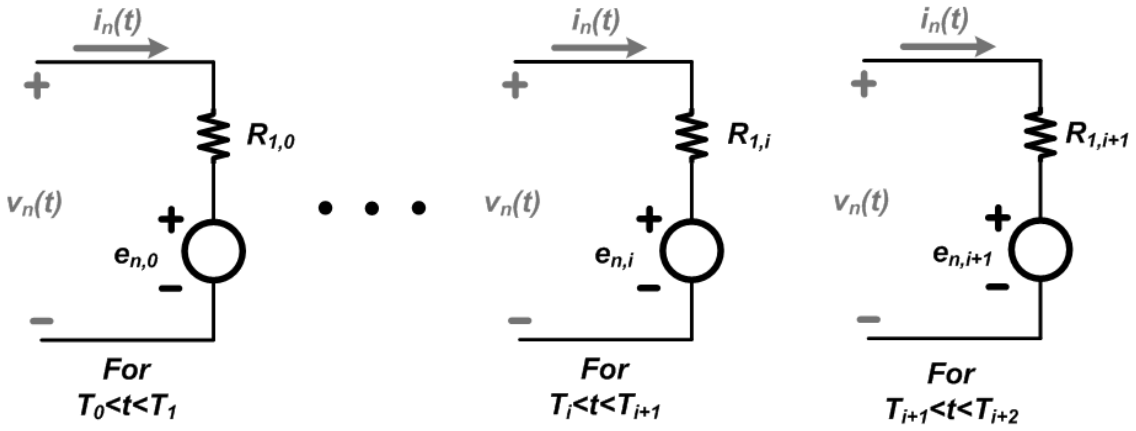

Fig. 3.18 – N$^{\text{th}}$ order Volterra equivalent model for the nonlinear resistor in different phases

The number of time phases is an important parameter that has major effect on the accuracy and simulation cost of the method. As the number of time phases increases, the simulation cost also increases, since the state transition matrix and zero-state vector should be calculated for all the time phases. The modified time-varying Volterra is more accurate as the number of time phases increases. As the number of time phases goes to infinity, the modified time-varying Volterra becomes identical to the time-varying Volterra presented in section 3.1. Choosing the number of time phases depends on the input bandwidth, as well as the nonlinearity of the circuit. It can be shown that in case of single tone input, employing 8 to 10 time phases per input period is sufficient to achieve comparable accuracy to time-varying Volterra. The nonlinear RC example of section 3.2 is simulated using the modified time-varying Volterra with 8 time phases per input period. The accuracy of the simulation results is similar to time-varying Volterra analysis. For steady-state analysis, the expansion points for all nonlinear devices are also periodic. Thus, the Volterra circuits are modeled as periodically switched linear circuits, where the switching frequency is the same as the input frequency. Periodically switched linear circuits are simulated in frequency-domain as described in [24], [25]. Simulation of the steady-state response of nonlinear circuits using the modified time-varying Volterra will be discussed in the next chapter.

3.6 Summary

In this chapter a new time-domain modification of Volterra analysis was presented. The proposed method uses a time-varying expansion point for the Volterra analysis to enable better accuracy comparing to conventional Volterra. As long as time-varying expansion point is chosen so that the difference between expansion point and exact response is small, the time-varying Volterra manages to give accurate results. It was shown that using a simple preliminary simulation of the circuit, pre-analysis, time-varying expansion point of nonlinear devices is determined. As long as strong nonlinearities are not considered, linear pre-analysis is sufficient to achieve good accuracy, as illustrated in the numerical example. On the other hand, when nonlinearity becomes stronger, using simple linear pre-analysis the time-varying Volterra does not achieve accurate enough results. This can be fixed by using a more accurate pre-analysis. However, this increases the computation of pre-analysis, which makes the overall method not suitable for simulation of strong nonlinear circuits.

Chapter 4
Time-Varying Volterra Analysis: Frequency-Domain Approach

In this chapter, the details of the proposed method in frequency-domain will be presented. The frequency-domain method uses the same methodology as the method described in chapter 3, i.e. time-varying Taylor series. Frequency-domain approach analyzes the time-varying Volterra circuits in frequency-domain. Since the frequency-domain method uses the same time-varying Taylor series, the convergence and accuracy properties of the method is the same as time-domain method discussed in chapter 3. Frequency-domain analysis of time-varying Volterra circuits, as well as the advantages and shortcomings of the method, will be discussed in this chapter.

The chapter is organized as follows. Section 4.1 describes the frequency-domain analysis of the time-varying Volterra circuits and compares the analysis with other frequency-domain approaches, i.e. Harmonic Balance and conventional Volterra analysis. In order to show the effectiveness of the method, section 4.2 discusses three nonlinear RC circuits simulated using the method. Section 4.3 presents the frequency-domain time-varying Volterra for multi-dimensional nonlinearities. Finally, section 4.4 summarizes the properties of the method comparing to other frequency-domain approaches.

4.1 Method Description

The proposed frequency-domain method employs time-varying Taylor expansion to express the behavior of nonlinear elements, similar to the time-domain method described in chapter 3. Similarly, the simulation procedure consists of pre-analysis and time-varying Volterra analysis. In this section we discuss time-varying Volterra analysis in frequency-domain, together with comparison of the method with Harmonic Balance.

4.1.1 Pre-Analysis

As discussed in chapter 3, pre-analysis is done using a fast simulation algorithm which does not need to be very accurate. It was shown in chapter 3 that accuracy of linear pre-analysis is sufficient for time-varying Volterra analysis. Linear pre-analysis is easily done in the frequency domain by solving the linearized circuit using [1],

$$(G + j\omega C)\mathcal{F}\{X_{PE}(t)\} = \mathcal{F}\{W_{PE}(t)\}. \tag{4.1}$$

where $X_{PE}(t)$ and $W_{PE}(t)$ are the unknown and input vectors respectively. Solving (4.1) requires LU factorization of $(G + j\omega C)$ at each frequency, and forward/backward substitution. In case of single-tone input, (4.1) should only be solved once, i.e. for the excitation frequency.

4.1.2 Time-Varying Volterra Analysis

Recalling from chapter 3, a nonlinear resistor is described using time-varying Taylor expansion as,

$$v_R(t) - V_0(t) = \hat{v}(t) = R_1(t)\hat{\imath}(t) + R_2(t)\hat{\imath}(t)^2 + R_3(t)\hat{\imath}(t)^3 + \cdots. \tag{4.2}$$

where,

$$\begin{aligned} R_1(t) &= \frac{df}{di_R}\bigg|_{i_R = i_0(t)'} \\ R_2(t) &= \frac{1}{2!}\frac{d^2 f}{di_R^2}\bigg|_{i_R = i_0(t)'} \\ R_3(t) &= \frac{1}{3!}\frac{d^3 f}{di_R^3}\bigg|_{i_R = i_0(t)'} \\ &\vdots \end{aligned} \tag{4.3}$$

$V_0(t)$ and $I_0(t)$ are the time-varying expansion point of Taylor series and the result of pre-analysis. Applying Schetzen's multi-linear method, the time-varying Volterra circuits of different orders for the resistor are generated as shown in Fig. 4.1. The time-varying Volterra circuits are described in the frequency-domain, assuming all the time-varying elements are periodic. This assumption is true for periodic inputs, which results in periodic expansion point for time-varying Volterra. In case of multi-tone inputs with non-commensurate frequencies, "almost-periodic" Fourier transform should be employed [10]. Taking the Fourier Transform (FT) of the time-varying resistor in Fig. 4.1, we'll get [14],

$$\mathcal{F}\{R_1(t)\} = \sum_{k=-\infty}^{+\infty} \hat{R}_{1,k}\delta(\omega - k\omega_0), \tag{4.4}$$

where $T_0 = 2\pi/\omega_0$ is the period of the time-varying resistor, and $\hat{R}_{1,k}$ is the kth frequency component of the time-varying resistor. Assuming the resistor is sufficiently approximated using the first K frequency components, we have,

$$\mathcal{F}\{R_1(t)\} \cong \sum_{k=-K}^{+K} \hat{R}_{1,k}\delta(\omega - k\omega_0). \tag{4.5}$$

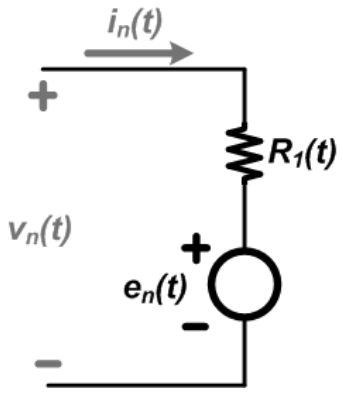

Fig. 4.1 - Nth order time-varying Volterra equivalent model for the nonlinear resistor

Similarly, time-varying capacitors, inductors and controlled sources are represented in the frequency-domain. Fig. 4.2 summarizes time-varying Volterra models for nonlinear elements in frequency-domain. Employing MNA, the n^{th} order time-varying Volterra circuit is formulated in frequency-domain as,

$$\mathcal{F}\{G(t)\}\otimes\mathcal{F}\{X_n(t)\} + j\omega\{\mathcal{F}\{C(t)\}\otimes\mathcal{F}\{X_n(t)\}\} = \mathcal{F}\{W_n(t)\}, \tag{4.6}$$

where $\otimes$ denotes convolution. It should be noted that, $G(t)$ and $C(t)$ are $M \times M$ matrices and $X_n(t)$ and $W_n(t)$ are $M \times 1$ vectors, where M is the size of the circuit matrix. $G(t)$ and $C(t)$ contain the time-varying resistors, inductors and capacitors and controlled sources, and thus are T_0 periodic. Approximating $\mathcal{F}\{G(t)\}$, $\mathcal{F}\{C(t)\}$, $\mathcal{F}\{X_n(t)\}$ and $\mathcal{F}\{W_n(t)\}$ with their first K frequency components, we'll get,

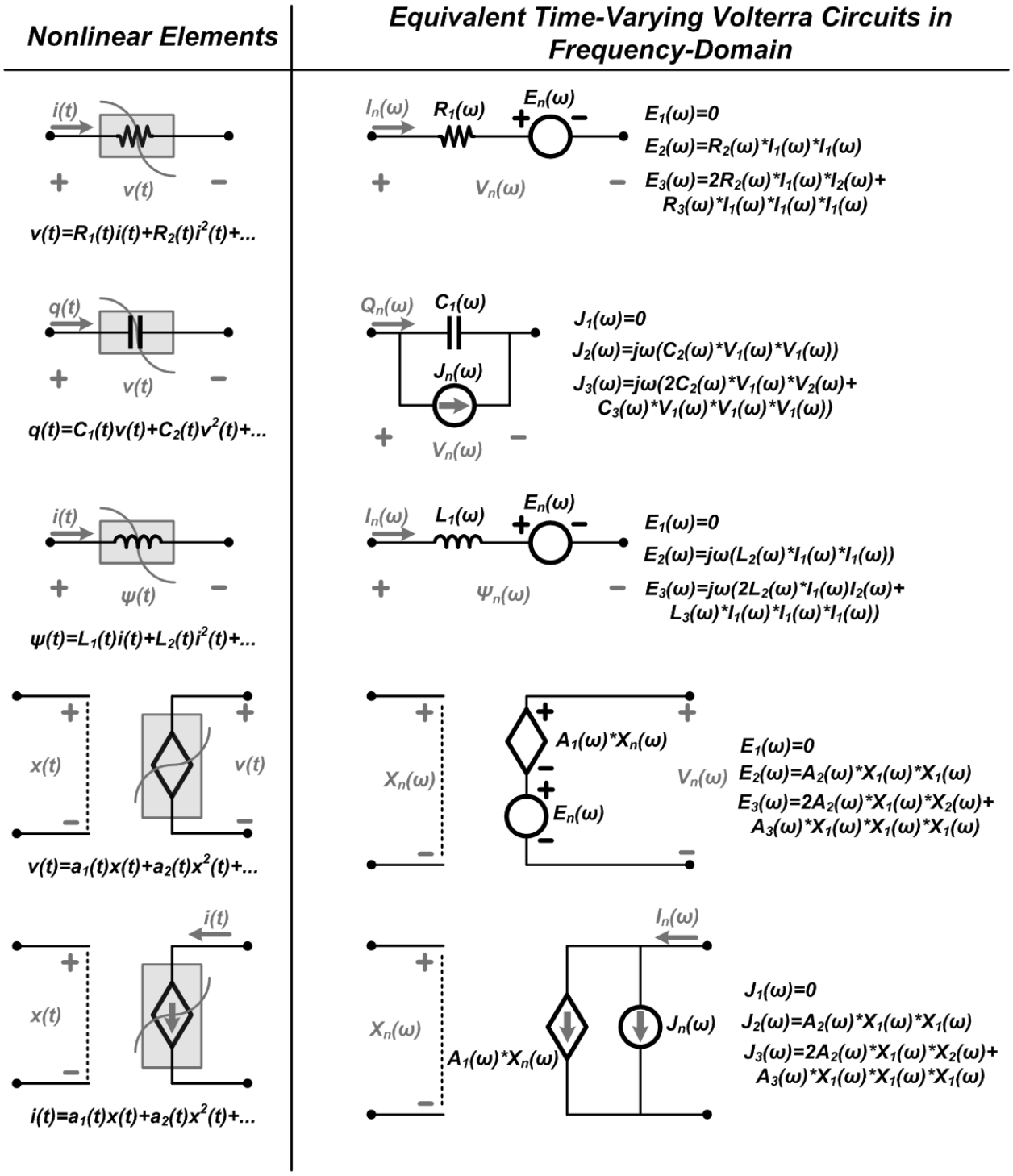

Fig. 4.2 - Nonlinear elements and their time-varying Volterra circuits in frequency-domain

$$\left\{\sum_{m=-K}^{+K}\hat{G}_m\delta(\omega-m\omega_0)\right\}\otimes\left\{\sum_{l=-K}^{+K}\hat{X}_{n,l}\delta(\omega-l\omega_0)\right\}$$
$$+j\omega\left\{\sum_{m=-K}^{+K}\hat{C}_m\delta(\omega-m\omega_0)\right\}\otimes\left\{\sum_{l=-K}^{+K}\hat{X}_{n,l}\delta(\omega-l\omega_0)\right\} \tag{4.7}$$
$$=\sum_{k=-K}^{+K}\widehat{W}_{n,k}\delta(\omega-k\omega_0),$$

where $\hat{X}_n(k\omega_0)$ and $\widehat{W}_n(k\omega_0)$ represent the kth frequency component of the unknown and input vector. Simplifying (4.7) results in,

$$\sum_{l=-K}^{+K}\sum_{m=-K}^{+K}\hat{G}_m\,\hat{X}_{n,l}\delta(\omega-(m+l)\omega_0)+\sum_{j=-K}^{+K}\sum_{i=-K}^{+K}j\omega_0(m+l)\hat{C}_m\,\hat{X}_{n,l}\delta(\omega-(m+l)\omega_0)$$
$$=\sum_{k=-K}^{+K}\widehat{W}_{n,k}\delta(\omega-k\omega_0). \tag{4.8}$$

Equating the coefficients of $\delta(\omega-k\omega_0)$, for every k, on both sides of (4.8) results in,

$$\sum_{m=-K}^{0}\{\hat{G}_m-jK\omega_0\hat{C}_m\}\hat{X}_{n,-m-k}=\widehat{W}_{n,-K},$$
$$\vdots$$
$$\sum_{m=-K}^{+K-1}\{\hat{G}_m-j\omega_0\hat{C}_m\}\hat{X}_{n,-m-1}=\widehat{W}_{n,-1},$$
$$\sum_{m=-K}^{+K}\hat{G}_m\,\hat{X}_{n,-m}=\widehat{W}_{n,0}, \tag{4.9}$$
$$\sum_{m=-K+1}^{+K}\{\hat{G}_m+j\omega_0\hat{C}_m\}\hat{X}_{n,-m+1}=\widehat{W}_{n,1},$$
$$\vdots$$
$$\sum_{m=0}^{+K}\{\hat{G}_m+jK\omega_0\hat{C}_m\}\hat{X}_{n,-m+K}=\widehat{W}_{n,K}.$$

Knowing the input vector, i.e. $\widehat{W}_{n,k}$ for $-K \le k \le +K$, together with circuit matrices, the unknown vector is calculated using the $2K+1$ equations given in (4.9), i.e. $\hat{X}_{n,k}$ for $-K \le k \le +K$. Rewriting (4.9) in the matrix form, we have,

$$T(\omega_0) \times \hat{X}_{M,n}(\omega_0) = \widehat{W}_{M,n}(\omega_0), \tag{4.10}$$

where,

$$\begin{aligned} \hat{X}_{M,n}(\omega_0) &= \begin{bmatrix} \hat{X}_{n,-K} & \dots & \hat{X}_{n,-1} & \hat{X}_{n,0} & \hat{X}_{n,1} & \dots & \hat{X}_{n,+K} \end{bmatrix}^T, \\ \widehat{W}_{M,n}(\omega_0) &= \begin{bmatrix} \widehat{W}_{n,-K} & \dots & \widehat{W}_{n,-1} & \widehat{W}_{n,0} & \widehat{W}_{n,1} & \dots & \widehat{W}_{n,+K} \end{bmatrix}^T. \end{aligned} \tag{4.11}$$

Also we have,

$$T(\omega_0) = \begin{bmatrix} T_{-K,0} & \cdots & T_{-K,-K+1} & T_{-K,-K} & 0 & \cdots & 0 \\ \vdots & \ddots & \vdots & \vdots & \vdots & \ddots & \vdots \\ T_{-1,K-1} & \cdots & T_{-1,0} & T_{-1,-1} & T_{-1,-2} & \cdots & 0 \\ T_{0,K} & \cdots & T_{0,1} & T_{0,0} & T_{0,-1} & \cdots & T_{0,-K} \\ 0 & \cdots & T_{1,2} & T_{1,1} & T_{1,0} & \cdots & T_{1,-K+1} \\ \vdots & \ddots & \vdots & \vdots & \vdots & \ddots & \vdots \\ 0 & \cdots & 0 & T_{K,K} & T_{K,K-1} & \cdots & T_{K,0} \end{bmatrix} \tag{4.12}$$

where,

$$T_{k,m} = \hat{G}_m + jk\omega_0 \hat{C}_m. \tag{4.13}$$

$T(\omega_0)$ matrix, called the conversion matrix, is similar to the transfer function for time-invariant circuits. However, since the circuit is time-varying, the output depends on the input at fundamental frequency and the harmonic frequencies. For a time-invariant circuit, $T(\omega_0)$ is a diagonal matrix. In order to find the unknown vector, one must solve (4.10) which require LU factorization of a $(2K+1)M \times (2K+1)M$ matrix, and $(2K+1)M$ forward/backward substitution. It should be noted that (4.10) must be solved for different orders of time-varying Volterra circuits. $T(\omega_0)$ matrix is constant for all the orders, however, $\widehat{W}_{M,n}(\omega_0)$ should be calculated based on the response of lower order circuits. Finally, the total response is

calculated by summing up the response of lower orders, i.e. $\hat{X}_M(\omega_0) = \hat{X}_{M,1}(\omega_0) + \hat{X}_{M,2}(\omega_0) + \hat{X}_{M,3}(\omega_0) + \cdots$.

The formulation presented, can be generalized for multiple-tone input signals as well. In case of multiple-tone inputs, the output will be a function of input frequencies and their harmonics as well as inter-modulation products of the input frequencies. This makes the size of frequency vector larger for multiple-tone inputs.

4.1.3 Comparison with Harmonic Balance

It is useful to compare the computation cost and accuracy of the frequency-domain time-varying Volterra with Harmonic Balance. In this section, we discuss the computation cost of the method and leave the accuracy comparison for the next section. Frequency-domain time-varying Volterra analysis requires pre-analysis, plus solving the time-varying Volterra circuits of different order, i.e. solving (4.10) for each order. Assuming N^{th} order time-varying Volterra analysis, the computation cost is approximated by,

$$Total\ Cost = C_{LU} + N \times C_{F/B} + N \times C_{W-Generation} + C_{Pre-Analysis}, \tag{4.16}$$

where C_{LU} is the cost of LU decomposition of $T(\omega_0)$, which only needs to be done once, and $C_{F/B}$ is the cost of forward/backward substitution. $C_{W-Generation}$ is the cost of calculating the input vector, i.e. $\widehat{W}_{M,n}(\omega_0)$, and $C_{Pre-Analysis}$ is the pre-analysis computation cost. Calculating the input vector requires taking the Fourier Transform (FT) of the input sources and Volterra model's dependent sources, which involves convolution of response of lower orders. $C_{W-Generation}$ can become significant in case of multiple-tone inputs. For the rest of this section, we concentrate on single-tone input. However, our calculations can be easily generalized for multiple-tone input as well.

The conversion matrix is sparse, because $\hat{G}(m\omega_0)$ and $\hat{C}(m\omega_0)$ are sparse matrices for $m \neq 0$. Thus, (4.10) is solved more efficiently using sparse matrix calculation methods [1]. Furthermore, since the circuit parameters are real functions of time, we have $\hat{G}(m\omega_0) = \hat{G}^*(-m\omega_0)$, $\hat{C}(m\omega_0) = \hat{C}^*(-m\omega_0)$, $\widehat{W}_n(m\omega_0) = \widehat{W}_n^*(-m\omega_0)$ and $\hat{X}_n(m\omega_0) = \hat{X}_n^*(-m\omega_0)$. Hence, the total computation cost is reduced by a factor of two. Using (4.12) it can be shown that for circuits with real parameters we have,

$$T(\omega_0) = \left(T^t(\omega_0)\right)^*. \tag{4.17}$$

Replacing $T(\omega_0) = L(\omega_0)U(\omega_0)$, where $L(\omega_0)$ and $U(\omega_0)$ are lower and upper triangular matrices respectively, we'll get,

$$T(\omega_0) = L(\omega_0)U(\omega_0) = \left(\left(L(\omega_0)U(\omega_0)\right)^t\right)^*,$$

$$\rightarrow L(\omega_0)U(\omega_0) = \left(U^t(\omega_0)\right)^*\left(L^t(\omega_0)\right)^*. \tag{4.18}$$

Knowing $U^t(\omega_0)$ and $L^t(\omega_0)$ are lower and upper triangular matrices respectively, we have,

$$L(\omega_0) = \left(U^t(\omega_0)\right)^*,$$

$$U(\omega_0) = \left(L^t(\omega_0)\right)^*, \tag{4.19}$$

for all the non-diagonal elements. Thus, calculating either $L(\omega_0)$ or $U(\omega_0)$ is sufficient, which means half the computation cost for LU decomposition. Similarly, the forward/backward substitution and input vector generation cost is reduced by a factor of two. Neglecting the pre-analysis computation cost, the overall computation cost is approximately,

$$Total\ Cost \cong \left((K+1)M\right)^3/3 + N\left(\left((K+1)M\right)^2 + C_{W-Generation}\right), \tag{4.20}$$

where K is the number of harmonics, N is the order of Volterra analysis, and M is the size of circuit matrix. In calculating (4.20), it is assumed that we do not use sparse matrix calculation algorithms. Sparse matrix algorithms will reduce the total cost.

Recalling from chapter 2, Harmonic-Balance balances the magnitude and phase of the harmonics for all the voltages and currents, by solving the Harmonic-Balance equation. Harmonic-Balance equation is a nonlinear equation and needs to be solved iteratively, using Newton-Raphson algorithm. The Jacobian matrix as well as the next iteration value should be calculated per iteration, using,

$$M\left(V^i\right)\left(V^{i+1} - V^i\right) = -F\left(V^i\right),$$

$$M(V) = \frac{\partial F(V)}{\partial V}, \tag{4.21}$$

where $M(.)$ is the Jacobian matrix and $F(.)$ is the nonlinear Harmonic Balance equation. Size of the Jacobian matrix and Harmonic-Balance equation is $(K+1)M \times (K+1)M$, where K is the number of harmonics and M is the number of unknown voltages/currents. Assuming I iterations for Newton-Raphson is required, Harmonic-Balance computation cost is calculated as,

$$Total\ Cost = I \times \left(C_{LU-Jacob} + C_{F/B} + C_{Jacob-Generation}\right), \tag{4.22}$$

where $C_{LU-Jacob} + C_{F/B}$ is the total cost of solving next iteration value per iteration, including LU decomposition of Jacobian matrix and forward/backward substitution. $C_{Jacob-Generation}$ is the cost of generating Jacobian matrix, which is time-consuming as the number of nonlinearities increases. Simplifying (4.23), we have,

$$Total\ Cost \cong I\left(\left((K+1)M\right)^3/3 + \left((K+1)M\right)^2 + C_{Jacob-Generation}\right). \tag{4.23}$$

Comparing (4.24) and (4.21), it can be seen that frequency-domain time-varying Volterra computation cost is less than Harmonic-Balance. $C_{Jacob-Generation}$ in (4.23) is usually more than $C_{W-Generation}$ in (4.20) for most applications, since the size of Jacobian matrix is $(K+1)M \times (K+1)M$, whereas time-varying Volterra input vector is $(2K+1)M \times 1$. However, Harmonic-Balance achieves better accuracy comparing to time-varying Volterra when dealing with strong nonlinearities, as it will be discussed in the next section. It should be noted that, this is a rough comparison between the full matrix solution of Harmonic Balance and time-varying Volterra analysis. Employing spars matrix algorithms, the total cost of both methods can be reduced further.

4.2 Numerical Example

This section presents simulation of a nonlinear RC circuit, shown in Fig. 4.3, using time-varying Volterra in frequency-domain. The circuit is the same as nonlinear RC circuit presented in section 3.2. The circuit is simulated using 3rd order frequency-domain time-varying Volterra, 3rd and 5th order frequency-domain conventional Volterra, Harmonic Balance and Newton-Raphson numerical integration. A detailed comparison between all the simulation methods will be presented in this section.

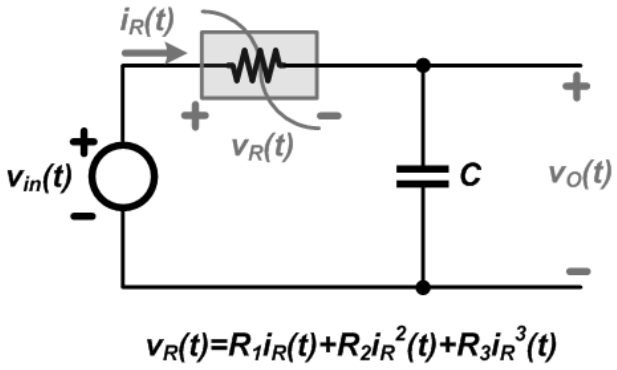

Fig. 4.3 - Nonlinear RC test circuit

First we discuss the conventional Volterra analysis. Circuit of different orders for conventional Volterra will be the same as the circuits shown in chapter 3, Fig. 3.5. The Volterra circuits are formulated in frequency-domain as,

$$(G + j\omega C)\mathcal{F}\{X_n(t)\} = \mathcal{F}\{W_n(t)\}, \tag{4.24}$$

where,

$$G = \begin{bmatrix} 0 & 0 & 0 & 1 & 1 \\ 0 & 0 & 0 & -1 & 0 \\ 1 & 0 & 0 & 0 & 0 \\ 1 & -1 & 0 & 0 & 0 \\ 0 & 1 & -1 & 0 & -R_1 \end{bmatrix},$$

$$C = \begin{bmatrix} 0 & 0 & 0 & 0 & 0 \\ 0 & 0 & C_0 & 0 & 0 \\ 0 & 0 & 0 & 0 & 0 \\ 0 & 0 & 0 & 0 & 0 \\ 0 & 0 & 0 & 0 & 0 \end{bmatrix}, \tag{4.25}$$

and,

$$\begin{aligned} \mathcal{F}\{W_1(t)\} &= [0 \quad 0 \quad \mathcal{F}\{v_{in}(t)\} \quad 0 \quad 0]^T, \\ \mathcal{F}\{W_2(t)\} &= [0 \quad 0 \quad 0 \quad \mathcal{F}\{e_2(t)\} \quad 0]^T, \\ &\vdots \\ \mathcal{F}\{W_5(t)\} &= [0 \quad 0 \quad 0 \quad \mathcal{F}\{e_5(t)\} \quad 0]^T. \end{aligned} \tag{4.26}$$

Assuming a single-tone at the input we have,

$$\mathcal{F}\{v_{in}(t)\} = \mathcal{F}\{A_{in}sin(\omega_0 t)\} = \frac{A_{in}}{j2}\delta(\omega-\omega_0) - \frac{A_{in}}{j2}\delta(\omega+\omega_0),$$

$$\mathcal{F}\{e_2(t)\} = R_2 I_{R1}(\omega) \otimes I_{R1}(\omega),$$

$$\vdots \tag{4.27}$$

$$\mathcal{F}\{e_5(t)\} = 2R_2 I_{R2}(\omega)\otimes I_{R3}(\omega) + 2R_2 I_{R1}(\omega)\otimes I_{R4}(\omega) + 3R_3 I_{R2}(\omega)\otimes I_{R2}(\omega)\otimes I_{R1}(\omega) + 3R_3 I_{R1}(\omega)\otimes I_{R1}(\omega)\otimes I_{R3}(\omega).$$

The total response for 5th order conventional Volterra is calculated as, $\mathcal{F}\{X(t)\} = \mathcal{F}\{X_1(t)\} + \mathcal{F}\{X_2(t)\} + \mathcal{F}\{X_3(t)\} + \mathcal{F}\{X_4(t)\} + \mathcal{F}\{X_5(t)\}$. For 3rd order Volterra the 4th and 5th order responses will be neglected. It can be seen that the complexity of the dependent sources increases significantly as the order of Volterra analysis increases. Also, calculating (4.27) will be expensive for multiple frequencies at the input, due to multiple convolution operations in (4.27).

The second method is 3rd order frequency-domain time-varying Volterra analysis. The first step is linear pre-analysis, which is the same as 1st order conventional Volterra. Using the result of pre-analysis, the time-varying Volterra circuits are created, which is the same as circuits shown in chapter 3, Fig. 3.6. The frequency-domain Volterra circuits are found out using Fourier transform, as shown in Fig. 4.3. We have,

$$v_{R-PE}(t) = f\big(i_{R-PE}(t)\big) = R_1 i_{R-PE}(t) + R_2 i_{R-PE}^2(t) + R_3 i_{R-PE}^3(t), \tag{4.28}$$

$$\rightarrow V_{R-PE}(\omega) = R_1 I_{R-PE}(\omega) + R_2 I_{R-PE}(\omega)\otimes I_{R-PE}(\omega) + R_3 I_{R-PE}(\omega)\otimes I_{R-PE}(\omega)\otimes I_{R-PE}(\omega).$$

For single-tone input, $i_{R-PE}(t)$ is also a single-tone, i.e. $I_{R-PE}(\omega) = \hat{I}_{R-PE}(-\omega_0)\delta(\omega-\omega_0) + \hat{I}_{R-PE}(+\omega_0)\delta(\omega+\omega_0)$, thus, we have,

$$V_{R-PE}(\omega) = \sum_{k=-3}^{+3} \hat{V}_{R-PE,k}\delta(\omega - k\omega_0). \tag{4.29}$$

Also, for time-varying Volterra coefficients we have,

$$\mathcal{F}\{\hat{R}_1(t)\} = R_1 + 2R_2 I_{R-PE}(\omega) + 3R_3 I_{R-PE}(\omega) \otimes I_{R-PE}(\omega),$$

$$\mathcal{F}\{\hat{R}_2(t)\} = R_2 + 3R_3 I_{R-PE}(\omega), \tag{4.30}$$

$$\mathcal{F}\{\hat{R}_3(t)\} = R_3.$$

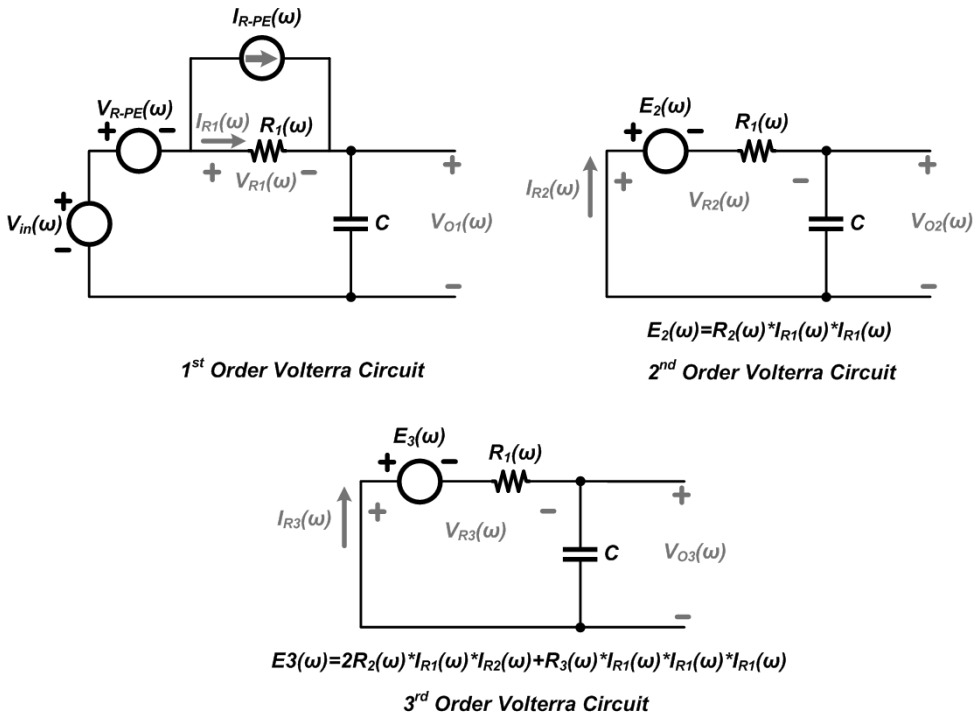

Fig. 4.4 - Varying Volterra circuits for different orders in frequency-domain

Time-varying Volterra circuits are characterized using MNA as,

$$G(t)X_n(t) + C\frac{dX_n(t)}{dt} = W_n(t), \tag{4.31}$$

where,

$$G(t) = \begin{bmatrix} 0 & 0 & 0 & 1 & 1 \\ 0 & 0 & 0 & -1 & 0 \\ 1 & 0 & 0 & 0 & 0 \\ 1 & -1 & 0 & 0 & 0 \\ 0 & 1 & -1 & 0 & -R_1(t) \end{bmatrix},$$

$$C = \begin{bmatrix} 0 & 0 & 0 & 0 & 0 \\ 0 & 0 & C_0 & 0 & 0 \\ 0 & 0 & 0 & 0 & 0 \\ 0 & 0 & 0 & 0 & 0 \\ 0 & 0 & 0 & 0 & 0 \end{bmatrix}, \tag{4.32}$$

Taking the Fourier transform of (4.32), we'll get,

$$\hat{G}(0) = \begin{bmatrix} 0 & 0 & 0 & 1 & 1 \\ 0 & 0 & 0 & -1 & 0 \\ 1 & 0 & 0 & 0 & 0 \\ 1 & -1 & 0 & 0 & 0 \\ 0 & 1 & -1 & 0 & -R_1 \end{bmatrix},$$

$$\hat{G}(k\omega_0) = \begin{bmatrix} 0 & 0 & 0 & 0 & 0 \\ 0 & 0 & 0 & 0 & 0 \\ 0 & 0 & 0 & 0 & 0 \\ 0 & 0 & 0 & 0 & 0 \\ 0 & 0 & 0 & 0 & -\hat{R}_1(k\omega_0) \end{bmatrix}, for\ k \neq 0, \tag{4.33}$$

and,

$$\hat{C}(0) = \begin{bmatrix} 0 & 0 & 0 & 0 & 0 \\ 0 & 0 & C_0 & 0 & 0 \\ 0 & 0 & 0 & 0 & 0 \\ 0 & 0 & 0 & 0 & 0 \\ 0 & 0 & 0 & 0 & 0 \end{bmatrix}, \tag{4.34}$$

$$\hat{C}(k\omega_0) = 0, for\ k \neq 0.$$

Using (4.33) and (4.34), the conversion matrix is constructed. For this example, we assume a total number of 6 harmonics is sufficient to achieve good accuracy, which makes the size of $T(\omega_0)$ to be 65×65.

The circuit is also simulated using Harmonic Balance simulation provided in ADS® software. ADS® uses advance algorithms to ensure convergence, as well as accuracy of the method. More information on Harmonic Balance simulation in ADS® can be found in [15]. Another method to simulate

the frequency-domain output of the circuit is to use transient numerical integration. The circuit is first solved in time-domain using Newton-Raphson and numerical integration, and then the frequency-domain response can be calculated using Fourier Transform (FT) of the steady-state part of the output voltage. Here, we use ELDO® to find the time-domain steady-state of the output, and then use FFT to find the output frequency spectrum. The CPU simulation time of the frequency-domain time-varying Volterra analysis is half the simulation time of ELDO® time-domain steady-state using the same machine. However, this is a rough comparison between the two methods, since ELDO® performs more actions during simulation than time-varying Volterra analysis.

Similar to section 3.2, three different cases of nonlinearities for the resistor will be examined. Case I discusses a mildly nonlinear resistor, i.e. $R_2, R_3 \ll R_1$. Similar to time-domain methods, all the methods simulate the circuit accurately. However, time-varying Volterra and Harmonic Balance are more accurate than conventional Volterra. For case II and III, the nonlinearity of the resistor is increased. Conventional Volterra fails to give accurate results, while time-varying Volterra and Harmonic Balance results are accurate. Harmonic Balance results are more accurate than time-varying Volterra, especially for case III.

4.2.1 Case I

First case deals with a mildly nonlinear resistor. The input of the circuit is a single-tone voltage source with a unity frequency and amplitude, i.e. $v_{in}(t) = \sin(2\pi t)$. The circuit parameters along with frequency-domain simulation parameters are summarized in Table 4.1.

Table 4.1 - Specifications of the test circuit and simulation parameters for Case I

Parameter	Value
Input Frequency, f_{in} (Hz)	1
Input Amplitude, A_{in} (Volts)	1
Resistor Parameters, R_1, R_2, R_3	$1, 0.05, 0.05$
Capacitor Values (F)	1
Maximum Number of Harmonics	6

The circuit is simulated using frequency-domain conventional Volterra, frequency-domain time-varying Volterra, Harmonic Balance and transient numerical integration in ELDO®. Table 4.2 and 4.3 summarize the magnitude and phase of the harmonics using different simulation methods. Time-domain numerical integration simulates the time-domain output voltage, thus, we should use FFT to find the magnitude and

phase of harmonics. This can also be done using the steady-state analysis provided in ELDO®. Steady-state analysis directly simulates the steady-state response of the circuit using shooting method [12].

The results of all the methods, i.e. conventional Volterra, time-varying Volterra and Harmonic-Balance, are close to the ELDO® simulations. Table 4.4 shows the error of different simulation methods comparing to ELDO® simulations. 3rd order conventional Volterra predicts the fundamental harmonic with acceptable accuracy, i.e. 0.8% relative error. However, the error becomes more significant for other harmonics, e.g. 9.8% relative error for DC component. Employing higher order Volterra, i.e. 5th order, the error is reduced one order of magnitude as shown in Table 4.4 (1.6% relative error for DC component). 3rd order time-varying Volterra gives more accurate results as compared to 3rd and 5th order conventional Volterra, up to 3 orders of magnitude smaller error for DC component. Harmonic Balance simulation result is the most accurate comparing to conventional and time-varying Volterra analysis. The fundamental harmonic error is similar to 3rd order time-varying Volterra, i.e. 0.6% relative error, while the DC component error is one order of magnitude smaller.

Table 4.2 – Comparison of the Magnitude of Harmonics for Case I

Frequency Component Magnitude	5th Order Volterra	3rd Order Volterra	3rd Order Time-Varying Volterra	Harmonic Balance	Transient Simulation/FFT
DC (dB)	−33.22	−34.258	−33.075	−33.076	−33.076
Fundamental (dB)	−22.364	−22.398	−22.368	−22.368	−22.368
2nd Harmonic (dB)	−61.84	−60.29	−61.567	−61.568	−61.567
3rd Harmonic (dB)	−72.324	−70.835	−72.098	−72.098	−72.0975
4th Harmonic (dB)	−91.055	–	−93.51	−93.514	−93.518
5th Harmonic (dB)	−106.66	–	−108.67	−108.712	−108.68
6th Harmonic (dB)	–	–	−122.31	−122.36	−122.53

Table 4.3 - Comparison of the Phase of Harmonics for Case I

Frequency Component Phase	5th Order Volterra	3rd Order Volterra	3rd Order Time-Varying Volterra	Harmonic Balance	Transient Simulation/FFT
DC Component (deg)	180	180	180	180	180
Fundamental (deg)	−171.23	−171.27	−171.23	−171.23	−171.23
2nd Harmonic (deg)	−68.56	−67.36	−68.25	−68.25	−68.25
3rd Harmonic (deg)	−151.51	−150.34	−151.25	−151.24	−151.24
4th Harmonic (deg)	−47.81	–	−49.34	−49.34	−49.34
5th Harmonic (deg)	−131.95	–	−133.18	−133.14	−133.14
6th Harmonic (deg)	–	–	−30.59	−30.78	−30.78

Table 4.4 – Error Comparison of Harmonics for Case I (Absolute Error)

Absolute Error of Frequency Component	5th Order Volterra	3rd Order Volterra	3rd Order Time-Varying Volterra	Harmonic Balance
DC (V)	3.6×10^{-4}	2.2×10^{-3}	1.0×10^{-7}	1.1×10^{-8}
Fundamental (V)	4.7×10^{-4}	5.9×10^{-4}	4.8×10^{-4}	4.8×10^{-4}
2nd Harmonic (V)	2.9×10^{-5}	1.3×10^{-4}	1.0×10^{-5}	1.0×10^{-5}
3rd Harmonic (V)	8.6×10^{-6}	3.8×10^{-5}	4.7×10^{-6}	4.6×10^{-6}
4th Harmonic (V)	6.9×10^{-6}	–	5.2×10^{-7}	5.2×10^{-7}
5th Harmonic (V)	9.6×10^{-7}	–	1.0×10^{-7}	1.0×10^{-7}
6th Harmonic (V)	–	–	2.7×10^{-8}	2.6×10^{-8}

4.2.2 Case II

Case II employs a stronger nonlinear resistor, compared to Case I. Using the same input source, i.e. single-tone input, the circuit is simulated in frequency-domain with the parameters shown in Table 4.5.

Table 4.5 - Specifications of the test circuit and simulation parameters for Case II

Parameter	Value
Input Frequency, f_{in} (Hz)	1
Input Amplitude, A_{in} (Volts)	1
Resistor Parameters, R_1, R_2, R_3	$1, 0.5, 0.5$
Capacitor Values (F)	1
Maximum Number of Harmonics	6

Table 4.6 and 4.7 summarize the simulation results of the circuit using conventional Volterra, time-varying Volterra, Harmonic Balance and ELDO®. 3rd and 5th order conventional Volterra no longer give accurate results and suffer from large errors, as large as 66% relative error in calculating DC component. 3rd order time-varying Volterra is able to predict the harmonics with good accuracy, i.e. 0.7% and 0.9% relative error for fundamental harmonic and DC component, respectively. Table 4.8 categorizes the absolute error of different simulation methods comparing to ELDO® simulations. Similar to Case I, Harmonic Balance simulation results are the most accurate results. Harmonic Balance and 3rd order time-varying Volterra show similar error for fundamental harmonic, i.e. 0.7% relative error, whereas, Harmonic Balance's simulation error for DC component is 2 orders of magnitude lower than 3rd order time-varying Volterra.

Table 4.6 - Comparison of the Magnitude of Harmonics for Case II

Frequency Component Magnitude	5th Order Volterra	3rd Order Volterra	3rd Order Time-Varying Volterra	Harmonic Balance	Transient Simulation/FFT
DC (dB)	-17.2	-12.258	-16.778	-16.674	-16.674
Fundamental (dB)	-23.962	-24.471	-23.627	-23.66	-23.659
2nd Harmonic (dB)	-53.04	-40.29	-47.308	-47.208	-47.203
3rd Harmonic (dB)	-48.3	-71.938	-64.653	-64.014	-63.999
4th Harmonic (dB)	-56.57	–	-66.017	-66.761	-66.672
5th Harmonic (dB)	-60.60	–	-82.929	-83.816	-83.337
6th Harmonic (dB)	–	–	-87.663	-88.088	-86.695

Table 4.7 - Comparison of the Phase of Harmonics for Case II

Frequency Component Phase	5th Order Volterra	3rd Order Volterra	3rd Order Time-Varying Volterra	Harmonic Balance	Transient Simulation/FFT
DC Component (deg)	180	180	180	180	180
Fundamental (deg)	−173.46	−173.11	−172.287	−172.313	−171.95
2nd Harmonic (deg)	−222.78	−67.364	−71.56	−71.493	−70.77
3rd Harmonic (deg)	−141.64	124.716	−159.123	−157.488	−156.405
4th Harmonic (deg)	−51.51	–	−55.34	−55.586	−54.136
5th Harmonic (deg)	54.16	–	48.897	48.249	49.898
6th Harmonic (deg)	–	–	−45.555	−41.906	−39.46

Table 4.8 - Error Comparison of Harmonics for Case II (Absolute Error)

Absolute Error of Frequency Component	5th Order Volterra	3rd Order Volterra	3rd Order Time-Varying Volterra	Harmonic Balance
DC (V)	9.4×10^{-2}	9.7×10^{-2}	1.7×10^{-3}	1.6×10^{-5}
Fundamental (V)	2.8×10^{-3}	5.9×10^{-3}	4.5×10^{-4}	4.1×10^{-4}
2nd Harmonic (V)	6.4×10^{-3}	5.3×10^{-3}	7.9×10^{-5}	5.5×10^{-5}
3rd Harmonic (V)	3.2×10^{-3}	6.3×10^{-4}	5.4×10^{-5}	1.2×10^{-5}
4th Harmonic (V)	1.0×10^{-3}	–	3.7×10^{-5}	1.2×10^{-5}
5th Harmonic (V)	8.6×10^{-4}	–	3.4×10^{-6}	4.1×10^{-6}
6th Harmonic (V)	–	–	6.7×10^{-6}	7.1×10^{-6}

4.2.3 Case III

Table 4.9 summarizes the circuit and simulation parameters for case III.

Table 4.9 - Specifications of the test circuit and simulation parameters for Case III

Parameter	Value
Input Frequency, f_{in} (Hz)	1
Input Amplitude, A_{in} (Volts)	1
Resistor Parameters, R_1, R_2, R_3	1, 1, 1.5
Capacitor Values (F)	1
Maximum Number of Harmonics	6

Simulation results for all the simulation methods are shown in Table 4.10 and 4.11. 3rd and 5th order conventional Volterra cannot simulate the circuit with good accuracy, since the circuit is even more nonlinear than case II. The relative error in simulating the DC component is as large as 200% for 5th order conventional Volterra. 3rd order time-varying Volterra is capable of simulating the circuit. However, the error is larger than the two cases before, i.e. 3.3% and 4.0% relative error for fundamental harmonic and DC component, respectively. Harmonic Balance simulation achieves better accuracy comparing to 3rd order time-varying Volterra, especially for DC component. However, the error in predicting the fundamental harmonic is close to 3rd order time-varying Volterra simulation, i.e. 3.2% relative error for fundamental harmonic. The absolute error of different simulation methods comparing to ELDO® simulations is summarized in Table 4.12.

Table 4.10 - Comparison of the Magnitude of Harmonics for Case III

Frequency Component Magnitude	5th Order Volterra	3rd Order Volterra	3rd Order Time-Varying Volterra	Harmonic Balance	Transient Simulation/FFT
DC (dB)	−5.77	−6.238	−14.450	−14.315	−14.319
Fundamental (dB)	−32.48	−30.037	−25.01	−25.15	−25.147
2nd Harmonic (dB)	−27.56	−34.27	−47.413	−46.969	−46.935
3rd Harmonic (dB)	−26.19	−49.713	−62.719	−60.375	−60.32
4th Harmonic (dB)	−44.43	–	−61.01	−62.538	−62.242
5th Harmonic (dB)	−39.95	–	−80.04	−81.658	−80.216
6th Harmonic (dB)	–	–	−79.22	−79.054	−77.111

Table 4.11 - Comparison of the Phase of Harmonics for Case III

Frequency Component Phase	5th Order Volterra	3rd Order Volterra	3rd Order Time-Varying Volterra	Harmonic Balance	Transient Simulation/FFT
DC Component (deg)	180	180	180	180	180
Fundamental (deg)	−179.2	−179.206	−173.189	−173.44	−173.08
2nd Harmonic (deg)	−70.35	−67.36	−74.658	−74.553	−73.84
3rd Harmonic (deg)	−150.34	48.14	−167.73	−159.978	−158.84
4th Harmonic (deg)	−47.81	–	−60.577	−60.731	−59.4
5th Harmonic (deg)	−88.85	–	49.817	43.146	42.565
6th Harmonic (deg)	–	–	−54.87	−47.85	−45.74

Table 4.12 - Error Comparison of Harmonics for Case III (Absolute Error)

Absolute Error of Frequency Component	5th Order Volterra	3rd Order Volterra	3rd Order Time-Varying Volterra	Harmonic Balance
DC (V)	7.0×10^{-1}	2.9×10^{-1}	9.42×10^{-3}	1.0×10^{-4}
Fundamental (V)	5.9×10^{-2}	2.4×10^{-2}	1.8×10^{-3}	1.7×10^{-3}
2nd Harmonic (V)	4.6×10^{-2}	1.5×10^{-2}	2.5×10^{-4}	4.3×10^{-4}
3rd Harmonic (V)	4.8×10^{-2}	4.1×10^{-3}	2.6×10^{-4}	1.3×10^{-4}
4th Harmonic (V)	5.2×10^{-3}	–	1.2×10^{-4}	1.3×10^{-4}
5th Harmonic (V)	9.9×10^{-3}	–	1.2×10^{-5}	1.8×10^{-4}
6th Harmonic (V)	–	–	3.6×10^{-5}	4.3×10^{-5}

4.3 Multi-Dimensional Nonlinearity

We generalize the frequency-domain time-varying Volterra method described before for multi-dimensional nonlinearities. Similar to time-domain time-varying Volterra, the time-varying Volterra circuits are found using Schetzen's multi-linear method, and then use Fourier transform to find the frequency-domain time-varying Volterra circuits. Fig. 4.5 shows the time-varying Volterra circuits for two-dimensional nonlinear elements in frequency-domain.

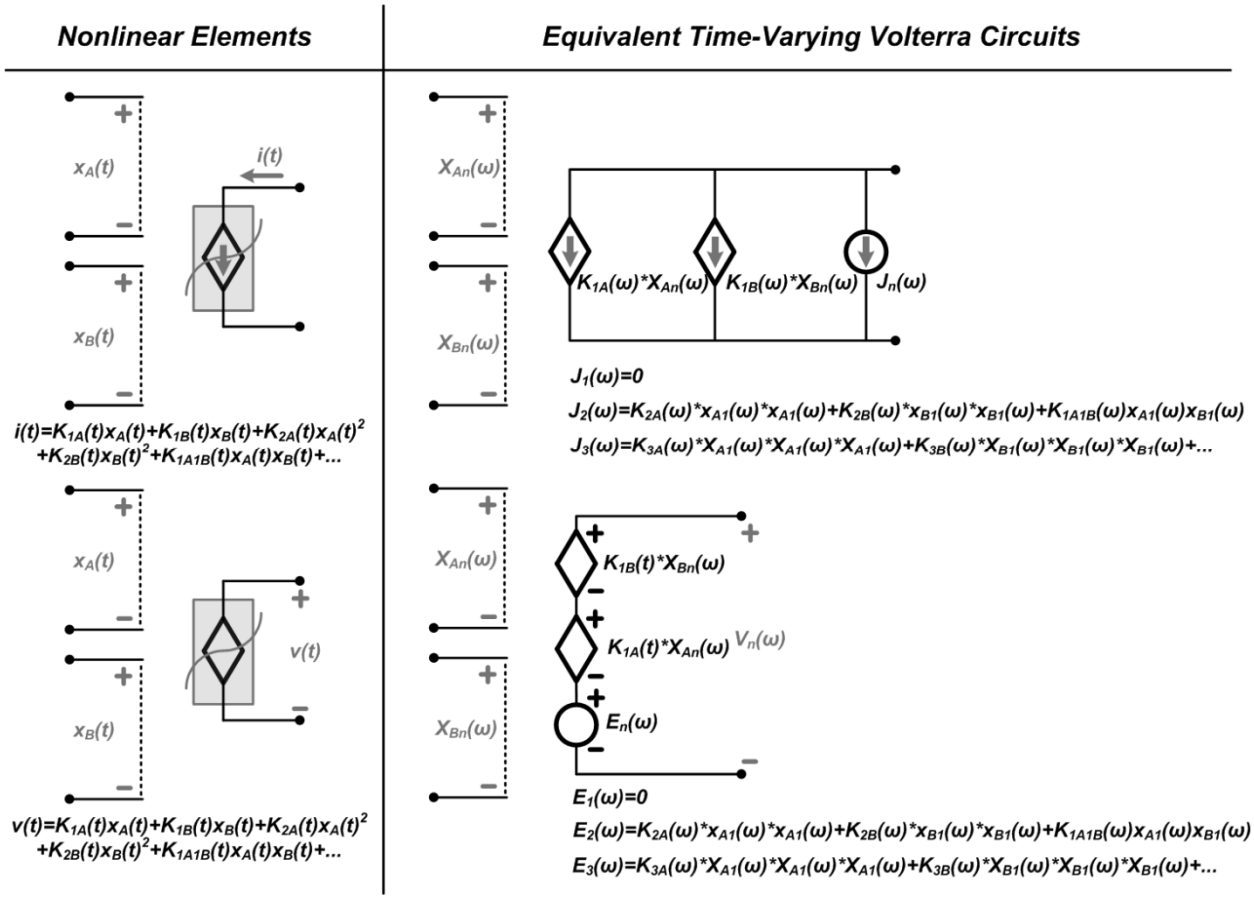

Fig. 4.5 – Two-dimensional nonlinear elements and their time-varying Volterra circuits in frequency-domain

4.4 Summary

In this chapter the frequency-domain simulation of time-varying Volterra was presented. Similar to time-domain approach, the method uses a time-varying expansion point for nonlinear elements and then applies Volterra analysis to enable better accuracy. Using numerical examples it was shown that the accuracy of the method is better than conventional Volterra, whereas Harmonic Balance results in better accuracy for strong nonlinearities. However, the computation cost of the method is less than Harmonic Balance and more than conventional Volterra.

Chapter 5
Power Amplifier Case Study

This chapter presents the application of the time-varying Volterra for simulation of a Class-F Power Amplifier. Class-F Power Amplifiers are a class of nonlinear Power Amplifiers that use harmonic tuning to achieve high efficiencies, theoretically 100%. This type of amplifiers cannot be simulated using conventional Volterra analysis, since the transistor changes region of operation [8], [22]. However, time-varying Volterra simulates the circuit with good accuracy. Basic operation of Class-F Power Amplifiers, details of simulation of the Class-F Power-Amplifier using time-varying Volterra as well as comparison with other simulation methods are discussed in this chapter.

The Chapter is organized as follows. Section 5.1 discusses the basics of Class-F Power Amplifiers and its design considerations. Section 5.2 presents the formulation of the Class-F Power Amplifier using time-varying Volterra in frequency-domain. The simulation results using conventional Volterra, time-varying Volterra and ELDO® steady-state analysis is presented in section 5.3. Finally, section 5.4 gives the concluding remarks.

5.1 Class-F Power Amplifier: Basics

Today's modern portable communication systems demand for low power consumption. Since RF Power Amplifiers dominate the power dissipation for transmitters, power efficient Power Amplifiers are becoming more and more important [16]. Class-F Power Amplifiers are a class of high efficiency amplifiers widely used. The goal in designing high efficiency amplifier is to minimize the dissipated power in the amplifying transistor, i.e. $P_{transistor}(t) = V_{DS}(t)I_D(t)$, thus, increasing the overall efficiency. Class-F Power Amplifiers load the transistor at different frequencies, i.e. fundamental and harmonics, to ensure a pulse waveform for drain-source voltage and half sinusoidal waveform for the drain current of the transistor, as shown in Fig. 5.1. In order to have such waveforms for the transistor, one must have [16],

$$Z_L(N\omega_0) = \begin{cases} 0 & even\ N \\ \infty & odd\ N \\ Z_L(opt) & N = 1 \end{cases}, \tag{5.1}$$

where Z_L is the load impedance seen by the drain of the transistor and ω_0 is the input frequency. $Z_L(opt)$ is the optimum load of the transistor which results in the maximum power delivered to the load.

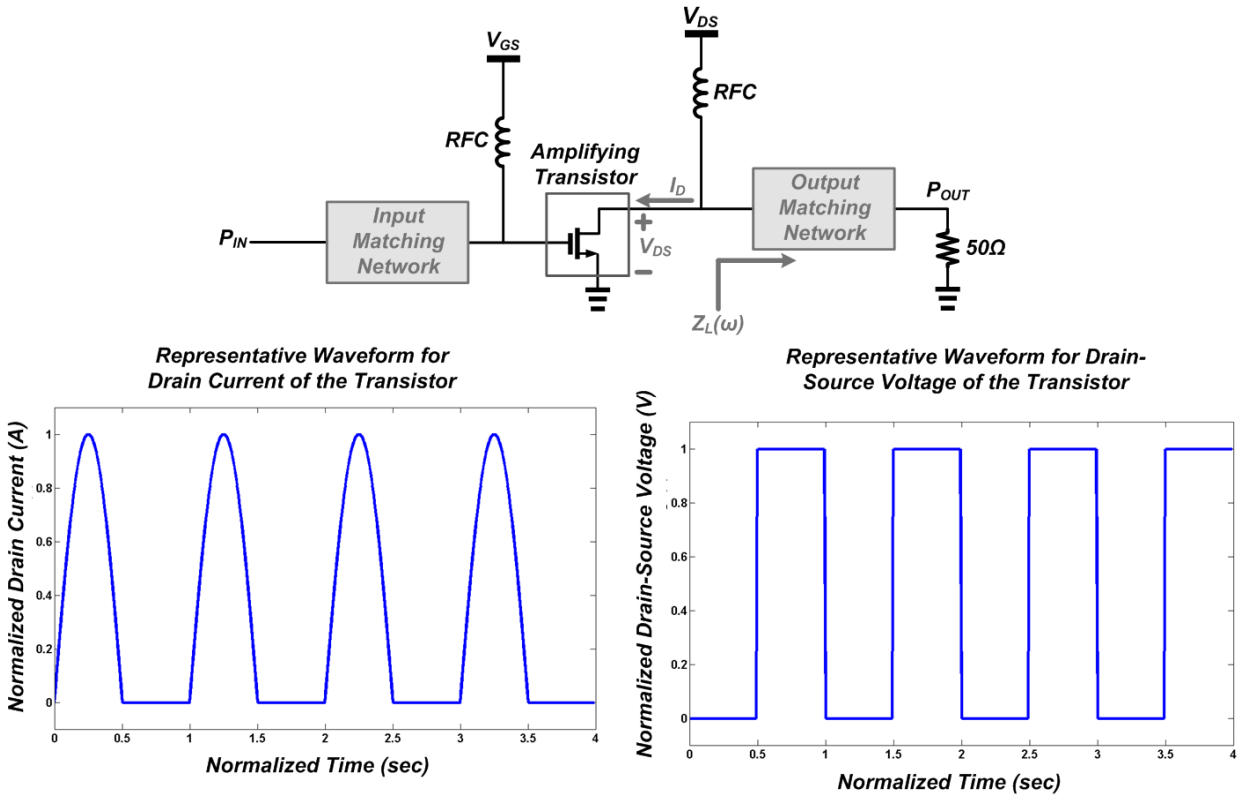

Fig. 5.1 – Class-F Power Amplifier

Fig. 5.2 shows the schematic of a Class-F Power Amplifier that satisfies (5.1) for first, second and third harmonic [17]. For simplicity the input matching network is not shown here. The combination of L_1, L_2 and C_B make sure that the impedance seen by the transistor is zero at second harmonic and infinity for third harmonic. The values for L_1, L_2 and C_B are calculated using,

$$L_1 = \frac{1}{6\omega_0^2 C_{out}}, \qquad L_2 = \frac{5}{3}L_1, \tag{5.2}$$

$$C_B = \frac{12}{5}C_{out},$$

where C_{out} is the output capacitance of the transistor. $L_{3\omega}$ and $C_{3\omega}$ are chosen to resonate at $3\omega_0$, also, the output π-matching network ensures the proper load for the transistor at fundamental frequency for maximum power delivered to the load. The reader is referred to [18] and [19] for detailed discussion on the design and properties of the output π-matching network.

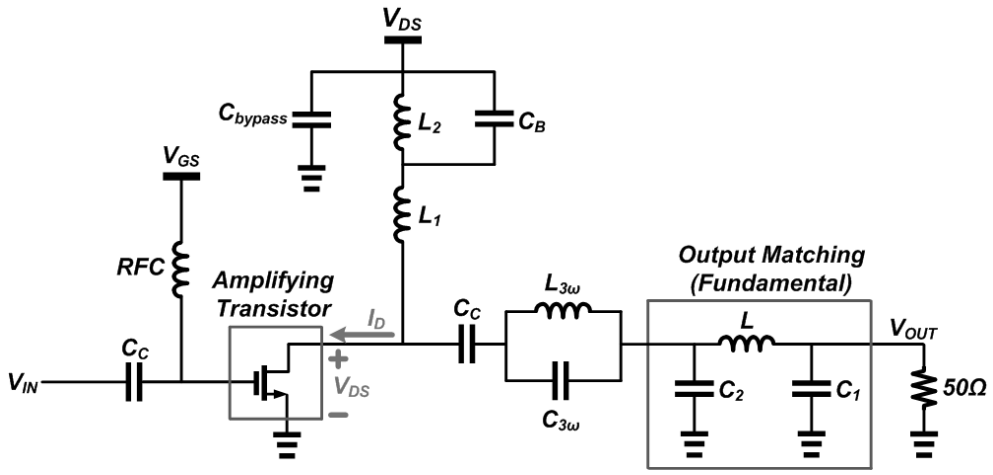

Fig. 5.2 – Schematic of a Class-F Power Amplifier (Input matching network is not shown for simplicity)

5.2 Formulation of Class-F Power Amplifier

The first step in simulating the Class-F Power Amplifier shown in Fig. 5.2 is to replace the transistor with its nonlinear equivalent model. For this case study, we have designed the Class-F Power Amplifier using $0.18\mu m$ CMOS technology NMOS transistors. The NMOS transistor is modeled for this application as shown in Fig. 5.3. The model contains two nonlinear capacitors, i.e. gate-source and drain-source capacitances, and a two-dimensional nonlinear voltage-controlled current source. The details about the validity, as well as, the accuracy of the model is found in Appendix A. Nonlinear elements in the model shown in Fig. 5.3 are characterized as,

$$C_{GS}(V_{GS}) = C_{GS0} + C_{GS1}V_{GS} + C_{GS2}V_{GS}^2 + \cdots + C_{GS10}V_{GS}^{10},$$
$$C_{DS}(V_{DS}) = C_{DS0} + C_{DS1}V_{DS} + C_{DS2}V_{DS}^2 + \cdots + C_{DS10}V_{DS}^{10}, \tag{5.3}$$

and,

$$\begin{aligned} I_D = f(V_{GS}, V_{DS}) = {} & a_{0,0} + a_{0,1}V_{DS} + a_{0,2}V_{DS}^2 + \cdots + a_{0,10}V_{DS}^{10} \\ & + \left(a_{1,0} + a_{1,1}V_{DS} + a_{1,2}V_{DS}^2 + \cdots + a_{1,10}V_{DS}^{10}\right)V_{GS} \\ & \vdots \\ & + \left(a_{10,0} + a_{10,1}V_{DS} + a_{10,2}V_{DS}^2 + \cdots + a_{10,10}V_{DS}^{10}\right)V_{GS}^{10}. \end{aligned} \tag{5.4}$$

For details of calculating the coefficients of nonlinear devices, the reader is referred to Appendix A.

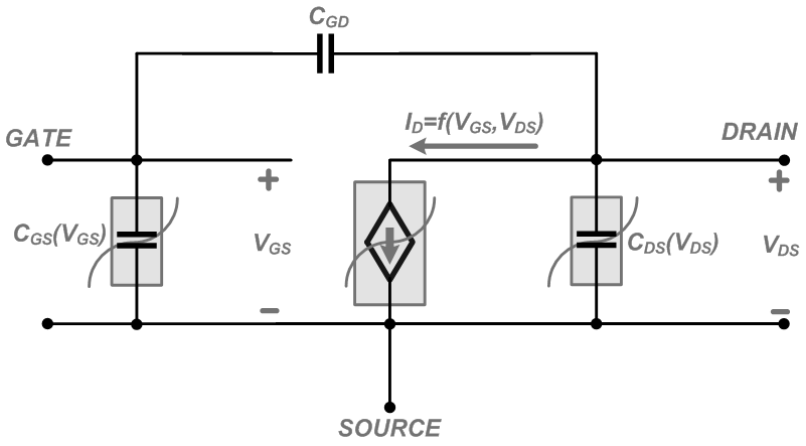

Fig. 5.3 – Nonlinear Transistor Model

Fig. 5.4 shows the Class-F Power Amplifier with the transistor replaced by the nonlinear model of Fig. 5.3. The amplifier is designed for the center frequency of $500MHz$, with circuit parameters summarized in Table 5.1.

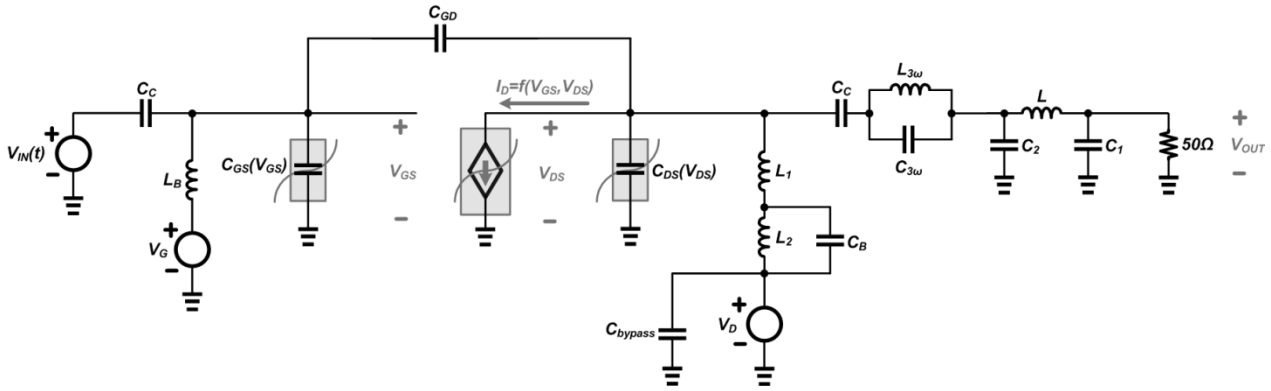

Fig. 5.4 – Class-F Power Amplifier with the transistor replaced by nonlinear model

Now we discuss the simulation of the Class-F Power Amplifier using time-varying Volterra analysis. The first step for time-varying Volterra analysis is linear pre-analysis. Pre-analysis circuit is constructed by linearizing all the nonlinear elements around their DC operating points. DC operating point of the transistor is easily calculated as,

$$V_{GS0} = V_G = 0.5\,V, \qquad V_{DS0} = V_D = 0.9\,V, \qquad I_{D0} = f(V_{GS0}, V_{DS0}) = 431.01\,\mu A\,. \tag{5.5}$$

Table 5.1 – Class-F Power Amplifier Parameters

Output Matching Parameters	
$\boldsymbol{L}$ **(nH)**	1.3786
$\boldsymbol{C_1, C_2}$ **(pF, pF)**	305.83, 96.73
3rd Harmonic Resonator Parameters	
$\boldsymbol{C_{3\omega}}$, $\boldsymbol{L_{3\omega}}$ **(pF, nH)**	11.258, 1
Biasing Circuit Parameters	
$\boldsymbol{L_B, L_1, L_2}$ **(μH, nH, nH)**	1, 68.15, 113.58
$\boldsymbol{C_B, C_C, C_{bypass}}$ **(pF, μF, μF)**	0.5947, 1, 1
$\boldsymbol{V_G, V_D}$ **(V, V)**	0.5, 0.9
Input Voltage Parameters	
Input Frequency (MHz)	500
Maximum Input Amplitude (V)	0.2

Fig. 5.5 shows the pre-analysis circuit using the linearized model for all nonlinear elements. The linearized capacitors and controlled current source are calculated using the equations below

$$g_{m1} = \frac{dI_D}{dV_{GS}}\bigg|_{V_{GS0}, V_{DS0}},$$

$$g_{DS1} = \frac{dI_D}{dV_{DS}}\bigg|_{V_{GS0}, V_{DS0}},$$

$$C_{GS-Lin} = C_{GS}(V_{GS})\,\Big|_{V_{GS} = V_{GS0}},$$

$$C_{DS-Lin} = C_{DS}(V_{DS})\,\Big|_{V_{DS} = V_{DS0}}. \tag{5.6}$$

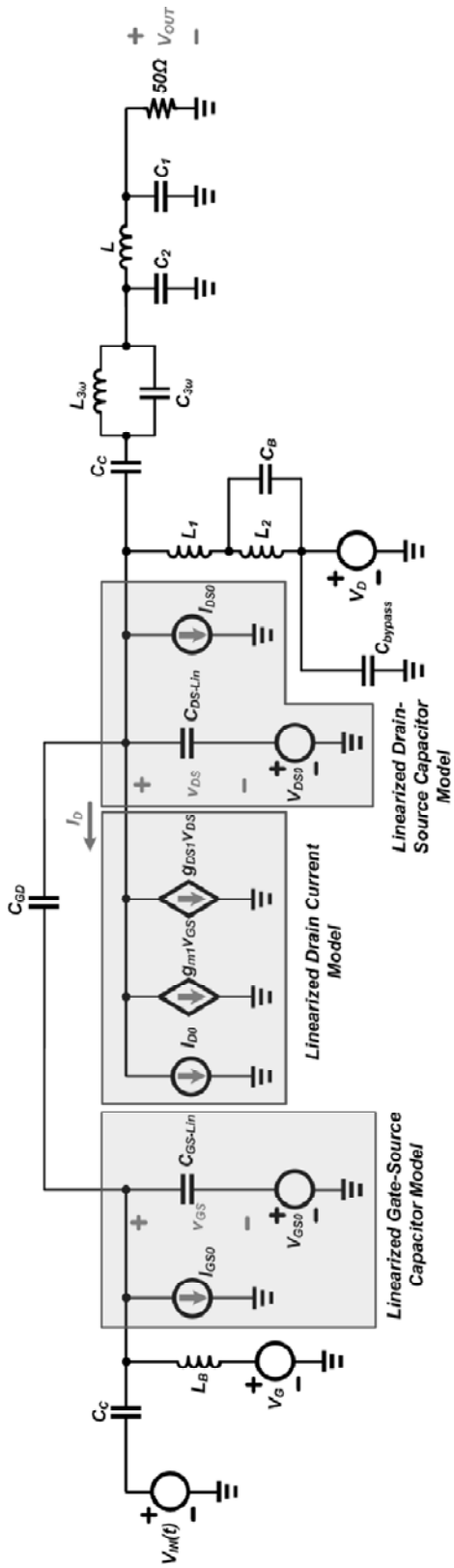

Fig. 5.5 – Linear Pre-Analysis circuit

The capacitor's linearized model contains a current source in parallel with the linear capacitor, i.e. I_{GS0} and I_{DS0}, which represents capacitor's DC operating point for charge. In other words,

$$I_{GS0} = \frac{d}{dt}(Q_{GS0}) = \frac{d}{dt}(C_{GS-Lin}V_{GS0}),$$
$$I_{DS0} = \frac{d}{dt}(Q_{DS0}) = \frac{d}{dt}(C_{DS-Lin}V_{DS0}). \quad (5.7)$$

As long as the operating point of the nonlinear capacitor is time independent, I_{GS0} and I_{DS0} will be zero and thus are removed from the model.

The next step in time-varying Volterra analysis is generating the time-varying Volterra models for all the nonlinear elements. Fig. 5.6 shows the time-varying Volterra circuits for different orders where all nonlinear elements are replace by their time-varying Volterra model. Generating time-varying Volterra models require calculating time-varying Volterra coefficients for all the nonlinear elements. The nonlinear controlled source coefficients are calculated as,

$$g_{m1}(t) = \frac{dI_D}{dV_{GS}}\bigg|_{V_{GS-PE}(t),V_{DS-PE}(t)'}$$
$$g_{DS1}(t) = \frac{dI_D}{dV_{DS}}\bigg|_{V_{GS-PE}(t),V_{DS-PE}(t)'}$$
$$g_{m2}(t) = \frac{1}{2!}\frac{d^2I_D}{dV_{GS}^2}\bigg|_{V_{GS-PE}(t),V_{DS-PE}(t)'} \quad (5.8)$$
$$g_{DS2}(t) = \frac{1}{2!}\frac{d^2I_D}{dV_{DS}^2}\bigg|_{V_{GS-PE}(t),V_{DS-PE}(t)'}$$
$$\vdots$$

Similarly, for the time-varying coefficients for the nonlinear capacitors we have,

$$C_{GS2}(t) = \frac{dC_{GS}(V_{GS})}{dV_{GS}}\bigg|_{V_{GS-PE}(t)'}$$

$$C_{DS2}(t) = \frac{dC_{DS}(V_{DS})}{dV_{DS}}\bigg|_{V_{DS-PE}(t)'}$$

$$C_{GS3}(t) = \frac{1}{2!}\frac{d^2C_{GS}(V_{GS})}{dV_{GS}^2}\bigg|_{V_{GS-PE}(t)'} \tag{5.9}$$

$$C_{DS3}(t) = \frac{1}{2!}\frac{d^2C_{DS}(V_{DS})}{dV_{DS}^2}\bigg|_{V_{DS-PE}(t)'}$$

where $V_{GS-PE}(t)$ and $V_{DS-PE}(t)$ are pre-analysis simulation results. Due to complexity, the symbolic expressions for time-varying coefficients are not shown here. Formulating the time-varying Volterra circuits using the method described in chapter 4, the time-varying Volterra circuits are analyzed in frequency-domain. The simulation results along with comparison with ELDO® steady-state results are presented in the next section.

5.3 Simulation Results

The Class-F Power Amplifier is simulated using 3rd order time-varying Volterra and ELDO® steady-state analysis. Here, we discuss the time-varying Volterra simulation for a single-tone input. However, multiple-tone inputs can also be simulated using this method. Table 5.2 to Table 5.4 summarizes the frequency components of the output voltage, transistor's drain-source voltage and supply current for 3rd time-varying Volterra and ELDO® steady-state simulation results for maximum input power. Time-varying Volterra simulation results are in good agreement with ELDO® steady-state simulation result. The amplifier was also simulated using 5th order conventional Volterra. However, the simulation results show large errors, i.e. more than 200% relative error for the output voltage of the amplifier and the simulation results are not shown here. Fig. 5.7 to Fig. 5.9 show the output of the amplifier, transistor's drain-source voltage and supply current respectively in time-domain for maximum input power. The time-domain results for time-varying Volterra are calculated using Inverse Fourier Transform. The time-varying Volterra simulation results show less than 0.2% relative error for the output voltage of the amplifier.

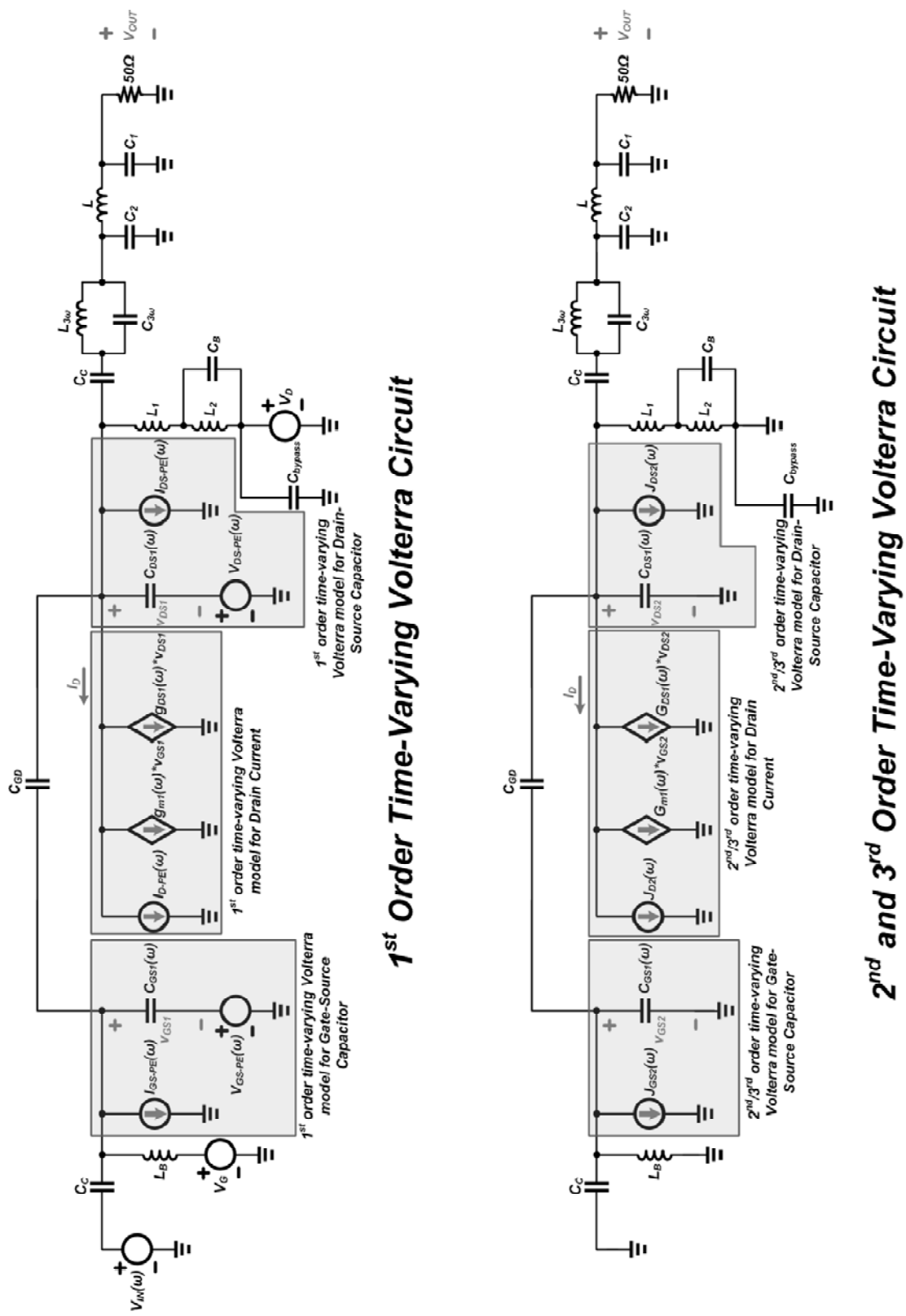

Fig. 5.6 – Time-Varying Volterra circuit for different orders

Table 5.2 – Simulation results for Drain-Source voltage of the transistor

Frequency Component Magnitude	3rd Order Time-Varying Volterra	ELDO Steady-State Simulation	Error of the Frequency Component
DC (dB)	-0.91515	-0.91515	7.6×10^{-8}
Fundamental (dB)	-7.09457	-7.11221	1.1×10^{-3}
2nd Harmonic (dB)	-137.573	-135.6896	6.4×10^{-8}
3rd Harmonic (dB)	-24.8446	-25.0862	1.574×10^{-3}
4th Harmonic (dB)	-61.73984	-61.24285	5.3×10^{-5}
5th Harmonic (dB)	-78.60462	-75.93401	4.5×10^{-5}
6th Harmonic (dB)	-76.124422	-80.42946	6.1×10^{-5}

Table 5.3 – Simulation results for the output voltage of the Class-F Power Amplifier

Frequency Component Magnitude	3rd Order Time-Varying Volterra	ELDO Steady-State Simulation	Error of the Frequency Component
DC (dB)	$-\infty$	-177.99	1.2×10^{-9}
Fundamental (dB)	-17.09473	-17.1123	3.6×10^{-4}
2nd Harmonic (dB)	-174.49	-171.77	2.3×10^{-9}
3rd Harmonic (dB)	-175.85	-168.689	2.9×10^{-9}
4th Harmonic (dB)	-123.961	-123.473	4.1×10^{-8}
5th Harmonic (dB)	-141.795	-139.318	3.2×10^{-8}
6th Harmonic (dB)	-141.313	-145.737	3.4×10^{-8}

Table 5.4 – Simulation results for the supply current of the Class-F Power Amplifier

Frequency Component Magnitude	3rd Order Time-Varying Volterra	ELDO Steady-State Simulation	Error of the Frequency Component
DC (dB)	-58.4617	-58.4236	5.2×10^{-6}
Fundamental (dB)	-69.26997	-69.2876	8.9×10^{-7}
2nd Harmonic (dB)	-69.8163	-69.808123	4.2×10^{-7}
3rd Harmonic (dB)	-77.4776	-77.7192	3.7×10^{-6}
4th Harmonic (dB)	-118.7497	-118.245	7.7×10^{-8}
5th Harmonic (dB)	-138.219	-136.086	6.4×10^{-8}
6th Harmonic (dB)	-76.124422	-80.42946	6.1×10^{-5}

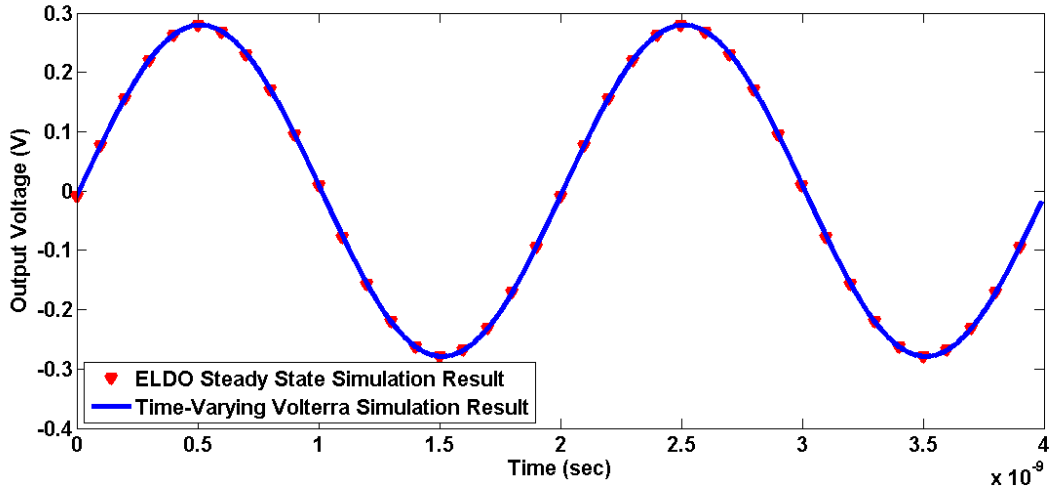

Fig. 5.7 – Output voltage of the amplifier for maximum input power

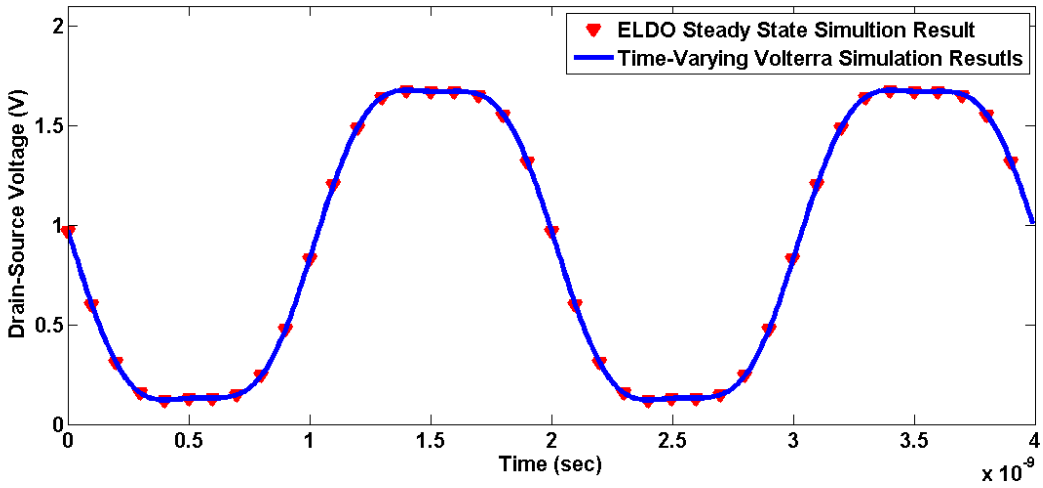

Fig. 5.8 – Transistor's Drain-Source voltage of the amplifier for maximum input power

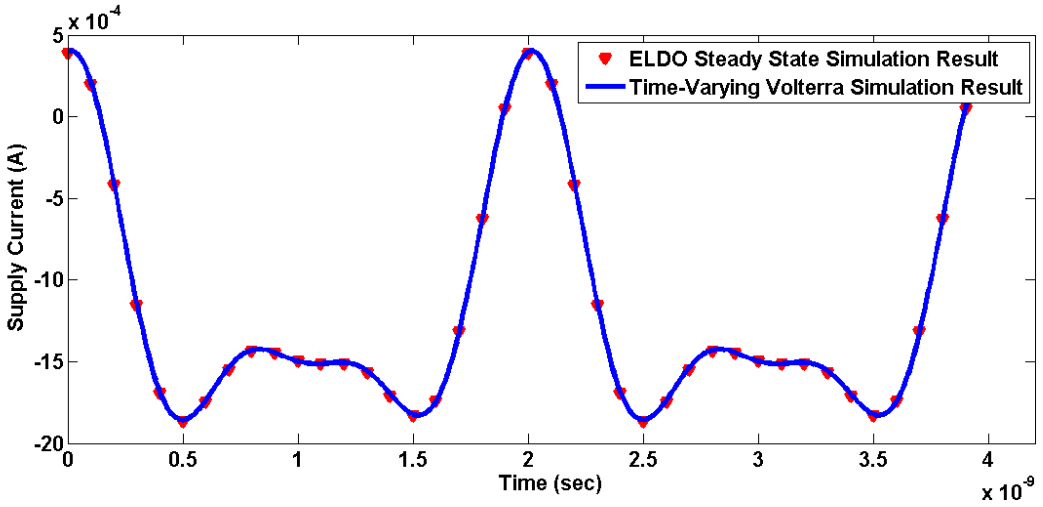

Fig. 5.9 – Power supply current of the amplifier for maximum input power

Furthermore, the amplifier is simulated for $6dB$ back-off input power, i.e. $6dB$ less than the maximum input power. The simulation results in time-domain are shown in Fig. 5.10 to Fig. 5.12. Fig. 5.13 shows output power versus input power for the amplifier using time-varying Volterra and ELDO® steady-state simulation results. The time-varying Volterra simulation results match ELDO® steady-state results with good accuracy. Similarly, simulation result for the drain efficiency of the

amplifier versus input power, shown in Fig. 5.14, are in good agreement with ELDO® steady-state simulation results.

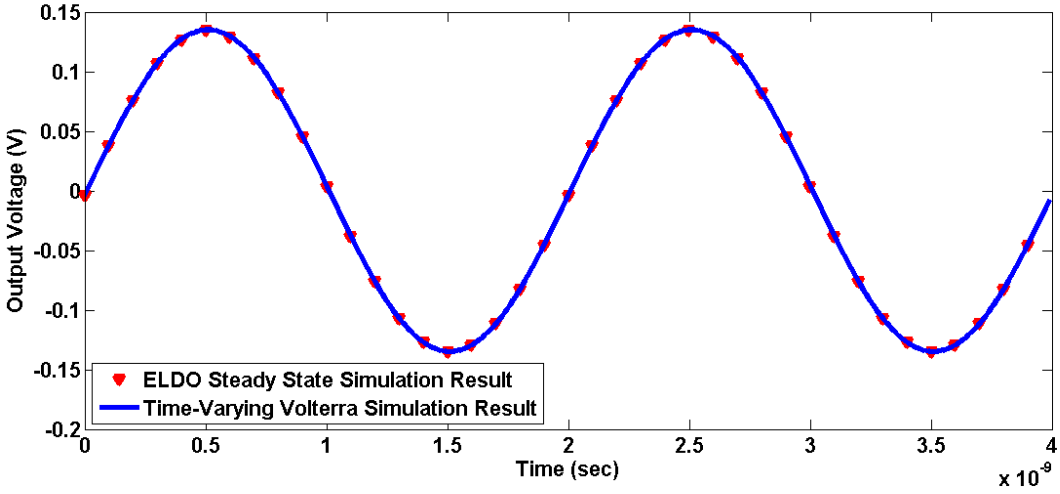

Fig. 5.10 – Output voltage of the amplifier for 6-dB back-off input power

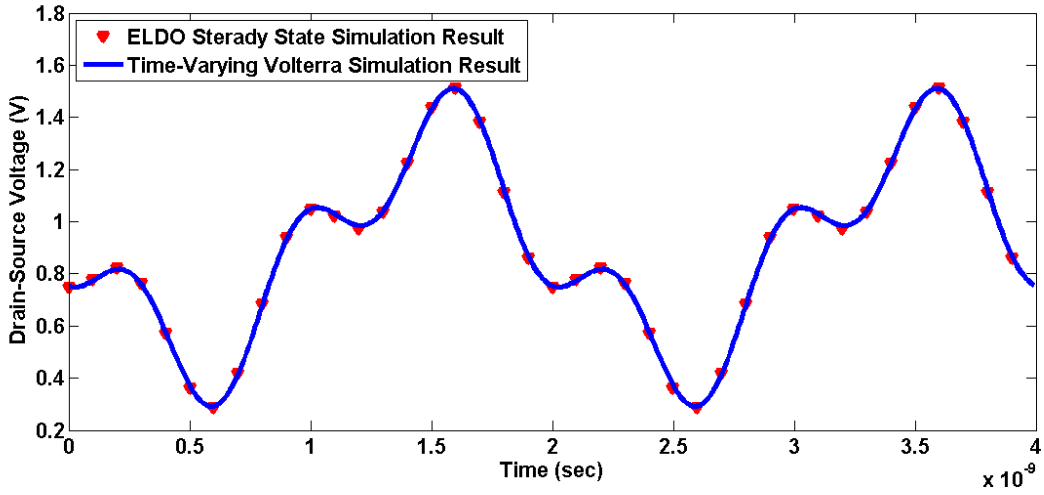

Fig. 5.11 – Transistor's Drain-Source voltage of the amplifier for 6-dB back-off input power

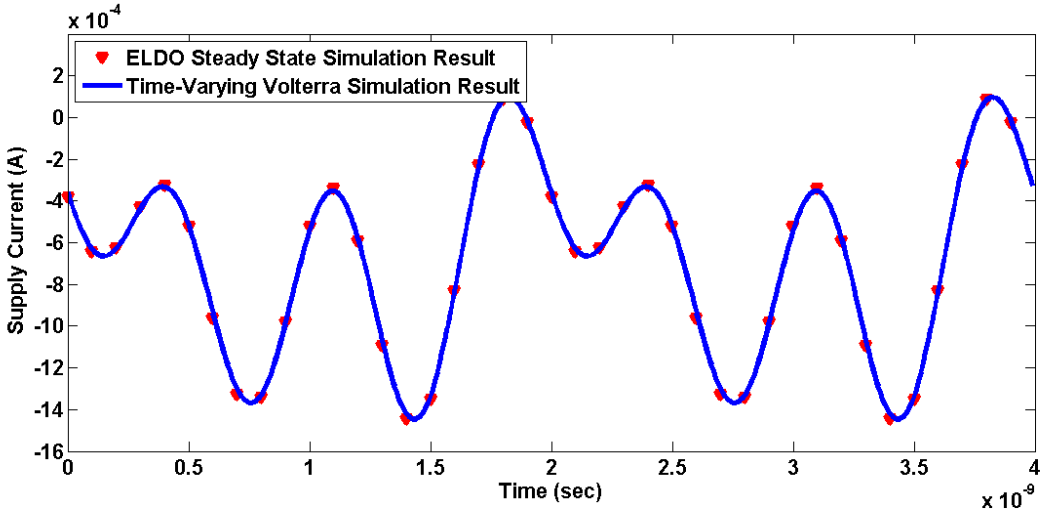

Fig. 5.12 – Power supply current of the amplifier for 6-dB back-off input power

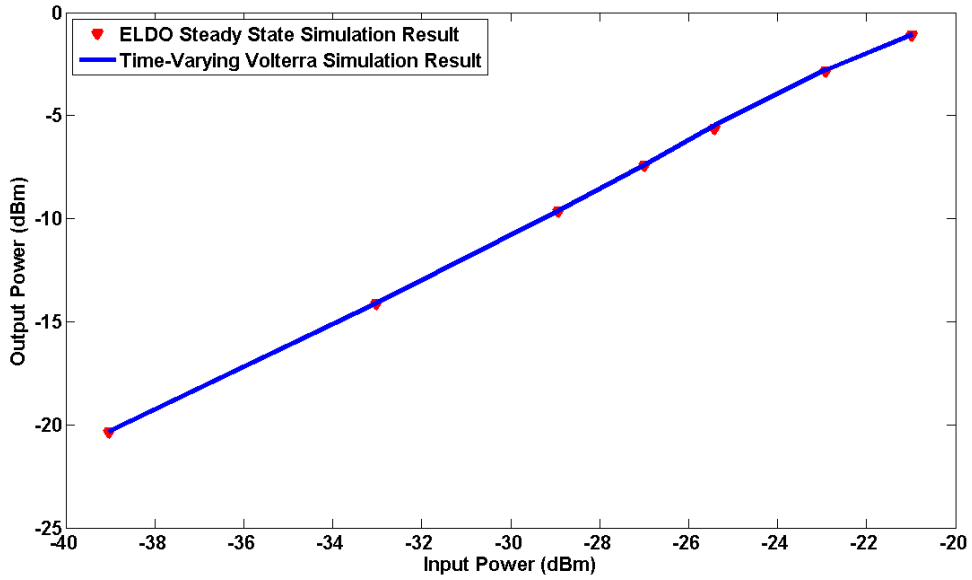

Fig. 5.13 – Output power vs. input power for the Class-F Power Amplifier

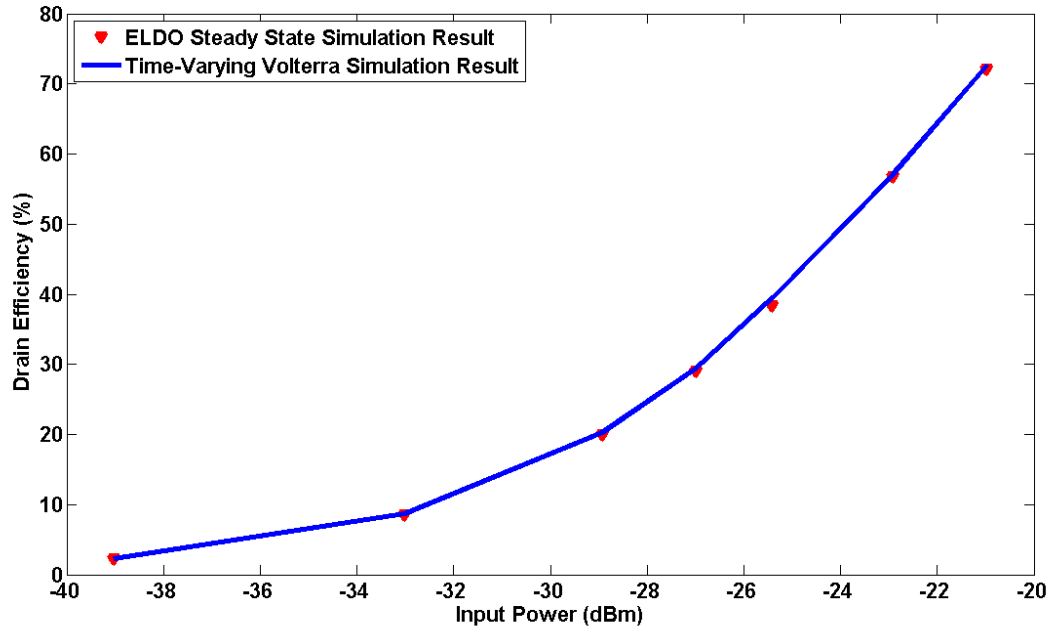

Fig. 5.14 – Drain Efficiency of the amplifier vs. input power

5.4 Conclusion

In this chapter a Class-F Power Amplifier was simulated using the proposed time-varying Volterra in frequency-domain. The simulation results show the effectiveness of the method to simulate transistor amplifiers with good accuracy. It was shown that the results show good accuracy comparing to ELDO® steady-state simulation results which uses shooting method [12] to simulate the steady-state solution of the circuit. Conventional Volterra, on the other hand, cannot simulate such a circuit.

Chapter 6
Conclusion and Future Work

This chapter presents the application of the proposed time-varying Volterra in circuit simulation. Also, possible future research work regarding time-varying Volterra is discussed here. The work presented in this thesis is the generalization of conventional Volterra analysis. Time-varying Volterra analysis manages to simulate a wider range of nonlinear circuits comparing to conventional Volterra, including saturated Power Amplifiers and mixers.

6.1 Application of Time-Varying Volterra in Circuit Simulation

Frequency-domain time-varying Volterra can be used to simulate nonlinear Power Amplifiers, mixers and nonlinear microwave circuits. The proposed method manages to simulate nonlinear circuits with large number of nonlinear elements without convergence issues of Harmonic Balance. Furthermore, the method can be generalized to simulate the sensitivity of nonlinear circuits. The sensitivity calculation would be similar to the work in [7]. Sensitivity analysis is important for performance optimization methods [26], as well as yield optimizations where sensitivity is used to calculate the yield gradient [27]. Another application for time-varying Volterra is for distortion decomposition calculation. The Volterra based distortion decomposition method presented in [28] can be generalized for time-varying Volterra analysis. Distortion decomposition is helpful to designers for low distortion designs. Distortion decomposition can be used to find the main sources of nonlinearities in the design. Thus designer can simplify the nonlinear models, which makes it easier to find symbolic expressions for distortion analysis [29].

The main contributions of this thesis are:

- Presenting time-domain time-varying Volterra analysis as a simulation method for nonlinear circuits.
- Applying the time-varying Volterra analysis in frequency-domain to simulate nonlinear RF/microwave circuits, e.g. Power Amplifiers.

6.2 Future Work

In this section possible future work regarding time-varying Volterra is presented. The frequency-domain time-varying Volterra method described in this thesis can be modified to achieve better

computation efficiency. Instead of employing a continuously time-varying expansion point for Taylor expansion, one can use multiple expansion points for Taylor series. This will be beneficial in case of periodic inputs. One can use a finite number of expansion points in each period of the input signal, e.g. 8 expansion points. Using the same concept, Volterra circuits of different orders can be generated similar to time-varying Volterra. However, the circuits of different order will be periodically switched linear circuits instead of time-varying linear. Periodically switched linear Volterra circuits for different order are simulated in either time- or frequency-domain as described in [25]. It should be noted that the number of expansion points determines the maximum frequency of the analysis, thus one should choose number of expansion points based on the application.

Time-varying Volterra can also be used for modeling purposes. Using multiple expansion points, different Volterra models can be constructed for a nonlinear circuit. Employing this method, the nonlinear circuit is modeled using different Volterra circuits for different input ranges. Using pre-analysis, the designer can determine the time phases in which different Volterra models are used. This can help in more accurate modeling of nonlinear circuits, such as saturated Power Amplifiers. Accurate modeling of saturated Power Amplifiers is an important part of linearizing Power Amplifier using pre-distortion algorithms [16].

Furthermore, the time-varying Volterra analysis may be modified to simulate harsher nonlinearities such as diodes. This may be achieved by employing a more sophisticated pre-analysis using a more sophisticated model for nonlinear elements in pre-analysis. For example harsh nonlinear elements may be replaced by a piecewise linear model, instead of the linearized model. Then time-varying Volterra can be applied using the result of pre-analysis.

Appendix A
Transistor Modeling

The model for CMOS transistors used in this thesis is based on polynomial fitting. There are different models for CMOS transistors in literature which some are physical-based and some are empirical models. BSIM3 [23] and EKV model [9] are two widely used physical-based models available for CMOS transistors. BSIM3 model is based on physical behavior of CMOS transistors with hundreds of empirical parameters added for accurate modeling. For this application we create our own empirical model for an NMOS transistor. The model includes a nonlinear voltage-controlled current source, which models the nonlinear drain current of the transistor, and nonlinear capacitors between gate, drain and source, as shown in Fig. A.1. It has been assumed that bulk of the transistor is connected to the source, thus the transistor can be modeled as a three-terminal device. The model, however, can be generalized to four-terminal device as well.

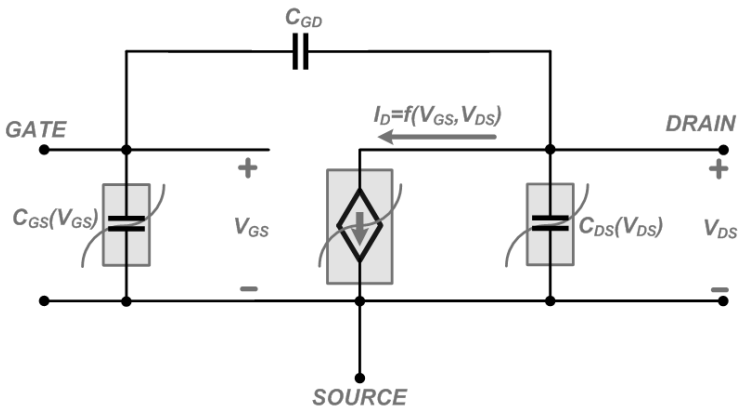

Fig. A.1 – Nonlinear transistor model

A.1 Drain Current Modeling

The drain current of an NMOS transistor is a nonlinear function of both gate-source and drain-source voltages, as shown below.

$$I_D = f(V_{GS}, V_{DS}). \tag{A.1}$$

In the EKV model [9] the drain current is modeled using the functions of the form, $\ln\left(1 + e^{\frac{v_p - v_s}{2}}\right)^2$. However, for this thesis we model the drain current using a 10th order two-dimensional polynomial as illustrated below.

$$\begin{aligned} I_D = f(V_{GS}, V_{DS}) = {} & a_{0,0} + a_{0,1}V_{DS} + a_{0,2}V_{DS}^2 + \cdots + a_{0,10}V_{DS}^{10} \\ & + \left(a_{1,0} + a_{1,1}V_{DS} + a_{1,2}V_{DS}^2 + \cdots + a_{1,10}V_{DS}^{10}\right)V_{GS} \\ & + \left(a_{2,0} + a_{2,1}V_{DS} + a_{2,2}V_{DS}^2 + \cdots + a_{2,10}V_{DS}^{10}\right)V_{GS}^2 \\ & \quad \vdots \\ & + \left(a_{10,0} + a_{10,1}V_{DS} + a_{10,2}V_{DS}^2 + \cdots + a_{10,10}V_{DS}^{10}\right)V_{GS}^{10}. \end{aligned} \tag{A.2}$$

This modeling requires 121 coefficients to be calculated, which can be done using polynomial fitting. The DC current of the transistor is first simulated using ELDO® for $0.1 < V_{GS} < 0.9$ and $0 < V_{DS} < 1.8$. ELDO® uses BSIM3v3 model for the transistors. Then using polynomial fitting function in MATLAB® all the coefficients in (A.2) are calculated to achieve minimum error.

A.2 Capacitor Modeling

The capacitors used in transistor modeling are usually multi-dimensional nonlinear capacitors. In other words,

$$\begin{aligned} C_{GS} &= f_1(V_{GS}, V_{DS}), \\ C_{DS} &= f_2(V_{GS}, V_{DS}), \\ C_{GD} &= f_3(V_{GS}, V_{DS}). \end{aligned} \tag{A.3}$$

However, for this thesis application we assume that the capacitors can be modeled with enough accuracy using a linear gate-drain capacitor and two one-dimensional nonlinear capacitors between gate-source and drain-source as shown in Fig. A.1.

$$C_{GS} \cong f_1(V_{GS}),$$

$$C_{DS} \cong f_2(V_{DS}), \tag{A.4}$$

$$C_{GD} = Constant.$$

It should be noted that as the frequency of application increases the effect of capacitor become more and more important and more accurate modeling is needed. Similar to the drain current, we approximate the nonlinear gate-source and drain-source capacitances using 10^{th} order polynomials.

$$C_{GS} = f_1(V_{GS}) = C_{GS0} + C_{GS1}V_{GS} + C_{GS2}V_{GS}^2 + \cdots + C_{GS10}V_{GS}^{10},$$

$$C_{DS} = f_2(V_{DS}) = C_{DS0} + C_{DS1}V_{DS} + C_{DS2}V_{DS}^2 + \cdots + C_{DS10}V_{DS}^{10}, \tag{A.5}$$

Extracting the capacitor values from BSIM3v3 model for different gate-source and drain-source biasing, the coefficients in (A.5) are determined using polynomial fitting function in MATLAB®.

A.3 Simulation Results

For this thesis we calculate the model in Fig. A.1 for an NMOS transistor in $0.18\mu m$ technology with $W = 240\mu m$ and $L = 0.18\mu m$. Fig. A.2 shows the drain current of the transistor using the 10^{th} order two-dimensional polynomial model as well as BSIM3v3 model. As it can be seen the results of polynomial model are in good agreement with BSIM3v3 model. The 10^{th} order two-dimensional polynomial model shows a maximum of 0.6% relative error for the drain current.

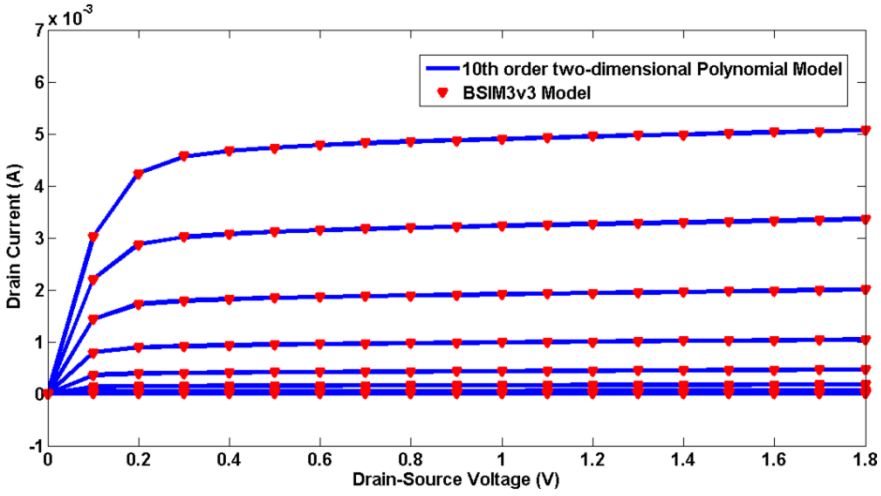

Fig. A.2 – Drain current of the transistor using 10th order two-dimensional polynomial model and BSIM3v3 model

The gate-source and drain-source capacitances of the transistor using the 10th order polynomial model and BSIM3v3 model are shown in Fig. A.3 and Fig. A.4. The 10th order polynomial model shows a relative error of less than 0.8% for the gate-source and drain-source capacitances comparing to BSIM3v3 model. It can be concluded that the circuit in Fig. A.1 with the polynomial models presented can model the transistor with good accuracy. For this thesis we use this model for the simulation of the Class-F Power Amplifier.

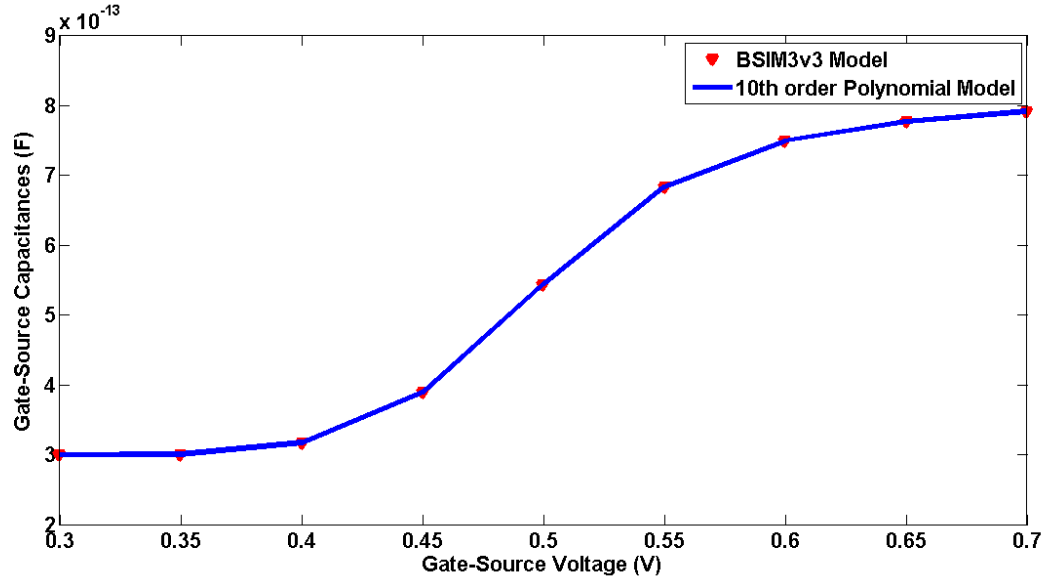

Fig. A.3 – Gate-Source capacitance of the transistor using 10th order polynomial model and BSIM3v3 model

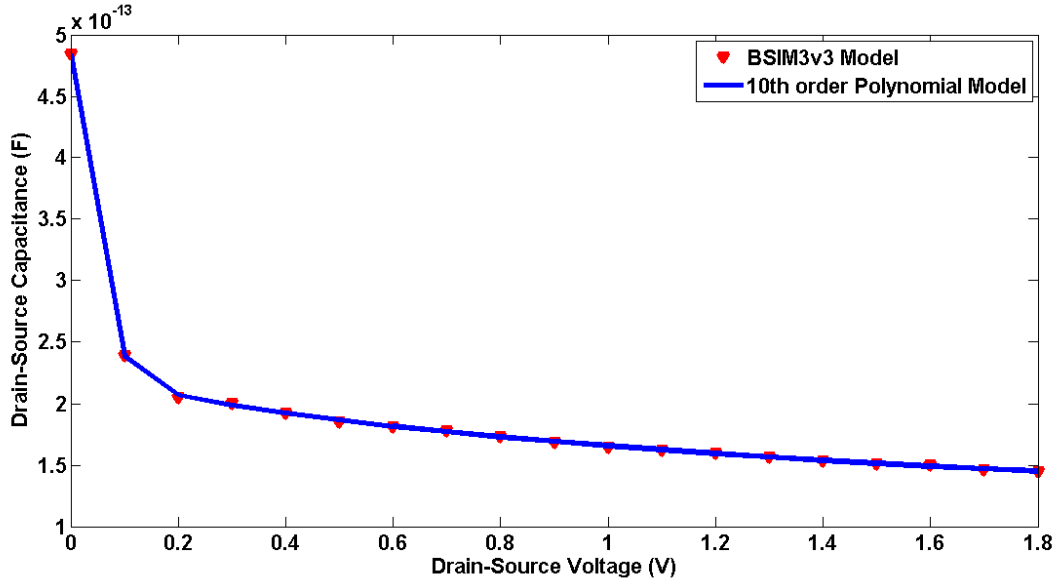

Fig. A.4 – Drain-Source capacitance of the transistor using 10th order polynomial model and BSIM3v3 model

Bibliography

[1] J. Vlach and K. Singhal, *Computer Methods for Circuit Analysis and Design*, 2nd ed., New York: Van Nostrand, 1994.

[2] K. Kundert, *The Designer's Guide to SPICE and Spectre*, Boston: Kluwer Academic Publishers, 1995.

[3] S. A. Maas, *Nonlinear Microwave and RF Circuits*, 2nd ed., Artech House, 2003.

[4] M. Schetzen, "Multilinear theory of nonlinear networks," *Journal of the Franklin Institue*, vol. 320, no. 5, pp. 221-247, 1985.

[5] V. Volterra, *Theory of functionals and of integral and integro-differential equations*, New York: Dover, 1959.

[6] P. Wambacq and W. Sansen, *Distortion Analysis of Analog Integrated Circuits*, Boston: Kluwer Academic Publishers, 1998.

[7] G. Zhu and A. Opal, "Sensitivity Analysis of Nonlinear Circuits using Volterra Series," in *Proc. IEEE ISCAS'06*, May 2006, pp. 5035-5038.

[8] I. Sarkas, D. Mavridis, and G. Papdopoulos, "Volterra Analysis Using Chebyshev Series," in *Proc. IEEE ISCAS'07*, May 2007, pp. 1931-1934.

[9] C. Enz, F. Krummenacher, and E. Vittoz, "An Analytical MOS Transistor Model Valid in All regions of Operation and Dedicated to Low Voltage and Low Current Applications," *Analog In. Circuits and Signal Processing*, vol. 48, no. 6, pp. 726-738, June 2001.

[10] S. A. Maas, *Nonlinear Microwave and RF Circuits*, Artech House, 1988.

[11] E. Isaacson and H. B. Keller, *Analysis of Numerical Methods*, New York: Wiley, 1966.

[12] *ELDO User's Manual*, Mentor Graphics Corporation, 2005.

[13] S. M. Sze, *Semiconductor Devices, Physics and Technology*, 2nd ed., New York: Wiley, 2002.

[14] A. V. Oppenheim, *Signals and Systems*, Upper Saddle River, N.J.: Prentice Hall, 1997.

[15] *ADS User's Manual*, Agilent Technologies, 2006.

[16] S. C. Cripps, *RF Power Amplifiers for Wireless Communications*, Artech House, 1999.

[17] F. Giannini, *Nonlinear Microwave Circuit Design*, Hoboken, N.J.: Wiley, 2004.

[18] T. H. Lee, *The Design of CMOS Radio-Frequency Integrated Circuits*, 2nd ed., New York: Cambridge University Press, 2004.

[19] B. Razavi, *RF Microelectronics*, Upper Saddle River, N.J.: Prentice Hall, 1998.

[20] J. A. Garcia, M. L. De la Fuente, J. C. Pedro, N. B. Carvalho, Y. Newport, A. Mediavilla, and A. Tazon, "Time-Varying Volterra Series Analysis of Spectral Regrowth and Noise Power Ration in

FET Mixers," *IEEE Tran. Microwave Theory and Techniques*, vol. 49, no. 3, pp. 545-549, March 2001.

[21] M. T. Terrovitis and R. G. Meyer, "Intermodulation Distortion in Current-Commutating CMOS Mixers," *IEEE J. Solid-State Circuits*, vol. 35, pp. 1461-1473, Oct. 2000.

[22] J. Vuolevi and T. Rahkonen, *Distortion in RF Power Amplifiers*, Norwood, MA: Artech House, 2003.

[23] Y. Cheng and C. Hu, *MOSFET Modeling & BSIM3 User's Guide*, Kluwer Academic Publisher, 1999.

[24] F. Yuan and A. Opal, "Distortion Analysis of Periodically Switched Nonlinear Circuits Using Time-Varying Volterra Series," *IEEE Trans. Circuits Syst.*, vol. 48, no. 6, pp. 726-737, June 2001.

[25] F. Yuan and A. Opal, *Computer Methods for Analysis of mixed-Mode Switching Circuits*, Kluwer Academic Publishers, 2004.

[26] G. Gielen and R. Rutenbar, "Computer-Aided Design of Analog and Mixed-Signal Integrated Circuits," *Proc. IEEE*, vol. 88, pp. 1825-1852, Dec. 2000.

[27] G. Stehr, *On the Performance Space Exploration of Analog Integrated Circuits*, PhD theis, Technische Universitat Munchen, Munich, 2005.

[28] G. Zhu and A. Opal, "Per-Element Decomposition in Distortion Analysis," in *Proc. IEEE ISCAS'07*, May 2007, pp. 449-452.

[29] X. Lie, P. Li, Y. Xu and L. Pileggi, "Analog and RF Circuit Macromodels for System-Level Analysis" *Proc. IEEE Design Automation Conference*, pp. 478-483, June 2003.

[30] G. Zhu, *Sensitivity Analysis and Distortion Decomposition of Mildly Nonlinear Circuits*, MASc. thesis, University of Waterloo, Waterloo, 2007.

[31] A. Opal, "Sampled data simulation of linear and nonlinear circuits," *IEEE Trans. On Computer-Aided Design*, vol. 15, no. 3, pp. 295-307, March 1996.

[32] A. Opal, "The transition matrix for linear circuits," *IEEE Trans. On Computer-Aided Design*, vol. 16, no. 5, pp. 427-436, May 1997.

[33] T. Quarles, A. R. Newton, D. O. Pederson and A. Sangiovanni-Vincentelli, *SPICE 3 Version 3F5 User's Manual*, Dept. Elec. Eng. Comp. Sci., Univ. of California, Berkeley, CA, Mar. 1994.

[34] P. Feldmann and J. Roychowdhury, "Computation of circuit waveform envelopes using an efficient matrix-decomposed harmonic balance algorithm," IEEE *International Conference on Computer-Aided Design: Digest of Technical Papers*, November 1996.

[35] K. Kundert, “Simulation methods for RF integrated circuits,” *Proc. IEEE/ACM Int. Conf. Computer-Aided Design (ICCAD)*, pp. 762-765, 1997.

[36] K. Kundert, “Introduction to RF simulation and its applications,” *IEEE J. Solid-State Circuits*, vol. 34, pp. 1298-1319, Sept. 1999.

[37] E. Dautbegovic, M. Condon and C. Brennan, “An efficient nonlinear circuit simulation technique,” *IEEE Tran. Microwave Theory and Techniques*, vol. 53, pp. 548-555, Feb. 2005.

[38] O. Ocali, M. A. Tan and A. Atalar, “A new method for nonlinear circuit simulation in time domain: NOWE,” *IEEE Trans. On Computer-Aided Design*, vol. 15, pp. 368-374, March 1996.